

7-2-2012

# Modeling gap effects in jointed rock

Tyler Baker

Follow this and additional works at: [https://digitalrepository.unm.edu/me\\_etds](https://digitalrepository.unm.edu/me_etds)

---

## Recommended Citation

Baker, Tyler. "Modeling gap effects in jointed rock." (2012). [https://digitalrepository.unm.edu/me\\_etds/55](https://digitalrepository.unm.edu/me_etds/55)

This Thesis is brought to you for free and open access by the Engineering ETDs at UNM Digital Repository. It has been accepted for inclusion in Mechanical Engineering ETDs by an authorized administrator of UNM Digital Repository. For more information, please contact [disc@unm.edu](mailto:disc@unm.edu).

Tyler A. Baker

---

*Candidate*

Mechanical Engineering

---

*Department*

This thesis is approved, and it is acceptable in quality and form for publication:

*Approved by the Thesis Committee:*

Dr. Tariq Khraishi, Chairperson

---

Dr. Howard L. Schreyer

---

Dr. Deborah Sulsky

---

# Modeling Gap Effects in Jointed Rock

by

**Tyler Baker**

B.S., Mechanical Engineering, University of Notre Dame, 2009

THESIS

Submitted in Partial Fulfillment of the  
Requirements for the Degree of

Master of Science  
Mechanical Engineering

The University of New Mexico

Albuquerque, New Mexico

May, 2012

# Modeling Gap Effects in Jointed Rock

by

**Tyler Baker**

B.S., Mechanical Engineering, University of Notre Dame, 2009

M.S., Mechanical Engineering, University of New Mexico, 2012

## Abstract

Joints represent planes of discontinuity in homogeneous media. The purpose of this investigation is to model joints and determine the effects on waves as they propagate through joints in rock. Properties of interest include energy dissipation, energy transmission, and changes in peak stress and impulse as waves propagate through one or more joints. Rather than combining rock joints into the constitutive model of the parent rock as typically done, this research seeks to model joints discretely. By capturing the behavior of individual rock joints, discrete effects on wave propagation are gathered. The ability to lump multiple joints into one equivalent joint is also explored. The key result is that joints affect short duration pulses more than long duration pulses. A single equivalent joint transmits less energy than a set of multiple joints.

# Contents

List of Figures	ix
List of Tables	xiii
<b>1 Introduction</b>	<b>1</b>
<b>2 Rock Joint Problem</b>	<b>3</b>
2.1 Rock Joints . . . . .	3
2.2 Wave Propagation through Jointed Rock . . . . .	6
2.3 Objective . . . . .	7
<b>3 Literature Survey</b>	<b>9</b>
3.1 Contiguous Rock Models . . . . .	9
3.1.1 Intact Rock . . . . .	10
3.1.2 Contact Behavior . . . . .	11
3.2 Large Rock Mass Models . . . . .	12
3.3 Aperçu . . . . .	13
<b>4 One-Dimensional Constitutive Models for Joints</b>	<b>14</b>

<i>Contents</i>	v
4.1 1D Joint Modeling Formulation . . . . .	14
4.1.1 Joint Closure . . . . .	15
4.1.2 Joint Opening . . . . .	17
4.2 Numerical Implementation of 1D Joint Model . . . . .	19
4.2.1 Joint Closure . . . . .	20
4.2.2 Joint Opening . . . . .	22
4.2.3 Other loading scenarios and summary . . . . .	22
4.2.4 Results of Driver Program for 1D Joint Model . . . . .	23
4.3 Gap Constitutive Model . . . . .	24
4.3.1 Results of Driver Program for 1D Gap Model . . . . .	24
4.4 1D Joint Model with Plasticity and Linear Elasticity . . . . .	25
4.4.1 Numerical Implementation of the Elastic-Plastic Joint Model . . . . .	27
4.4.2 Calculation of $E_g$ . . . . .	28
4.4.3 Results of Driver Program for 1D Elastic-Plastic Joint Model . . . . .	29
4.5 Experimental Validation of 1D Joint Model . . . . .	30
4.6 MPM Code, Gap Model, and Analytical Solution . . . . .	31
4.6.1 Gap Model Analysis . . . . .	32
4.6.2 Analytical Solution to Determine Closure Potential . . . . .	34
4.6.3 Proposed Boundary Condition Characterization . . . . .	35
<b>5 Basic Features of Wave Propagation through a Joint</b>	<b>37</b>
5.1 One-Dimensional Bar Problem . . . . .	37

<i>Contents</i>	vi
5.2 Gap, Plastic Joint, and Elastic-Plastic Joint Comparison . . . . .	39
5.2.1 No Discontinuity . . . . .	40
5.2.2 Gap Discontinuity . . . . .	40
5.2.3 Plastic Joint Discontinuity . . . . .	42
5.2.4 Elastic-Plastic Joint Discontinuity . . . . .	44
<b>6 Effects of Parameters on Wave Propagation through Single Joint</b>	<b>47</b>
6.1 Program of Single Joint Study . . . . .	47
6.2 Single Discontinuity Study . . . . .	49
6.2.1 Gap . . . . .	49
6.2.2 Plastic Joint . . . . .	51
6.2.3 Elastic-Plastic Joint . . . . .	53
6.3 Single Joint Conclusions . . . . .	54
<b>7 Effects of Parameters on Wave Propagation through Two Joints</b>	<b>56</b>
7.1 Two Gaps Study . . . . .	58
7.1.1 Two Gaps In-Depth . . . . .	61
7.2 Two Plastic Joints Study . . . . .	64
7.2.1 Two Joints In-Depth . . . . .	68
7.3 Summary of Multiple Joints . . . . .	70
<b>8 Conclusion</b>	<b>71</b>
8.1 Summary . . . . .	71
8.2 Future Work . . . . .	72

<i>Contents</i>	vii
<b>A Convergence Study with a Single Gap</b>	<b>73</b>
<b>B Convergence Study with Two Gaps</b>	<b>77</b>
<b>C Nondimensionalization Scheme</b>	<b>81</b>
C.1 Dimensioned Quantities . . . . .	81
C.2 Equations . . . . .	82
C.3 Proposed Dimensionless Quantities . . . . .	82
<b>D Material Point Placement</b>	<b>85</b>
<b>E Complete Figures</b>	<b>90</b>
E.1 Single Gap . . . . .	91
E.2 Single Plastic Joint . . . . .	92
E.3 Single Elastic-Plastic Joint . . . . .	93
<b>F Lumping Joints Study</b>	<b>94</b>
F.1 Gaps, $u_{g0} = 1.5\text{mm}$ . . . . .	96
F.2 Gaps, $u_{g0} = 0.5\text{mm}$ . . . . .	97
F.3 Plastic Joints, $u_{g0} = 1.5\text{mm}$ . . . . .	98
F.4 Plastic Joints, $u_{g0} = 0.5\text{mm}$ . . . . .	99
F.5 Elastic-Plastic Joints, $u_{g0} = 1.5\text{mm}$ . . . . .	100
F.6 Elastic-Plastic Joints, $u_{g0} = 0.5\text{mm}$ . . . . .	101
<b>G Joint Spacing Study</b>	<b>102</b>
G.1 Gaps . . . . .	104



<i>Contents</i>	viii
G.2 Plastic Joints . . . . .	105

# List of Figures

2.1	Two sets of joints with terminating planes . . . . .	4
2.2	Jointed rock in Carlsbad Cavern. Photograph provided by Stephen Bespalko. . . . .	5
2.3	The traction $\boldsymbol{\tau}$ acting on the joint with shear and normal components and the joint discontinuity $[\boldsymbol{u}]$ . . . . .	5
2.4	Rock joint and its numerical representation . . . . .	6
2.5	Wave propagating towards a joint set . . . . .	7
4.1	The joint “hardening” function $g(\bar{u}_g)$ when $\bar{u}_g \leq 1$ . . . . .	16
4.2	Impact of $m$ on the shape of the joint “hardening” function $g(\bar{u}_g)$ . .	17
4.3	Joint with prescribed positive strain increments . . . . .	18
4.4	Joint Driver Loading Cycle . . . . .	23
4.5	Gap Driver Loading Cycle . . . . .	25
4.6	Elastic-Plastic Joint Driver Loading Cycle . . . . .	29
4.7	Experimental configuration . . . . .	30
4.8	Driver output . . . . .	31
4.9	Verification run where the green dot represents a gap in the middle of the bar. . . . .	32

<i>List of Figures</i>	x
4.10 Gap Model Verification . . . . .	33
5.1 Notation for the problem of a bar with a single discontinuity . . . . .	38
5.2 Results of wave propagation through a bar without a discontinuity . . . . .	40
5.3 Results of wave propagation through a bar with a gap . . . . .	41
5.4 Results of wave propagation through a bar with a plastic joint . . . . .	43
5.5 Results of wave propagation through a bar with an elastic-plastic joint . . . . .	45
6.1 Single Discontinuity Study . . . . .	47
6.2 Plots of results for wave propagation through a single gap with $u_p = 1.5\text{mm}$ . . . . .	50
6.3 Plots of results for a wave transmitted through a single plastic joint with $u_p = 1.5\text{mm}$ . . . . .	52
6.4 Plots of results for a wave transmitted through a single, elastic-plastic joint with $u_p = 1.5\text{mm}$ . . . . .	54
7.1 Transmitted energy results for multiple gap study . . . . .	57
7.2 Plots of stress for different gap spacings (blue dots denote locations of gaps) . . . . .	60
7.3 Results for transmitted energy due to gap spacing . . . . .	61
7.4 Stress plots at various time of wave propagation through two gaps spaced 40 material points apart (blue dots denote gap locations) . . . . .	63
7.5 $\bar{u}$ versus time for each gap . . . . .	63
7.6 Plots of material point stress for multiple joint spacing (blue dots denote joint locations) . . . . .	64
7.7 Energy versus time plots for multiple joint spacings . . . . .	66

<i>List of Figures</i>	xi
7.8 Energy transmission of multiple joint spacings . . . . .	67
7.9 Material point stress plotted at different times (blue dots denote joint locations) . . . . .	69
7.10 $\bar{u}$ versus time for each joint . . . . .	70
A.1 Mesh refinement for wave propagation through a gap, 1 material point per cell . . . . .	74
A.2 Mesh refinement for wave propagation through a gap, 1 material point per cell . . . . .	75
A.3 Mesh refinement for wave propagation through a gap, 1 material point per cell . . . . .	75
A.4 Mesh refinement for wave propagation through a gap, 1 material point per cell . . . . .	76
B.1 Mesh refinement for wave propagation through two gaps, 1 material point per cell . . . . .	78
B.2 Mesh refinement for wave propagation through 2 gaps, 1 material point per cell . . . . .	79
B.3 $\bar{u}$ versus time for first gap . . . . .	80
B.4 $\bar{u}$ versus time for second gap . . . . .	80
D.1 Stress as a function of $x$ for different times using 50 material points located close to the cell boundary to discretize the bar . . . . .	87
D.2 Stress as a function of $x$ for different times using 128 material points centered in the cells to discretize the bar . . . . .	88

D.3	Stress as a function of $x$ for different times using 50 material points located close to the cell boundary to discretize the bar with a gap in the center of the bar . . . . .	88
D.4	Stress as a function of $x$ for different times using 128 material points centered in the cells to discretize the bar with a gap in the center of the bar . . . . .	89
E.1	Results of single gap study, $u_p = 1.5\text{mm}$ . . . . .	91
E.2	Results of single plastic joint study, $u_p = 1.5\text{mm}$ . . . . .	92
E.3	Results of single elastic-plastic joint study, $u_p = 1.5\text{mm}$ . . . . .	93
F.1	Layout of Discontinuity Lumping Study . . . . .	94
F.2	Results of lumping multiple gaps, $u_{g0} = 1.5\text{mm}$ . . . . .	96
F.3	Results of lumping multiple gaps, $u_{g0} = 0.5\text{mm}$ . . . . .	97
F.4	Results of lumping multiple plastic joints, $u_{g0} = 1.5\text{mm}$ . . . . .	98
F.5	Results of lumping multiple plastic joints, $u_{g0} = 0.5\text{mm}$ . . . . .	99
F.6	Results of lumping multiple elastic-plastic joints, $u_{g0} = 1.5\text{mm}$ . . .	100
F.7	Results of lumping multiple elastic-plastic joints, $u_{g0} = 0.5\text{mm}$ . . .	101
G.1	Layout of Discontinuity Spacing Study . . . . .	103
G.2	Results of spacing two gaps, $u_{g0} = 1.5\text{mm}$ . . . . .	104
G.3	Results of spacing two plastic joints, $u_{g0} = 1.5\text{mm}$ . . . . .	105

# List of Tables

6.1	Inputs used for the single joint sets . . . . .	48
7.1	Inputs used for gap spacing . . . . .	58
7.2	Energy dissipated in closing the joints . . . . .	66
F.1	Inputs used for multiple joints . . . . .	95
G.1	Inputs used for joint spacing . . . . .	103

# Chapter 1

## Introduction

This thesis presents the results of research done on the modeling of rock joints. A rock joint is numerically considered a discontinuity of the rock medium. The published constitutive models for rock do not discretely model the rock joints. Further, the current literature does not seem to present any studies or findings on the interaction of a joint with a propagating wave or explore a joint's impact on wave propagation, such as energy transmission or wave impulse.

The thesis work develops a discrete one-dimensional constitutive model for rock joints that will be used in a study of the effects of rock joints on wave propagation through rock media.

The thesis tasks are:

- (a) Develop a one-dimensional discrete constitutive model for joints under normal loading.
- (b) Implement the one-dimensional model into a dynamic Material Point Method code to study the result of the joint on wave propagation.
- (c) Consider multiple joints and their impact on wave-propagation.
- (d) Determine when it is reasonable, if ever, to replace a set of joints with one equivalent joint in order to make numerical simulations simpler and less costly.

The results are conclusions about how a single joint or multiple joints affect the peak stress, the energy, and the impulse of a one-dimensional sinusoidal pulse. This development provides the framework for a corresponding investigation of three-dimensional wave impingement on a single joint or multiple joints oriented obliquely to the direction of wave propagation.



## Chapter 2

# Rock Joint Problem

The masters research problem is primarily a one-dimensional study of rock joints and the impact of joints on wave propagation through rock. A one-dimensional constitutive model has been developed to represent joint behavior under normal loading. This model is used to characterize wave behavior and to quantify the effect of joints on wave propagation in one dimension.

### 2.1 Rock Joints

Rocks often contain discontinuous planes of weakness which traverse the rock mass. Planes of weakness depend on the length of discontinuity, ranging from small cracks called fissures to joints to large faults. Fissures can be contained in handheld specimens. Joints occur in larger rock masses. Faults span long distances and continuously intersect rock and other types of discontinuities (Goodman [8]). Given the large range in sizes of discontinuities that exist in rocks, the focus of this research is limited to discontinuities associated with joints.

A joint is composed of two parallel faces of rock, which have fractured due to external forces, such as folding, or cooling (in igneous rock). The faces are separated by some length to leave a void. Over time, water flows through the void leaving be-

hind mineral deposits and sediment, which forms gouge. Another joint characteristic is asperities. Depending on how the initial fracture occurred, two rock faces could have varying degrees of surface roughness. The asperities form the overall structure of surface roughness. The essential characteristics of a joint are the asperities and gouge. The joint has resistance to shear because of these characteristics. In normal compressive loading, the joint exhibits nonlinear increase in stress with gap closure. In normal tensile loading, the joint exhibits little or no strength.

Joints appear as parallel planar cracks. The spacing between cracks may vary from centimeters to as much as 10 meters (Goodman [8]). Typically, joints appear in sets, as opposed to sporadically spaced and oriented discontinuities. These parallel discontinuities are uniformly spaced and end along an intersecting joint called a terminating plane (Figure 2.1). A system of joints is more than one set of joints contained in the rock mass. Jointed igneous and metamorphic rock usually have systems of three or more joint sets. One set will have planes of weakness parallel to the bedding planes of the rock. The subsequent sets form in other directions creating a rock mass that is composed of individual blocks with discontinuities along their surfaces (Figure 2.2).

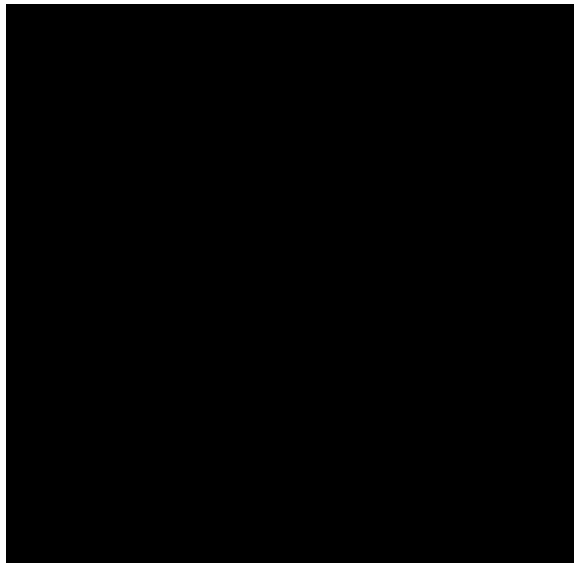


Figure 2.1: Two sets of joints with terminating planes

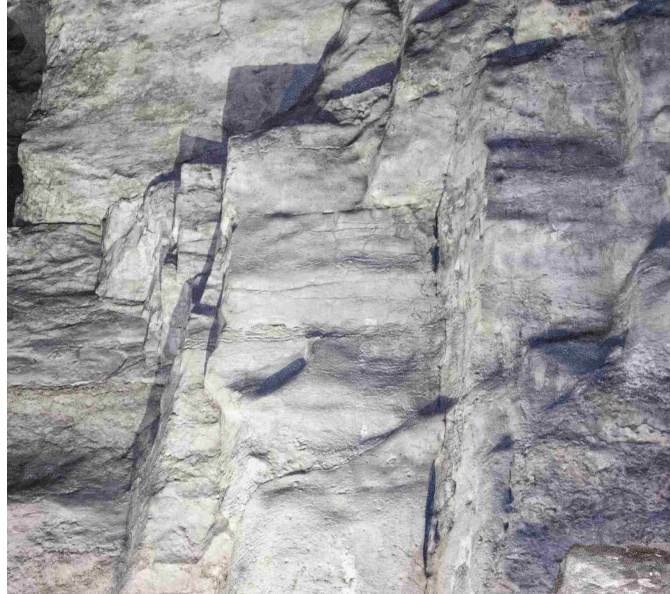


Figure 2.2: Jointed rock in Carlsbad Cavern. Photograph provided by Stephen Bepalko.

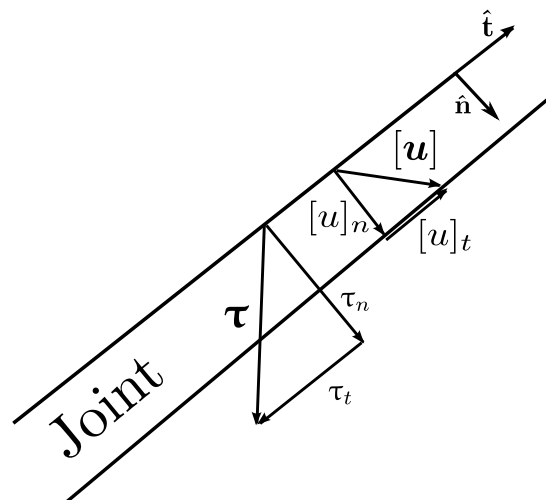


Figure 2.3: The traction  $\boldsymbol{\tau}$  acting on the joint with shear and normal components and the joint discontinuity  $[\boldsymbol{u}]$

The discontinuity  $[\boldsymbol{u}]$  and  $\boldsymbol{\tau}$  represent the relative displacement and traction, respectively, acting on the parent rock faces (Fig 2.3). These vectors have normal and tangential components. The faces of the joint typically exhibit asperities which inhibit shearing motions. Mathematical models typically idealize the joint faces as

planes with the effects of asperities taken into account through a function for shear resistance (Fig 2.4).

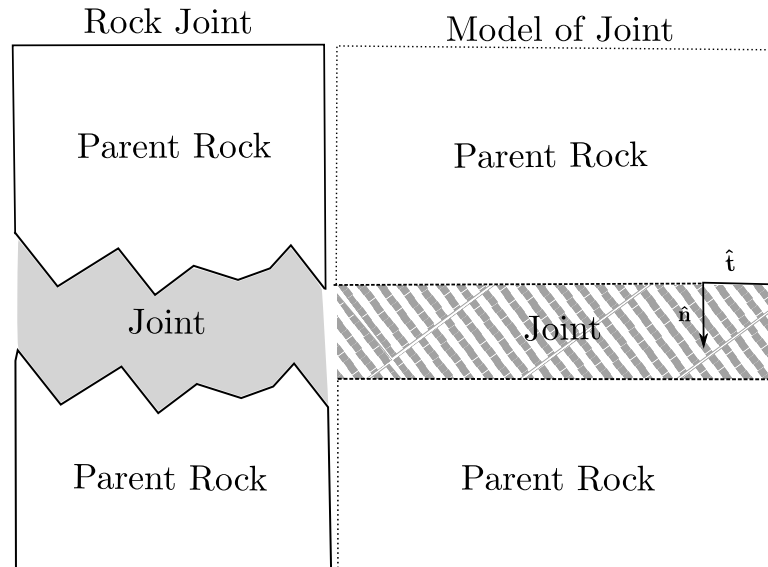


Figure 2.4: Rock joint and its numerical representation

## 2.2 Wave Propagation through Jointed Rock

The problem for the one-dimensional study of rock joint behavior is a compressive wave propagating through a rock joint or joint set oriented normally to the direction of wave travel (Figure 2.5). The study determines the characteristics of the wave after propagating through a joint. The effects of a joint on a compressive wave are energy dissipation, wave reflection, and change of shape. The parent rock, modeled as a linear elastic medium, is assumed to contain either a single joint or sets of joints. The effects of one, two, and three joints on wave propagation are analyzed. For large-scale analyses, it is important to know when two or more joints can be replaced with a single equivalent joint. This issue is also addressed.

The joint compresses as the wave propagates through it. This behavior is called closure since the width of the discontinuity decreases with compressive stress. Closure requires energy, provided by the compressive wave. One result of joint-wave

interaction is the dissipation of energy. The portion of the wave that reflects off the joint travels opposite to the initial direction and becomes a tensile wave. This reflected portion can also be calculated to properly determine the effects of joints. A part of the wave propagates through the joint as a compressive wave.

The amount of energy dissipation is dependent on the joint properties. A weathered joint filled with gouge and mineralization has a resistance to joint closure. Energy is dissipated during closure because the gouge resists closure and does not allow the intact rock faces to come fully into contact. A fresh joint, called a gap, with no relative shear motion closes with no resistance because the asperities of the rock faces line up. All of the energy remains in the parent rock. Some energy reflects off the joint and some passes through the joint if the free surfaces come into contact. Until the two faces of intact rock come into contact, a fresh, unfilled joint acts as a free surface and the wave is reflected.

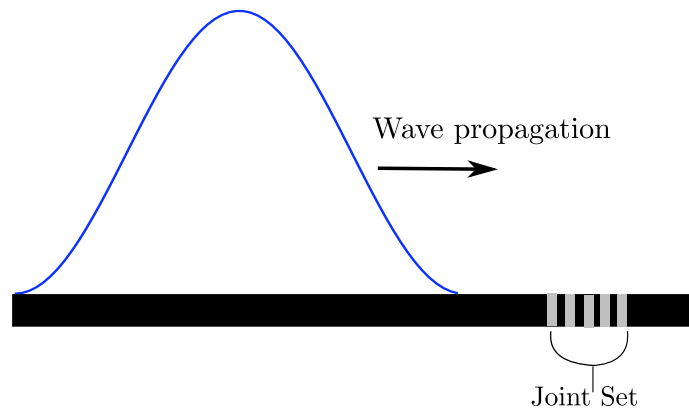


Figure 2.5: Wave propagating towards a joint set

## 2.3 Objective

The research objective is to numerically model the characteristics of wave-joint interaction in jointed rock. The main focus is the proper representation of wave-joint interaction for one-dimensional motion. The features that are studied include the

amount of energy transmitted through a joint, the impulse of the transmitted wave in comparison with the impulse provided by the initial wave, and the reduction of peak stress in an initial wave altered by a joint. Then, the results of modeling several joints sequentially are obtained and compared with modeling the joint set as one equivalent joint.

# Chapter 3

## Literature Survey

Rock is numerically modeled two ways. The first approach is to model individually, or discretely, the behavior of the contiguous rock and the rock material between joints and discontinuities. The second approach models large rock masses at the field scale and incorporates the effect of joints and discontinuities as well as the intact rock into an equivalent continuum (Bazant [2]). Which of the approaches used is largely based on the scale of the problem. Contiguous rock models capture the micromechanics, and large rock mass models capture the phenomenological effects of the contiguous rock and all other structural aspects of rock.

### 3.1 Contiguous Rock Models

Within the scope of the contiguous rock approach, some formulations model the behavior of the intact rock and others model the contact behavior of the contiguous rock blocks.

### 3.1.1 Intact Rock

Classically, intact rock models use a Mohr-Coulomb or a Hoek-Brown failure criterion. The most recent advances use models based on the micromechanics of rock (Bazant [2]). Hoek and Brown considered the uniaxial compressive strength of intact rock and used a largely empirical approach to model rock based on their relation between a rock mass rating and a geological strength index (Jing [11]).

In 2000, Shao and Rudnicki [15] developed a microcrack-based continuous damage model. They modeled brittle geomaterials under a compression dominated stress field. The approach combined micromechanical models with a damage evolution law. But, they only considered the triaxial compression loading path. Another recent advancement is Bazant's microplane model [3], which incorporates the pore collapse of isotropic rock. The model addresses shear-enhanced compaction, a phenomenon where compaction is enhanced as the deviatoric stress is increased. The model is largely based on the microplane model already used for concrete and captures the hardening and softening of porous rock. Fossum and Brannon [7] created a viscoplastic model for rock. Over a broad range of strain rates at laboratory scale, they identified the key features of rock micromechanics to be pore collapse and microcracking. Their idea is that pore collapse and microcracking cause the macroscale transition from volumetric compaction to dilatation under triaxial compression. Their current efforts are focused on applying the micromechanics model to field scale incorporating rock joints. Hu [9] developed an approach for anisotropic plasticity and damage in semi-brittle rocks based on a discrete thermodynamic approach. His approach is that frictional sliding of weakness planes generate macroscopic plastic deformation. The model captures more easily the coupling between anisotropic plasticity and induced damage when compared with classical constitutive models.

These intact rock approaches reflect the micromechanics of rock. One point of concern though is the scalability. Over a large rock mass, the models may not accurately depict the behavior of jointed rock because of its many discontinuous features. Also, these authors do not consider high-rate compressive waves as well as



the possible tensile waves reflected off of free or failed surfaces.

### 3.1.2 Contact Behavior

The models for the contact between intact rock blocks consider either the asperities of each rock surface or a granular fill between the two surfaces. These models indirectly consider joint behavior but do not address joints directly. In 1972, Barton [1] first introduced the Joint Roughness Concept and mathematically used fractals to represent the surface roughness of intact rock blocks. Plesha [14] developed a constitutive model for rock discontinuities with dilatancy and surface degradation. He idealized surface microstructure as interlocking asperity surfaces. The key feature his model addressed was dilatancy. He defined dilatancy as “a tendency of two contacting bodies to separate during relative tangential motion due to the sliding of asperity surfaces of one body on those of another.” The model accounted for asperity wear as a function of high compressive stress. The higher the compressive stress, the quicker asperities would degrade resulting in a loss of strength after the initiation of sliding. Huang’s microstructural constitutive model [10] considered rock surfaces with regular asperities as triangle-shaped teeth. He identified three mechanisms to influence the contact of rock surfaces to be sliding, separation of asperity contact-faces, and shear fracture of asperities. He used a Mohr-Coulomb criterion with a cohesion factor and focused on the properties of individual asperity faces. In 2010, Trivedi [16] proposed a model that considered the contact between rock surfaces to contain granular fill as opposed to the asperities of Plesha’s model. The strength and dilatancy of joints followed the soil mechanics constitutive equations. He identified a relationship between dilatancy and joint strength due to the progressive failure of the granular media.

The contact models effectively predict joint surface sliding for both fresh joints (contacting asperities) and filled joints (granular media). However, they do not address joint closure or wave propagation due to compressive waves. These models cannot be implemented on a large scale because each focuses on such a small scale.

Individual asperities or granular characteristics would not be known for a jointed rock mass of significant size.

## 3.2 Large Rock Mass Models

To model jointed rock on a larger scale, constitutive models are developed based on a homogenization of the rock volume. The mathematical homogenization of the rock mass smears the mechanical properties of joints and intact rock evenly over the volume. Usik Lee [12] outlined a general smeared continuum damage mechanics model based on constitutive equations of damaged material using a micromechanical or phenomenological approach. He homogenizes (or averages) the mesostructural field of defects within a representative volume element (RVE). The micromechanical behavior of the RVE effectively becomes a continuum. Lee points out that most models introduce internal variables to describe damage indirectly and are not always physically interpretable. The basis for his model is the Strain Energy Equivalence Principle (SEEP). According to Lee, the SEEP is “when the damaged material volume cell and its equivalent continuum model have identical displacements on their boundaries, they contain equal strain energy.” Cai and Horii [5] present a model using the same principle applied directly to highly jointed rock masses. They formulate the stress-strain relations of jointed rock masses by taking the volume average of stress and strain within the RVE, where the relative displacement of the joints is required. The mechanical behavior is then represented with an elasto-plastic constitutive law based on classical plasticity theory. The approach calls for determining the RVE, which is quite difficult as presented by Chalhoub [6]. Chalhoub proposes a geometrical approach to determining the RVE rather than a more computationally demanding mechanical approach. He proposes that the mechanical RVE can be determined by analyses carried out on the geometrical parameters of the rock mass. The most important geometrical parameter he identifies is the density of rock joints. The downside is that his approach is based on the assumption that all joints within the RVE have the same mechanical properties. At the 2010 Ground Shock

and Faulted Media Workshop, Brannon [4] outlined her approach for a homogenized rock-joint formulation. The homogenized formulation is aimed at a scale too large to model joints explicitly. Similar to Cai, she proposed an “equivalent continuum.” Her formulation assumed joints to be parallel and evenly spaced.

The smeared continuum approach to jointed rock makes sense for large scale applications. The downside to this approach is the scalability of either the micromechanics or phenomena the formulations predict. The homogenization of the rock volume is based on the assumption that all rock joints have equivalent mechanical and geometrical properties, which may not always be the case for jointed rock. For the purposes of this proposal, joint behavior and its effect on wave propagation cannot be discretely calculated within a smeared representative volume element.

### 3.3 Aperçu

Many jointed rock modeling approaches do not reflect specific constitutive features of joints. Capturing parent rock and joint effects in the same model makes sense for certain applications, especially large-scale computational analysis. But, the models are unable to represent discrete joints for analysis.

In effort to address the current void of rock joint effects in the literature, the objective of this research is to provide a basis for joint-specific constitutive models in a numerical setting. The proposed models aim to capture the features of individual rock joints. Once those features are addressed, computational analysis can ascertain the impact of rock joints within the scope of numerical geomechanics.

The most closely related work to the proposed approach is Wang’s joint model [17]. Wang used a classical plasticity formulation for a rock joint of thickness approaching zero. He modeled joint closure and normal loading. His approach is not directly applicable to the scope of this research because a joint in the proposed research context is considered to have a thickness and possibly gouge between the parent rock faces.

## Chapter 4

# One-Dimensional Constitutive Models for Joints

The term “joint” will be used to describe a discontinuity of the parent rock that has some resistance to closure of the discontinuity. A joint is physically understood as a rock with fractures that have weathered and accumulated gouge and mineralization between the two parent rock faces defining each fracture. This accumulated material provides resistance if the fracture is compressed. The term “gap” will be used to describe a discontinuity of the parent rock that has no resistance to closure. A gap is a fresh rock fracture that has had no shearing motion. Therefore, the parent rock faces of a gap can come into contact with no resistance to closure.

The subsequent sections of this chapter outline the formulation for the 1D joint models. Experimental data are provided with the development of the 1D model.

### 4.1 1D Joint Modeling Formulation

This section outlines the model for handling joint closure and opening in which only the component of traction in the normal direction is considered.

To begin, consider a linear elastic bar of rock material. Along the bar is an existing

discontinuity of known initial length  $u_{g0}$ .  $u_g$  is defined to be the discontinuity length at a certain time. Prior to any deformation,  $u_g = u_{g0}$ . This existing discontinuity is a joint composed of gouge, which is sediment and mineral particles that coalesced within the crack after its initial formation. The joint has strength in compression and no strength in tension. First, nondimensionalize the length of the discontinuity  $u_{g0}$  by proposing  $\bar{u}_g = \frac{u_g}{u_{g0}}$ . In further discussion,  $\bar{u}_g$  will be referred to as the dimensionless discontinuity size. If the joint has opened beyond its initial size  $u_{g0}$ , then  $\bar{u}_g > 1$  and the process is joint opening. If the joint has closed from its initial size  $u_{g0}$ , then  $\bar{u}_g < 1$  and the process is joint closure. At this point in the discussion, no loading has been applied to the joint and neither joint closure nor opening has occurred. Therefore,  $\bar{u}_g$  has an initial dimensionless value of 1. A function  $F(\sigma_{el}, \bar{u}_g)$  is defined later to identify the state of joint closure, where  $\sigma_{el}$  is the stress. A joint “hardening” function  $g(\bar{u}_g)$  relates joint closure to stress. This function has parameters that will be given values to match experimental data for normal loading of joints. The joint function is chosen to be of the form

$$F = -\sigma_{el} + g(\bar{u}_g). \quad (4.1)$$

If  $F < 0$ , no joint closure occurs. If  $F = 0$ , the joint may close. And,  $F > 0$  is not allowed. A distinction must be made in regimes of joint closure or joint opening. As noted earlier, joints resist compression but have no strength in tension.

### 4.1.1 Joint Closure

The state of joint closure is governed by the joint function  $F(\sigma_{el}, \bar{u}_g)$  as defined in Equation (4.1). The “hardening” function is chosen to be of the form

$$g(\bar{u}_g) = \sigma_g \left( 1 - \frac{1}{\bar{u}_g^m} \right) e^{\bar{u}_g^m}, \quad (4.2)$$

where  $\sigma_g$  is a material-based parameter with dimensions of stress and  $m$  is another material based dimensionless parameter. Such a form gives qualitative joint closure characteristics consistent with experimental data for a granular filled joint (Li and Ma [13]). Assume the joint is at its initial state prior to any loading. For a given

increment in joint closure  $\Delta \bar{u}_g < 0$ ,  $\bar{u}_g < 1$ . The stress in the joint is  $\sigma_{joint} = g(\bar{u}_g)$ . Figure 4.1 shows the characteristics of the joint closure function  $g(\bar{u}_g)$ . Li and Ma's publication will be used to calibrate the constitutive model to their published data. The important difference between joint and gap behavior is that the joint "hardening" function for a gap is

$$g(\bar{u}_g) = 0. \quad (4.3)$$

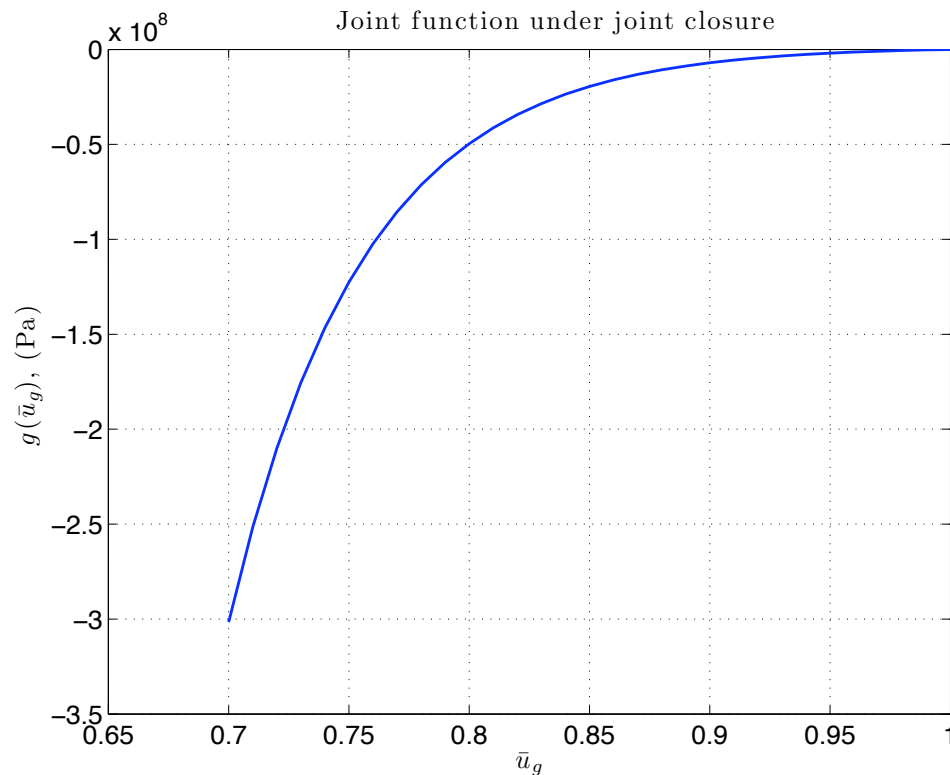


Figure 4.1: The joint "hardening" function  $g(\bar{u}_g)$  when  $\bar{u}_g \leq 1$

An investigation was conducted to illustrate the effects of different values of  $m$  in the joint closure function  $g(\bar{u}_g)$ . In Figure 4.2, various values of  $m$  are prescribed to show the effect of the characteristic material parameter on the shape of  $g(\bar{u}_g)$ . The importance of this investigation is to demonstrate that as the value of  $m$  grows larger, the joint will have less resistance to closure. The parameter  $m$  can be used to better match the constitutive model predictions to experimental data.

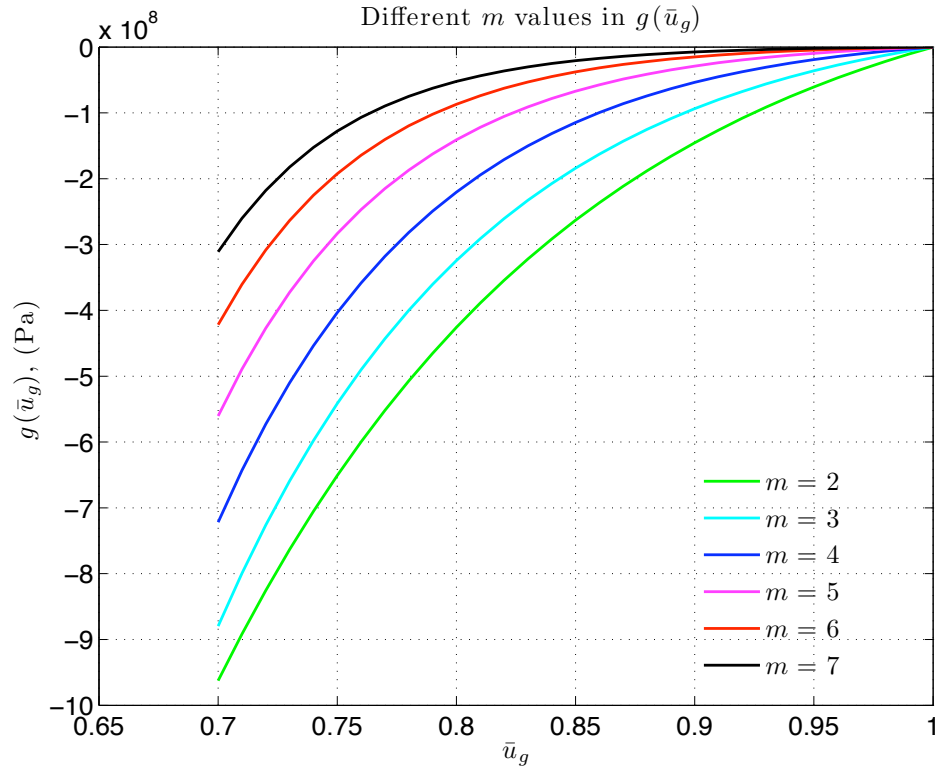


Figure 4.2: Impact of  $m$  on the shape of the joint “hardening” function  $g(\bar{u}_g)$

### 4.1.2 Joint Opening

Joint opening is simpler than joint closure because the experimental data suggest joints do not have any tensile strength. When a joint is put under a tensile load from a zero stress state, the load cannot be sustained and the joint will immediately open up. The need for a decohesion function is unnecessary whenever a tensile load is applied from a zero stress state. The joint will open up immediately and have zero stress. Suppose a joint is again at its initial size  $u_{g0}$  and a tensile load is applied. Figure 4.3 illustrates this process and relates  $\bar{u}_g$  to the stress  $\sigma$ , at the gap. The notion that rock joints have zero tensile strength does not appear plausible intuitively. However, the joint gouge between fractured rock faces is a granular media. Granular media do have zero tensile strength. Yet, jointed rock can allow for tensile waves to propagate through in physical testing. The hypothesis for this phenomenon is that there is an “in situ” stress consisting of confining pressure so that rock joints

do not simply open up during underground wave propagation. Further investigation needs to be done in a 2D or 3D implementation to test this hypothesis, which is beyond the scope of the proposed research.

Consider a joint under a compressive load that has intact rock on either side of its plane of discontinuity. The numerical implementation of a joint spreads its effect over a portion of the parent rock containing the joint, so the intact rock must also be considered. If a positive (tensile) increment in strain is applied from a compressive state, the magnitude of the strain increment matters. If the strain increment is large enough that the intact rock returns to zero strain and the joint returns to its initial joint size  $u_{g0}$ , the element containing the joint will have zero stress. If the strain increment is not large enough to unload the joint and intact rock to a zero stress state, then the joint closure routine will be followed with a positive strain increment.

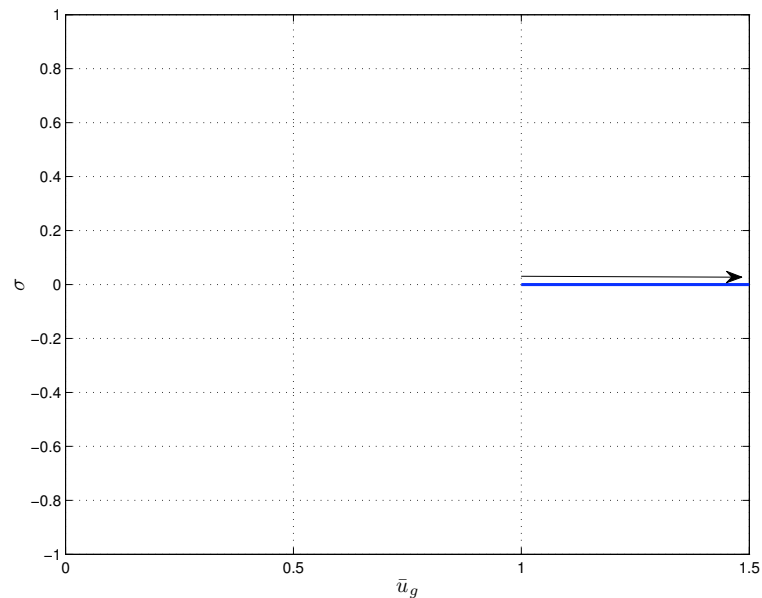


Figure 4.3: Joint with prescribed positive strain increments



## 4.2 Numerical Implementation of 1D Joint Model

Begin by considering a material point with a domain of length  $h$ . The material point has an elastic region and a joint discontinuity of initial size  $u_{g0}$ , where  $u_{g0} \ll h$ . Within the material point domain, there is a continuous stress ( $\sigma_{el}$ ) in the elastic region and joint. There is both an elastic strain ( $\varepsilon_{el}$ ) and a joint strain ( $\varepsilon_g$ ). The elastic region has a Young's Modulus of  $Y$ . To describe the strain over the domain in consideration, there is also a total strain  $\varepsilon_{tot}$ . The total strain and total strain increments are given by

$$\varepsilon_{tot} = \varepsilon_{el} + \varepsilon_g \quad (4.4)$$

$$\Delta\varepsilon_{tot} = \Delta\varepsilon_{el} + \Delta\varepsilon_g. \quad (4.5)$$

Every time step gives an increment in strain ( $\Delta\varepsilon_{tot}$ ) at the material point under consideration. For the purpose of explaining the numerical implementation, the current time step is the  $k$ -th time step. The state of stress and strain of the material point is known at the  $k$ -th time step. The numerical implementation will determine the state of stress and strain at the material point at the  $(k+1)$ -th time step, the next time step. Therefore, stress and strain values with an superscript  $k$  denote the values at the current time step and values with an superscript  $k+1$  denote the values at the next time step. Also, the joint will be non-dimensionalized as shown earlier, where  $\bar{u}_g^k = \frac{u_g^k}{u_{g0}}$ .

Given the basic description of joint behavior under normal loading in 1D, the numerical implementation of the joint model is detailed. The implementation for the model is based upon the following premises:

- (a) Every joint is contained within an element of length  $h$ . The element has nodal displacements  $u_2$  and  $u_1$ . The total strain across the element is  $\varepsilon_{tot} = \frac{u_2 - u_1}{h}$ .
- (b) Every joint starts with an initial discontinuity size  $u_{g0}$ . Under no loading, a material point (or element using one material point per element) with a joint has an associated strain due to the joint size. Therefore, the total strain across

the material point domain is  $\varepsilon_{tot} = \frac{u_{g0}}{h}$ , where  $h$  is the material point (element) domain length. The material point also has an equal initial joint strain  $\varepsilon_g = \frac{u_{g0}}{h}$ .

- (c) During joint closure, the hardening function  $g(\bar{u}_g)$  is followed.
- (d) During joint opening, the joint assumes no stress and simply opens up for a given strain increment.
- (e) In the context of numerical modeling within the MPM, the stress within the joint must be equal to that of the stress over the rest of the material point domain, which is intact rock.

### 4.2.1 Joint Closure

For the material point under consideration at time  $t^k$ , suppose an increment in total strain  $\Delta\varepsilon_{tot}^k$  is negative and that the material point's domain was already under a compressive load. Therefore, the material point would stay under a compressive load and the joint would close further. To begin, assume that the full increment of total strain is added to the elastic strain. If the increment in strain is fully specified to the elastic strain, then the joint strain and the joint size stay the same as the previous time step. The trial strain increments are as follows:

$$\varepsilon_{el}^{k+1} = \varepsilon_{el}^k + \Delta\varepsilon_{tot}^k \quad (4.6)$$

$$\varepsilon_g^{k+1} = \varepsilon_g^k \quad (4.7)$$

$$\bar{u}_g^{k+1} = \bar{u}_g^k. \quad (4.8)$$

These values for strains are used for the first iteration of the Newton-Raphson scheme to solve for the joint discontinuity over the material point domain. With the proposed strains, the stresses are found using either an elastic assumption or the joint closure function  $g(\bar{u}_g)$ .

$$\sigma_{el}^{k+1} = Y\varepsilon_{el}^{k+1} \quad (4.9)$$

$$\sigma_{joint}^{k+1} = g(\bar{u}_g^{k+1}) \quad (4.10)$$

The decohesion function  $F(\sigma_{el}, \bar{u}_g)$  is then calculated as follows:

$$F = -\sigma_{el}^{k+1} + g(\bar{u}_g^{k+1}). \quad (4.11)$$

The stresses in the elastic and joint regions will not be equal.  $-\sigma_{el}^{k+1}$  will be greater than  $g(\bar{u}_g^{k+1})$ , resulting in  $F$  being greater than zero. Now, the joint is allowed to close in a procedure that forces  $F$  to zero. In the implementation, requiring  $F$  to be zero is too strict for a reasonable number of iterations. The actual requirement becomes that of enforcing  $F$  to be a very small positive number  $\varepsilon$ . This ensures that the stresses in the elastic region and joint regions will be equal. Given the current values of  $\sigma_{el}^{k+1}$  and  $\sigma_g^{k+1}$ ,  $F$  will be positive. To find the values of  $\sigma_{el}^{k+1}$  and  $\bar{u}_g^{k+1}$  for which  $F$  is zero requires the Newton-Raphson scheme. Following the Newton-Raphson scheme, the derivatives of  $g(\bar{u}_g^{k+1})$  and  $\sigma_{el}^{k+1}$  are found to give  $\dot{F}$ .

$$\frac{\partial g^{k+1}}{\partial \bar{u}_g^{k+1}} = \frac{\sigma_g m}{e^{\bar{u}_g^{k+1} m} (\bar{u}_g^{k+1})^{(m+1)} (\bar{u}_g^{k+1})^{(m+1)}} \quad (4.12)$$

$$\frac{\partial \sigma_{el}^{k+1}}{\partial \varepsilon_{el}^{k+1}} = -Y \quad (4.13)$$

$$\dot{F} = -\frac{\partial \sigma_{el}^{k+1}}{\partial \varepsilon_{el}^{k+1}} \varepsilon_{el}^{k+1} + \frac{\partial g(\bar{u}_g^{k+1})}{\partial \bar{u}_g} \dot{\bar{u}}_g \quad (4.14)$$

Using (4.14),  $\bar{u}_g^{k+1}$  is updated by

$$\Delta \bar{u}_g^{k+1} = -\frac{F}{\dot{F}} \quad (4.15)$$

$$\bar{u}_g^{k+1} = \bar{u}_g^{k+1} + \Delta \bar{u}_g^{k+1}. \quad (4.16)$$

For the new value of  $\bar{u}_g^{k+1}$ , a new gap strain is found by

$$\varepsilon_g^{k+1} = \frac{\bar{u}_g^{k+1} u_{g0}}{h}. \quad (4.17)$$

And, with a new value of gap strain, comes a new value in elastic strain.

$$\varepsilon_{el}^{k+1} = \varepsilon_{tot}^{k+1} - \varepsilon_g^{k+1} \quad (4.18)$$

Using these new values of strain, the process can be repeated, whereby the stresses in the elastic region and the joint region are found. Given a new value of  $F$ , if  $F$  does not meet the requirement of having a value less than a small positive number,

the process of using the Newton-Raphson scheme is repeated until  $F$  does meet the requirement. The corresponding values for  $\varepsilon_g^{k+1}$  and  $\varepsilon_{el}^{k+1}$  become the strains associated with the material point at time  $t^{k+1}$  once the Newton-Raphson scheme is complete.

### 4.2.2 Joint Opening

For the material point under consideration at time  $t^k$ , suppose an increment in total strain  $\Delta\varepsilon_{tot}^k$  is positive and that the material point's only strain comes from the joint discontinuity. Therefore,  $\varepsilon_{tot}^k = \varepsilon_g^k = \frac{u_{g0}}{h}$  and  $\varepsilon_{el}^k = 0$ . Because joints cannot withstand any tensile loading, the stress across the material point will be initially discontinuous and must be resolved. The elastic region of the material point's domain will have zero stress because all of the strain increment is automatically put onto the joint and the stress is continuous. In summary, given a positive total strain increment from an initial zero stress, all strain will be applied to the jointed region of the material point.

$$\varepsilon_{tot}^{k+1} = \varepsilon_{tot}^k + \Delta\varepsilon_{tot}^k \quad (4.19)$$

$$\varepsilon_{el}^{k+1} = 0 \quad (4.20)$$

$$\varepsilon_g^{k+1} = \varepsilon_g^k + \Delta\varepsilon_{tot}^k \quad (4.21)$$

### 4.2.3 Other loading scenarios and summary

Consideration must be given to the loading scenario where a joint is in compression and a positive strain increment is prescribed at time  $t^{k+1}$ . Assume the total prescribed increment in strain  $\Delta\varepsilon_{tot}^{k+1}$  has a large enough magnitude that when initially prescribed to the elastic region  $\varepsilon_{el}^{k+1}$  is greater than zero (under tension). This could satisfy the condition that  $F \leq 0$  but there would be a discontinuity in stress between the elastic and joint regions of the material point. Therefore, a check is performed at the end of the Newton-Raphson scheme to check if  $\sigma^{k+1} = Y\varepsilon_{el}^{k+1} > 0$ . Assuming

$\sigma^{k+1} > 0$ , the strains are modified as follows:

$$\varepsilon_g^{k+1} = \varepsilon_g^{k+1} + \varepsilon_{el}^{k+1} \geq \frac{u_{g0}}{h} \quad (4.22)$$

$$\varepsilon_{el}^{k+1} = 0 \quad (4.23)$$

$$\sigma^{k+1} = 0. \quad (4.24)$$

#### 4.2.4 Results of Driver Program for 1D Joint Model

A driver program was used to prescribe increments in strain for a joint and its associated elastic region. A load-unload-load path was prescribed to demonstrate how the model deals with unloading. The results of the run are shown in Figure 4.4.

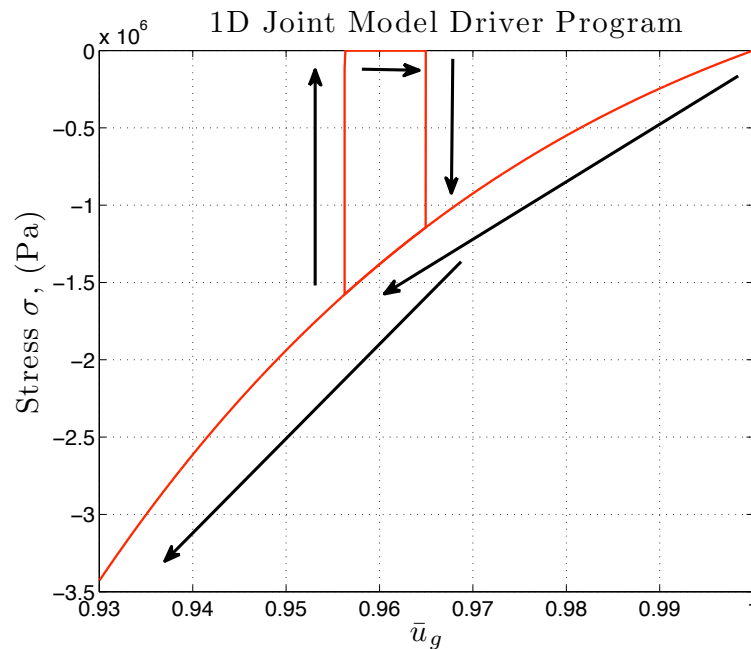


Figure 4.4: Stress as a function of displacement discontinuity for a joint going through a load-unload-load cycle.

The results demonstrate that the joint constitutive model unloads vertically, as outlined in Section 4.2.2. The physical meaning is that all of the joint deformation is plastic deformation. The joint unloads vertically from the value of stress when the

function  $F = 0$  and then loads vertically back to the value of stress when  $F = 0$ . During unloading, all of the positive strain increments ( $\Delta\varepsilon_{tot}$ ) are allocated to the strain ( $\Delta\varepsilon_{el}$ ) of the elastic region.

### 4.3 Gap Constitutive Model

A gap is a discontinuity in displacement with no resistance to closure. A gap is simply a joint that has not had any coalescence of gouge or mineralization to resist closure back to its initial state prior to the initial fracturing. For one-dimension, with no resistance to closure or opening, a gap simply closes or opens based on the the increment in strain  $\Delta\varepsilon_{tot}^{k+1}$ .

To simplify the explanation of the implementation of the gap constitutive model, consider the parameters used to describe the behavior of a joint in Section 4.1. The gap has an initial size  $u_{g0}$ . A dimensionless gap size describes the gap at a time  $t^k$  as  $\bar{u}_g^k = \frac{u_g^k}{u_{g0}}$ . The initial total strain in the gap is  $\varepsilon_g^0 = \frac{u_{g0}}{h}$ , where  $h$  is the element size that the gap is in. The total strain in the element  $\varepsilon_{tot}^k$  is the sum of the gap strain and elastic strain ( $\varepsilon_g^k + \varepsilon_{el}^k$ ). A decohesion function  $F$  governs the gap and is the same as the function used in a joint (Equation 4.1). The difference is the “hardening” function  $g(\bar{u}_g)$  for a gap is

$$g(\bar{u}_g) = 0. \quad (4.25)$$

The modification to the “hardening” function is the only difference between a joint and a gap. The formulation and numerical implementation is otherwise identical to the joint formulation show in Sections 4.1 and 4.2.

#### 4.3.1 Results of Driver Program for 1D Gap Model

The gap constitutive model was used through the same load-unload-load cycle in Figure 4.4. The gap cannot sustain any load whether in tension or compression (Fig

4.5). The different legs of the loading path overlap because until the gap fully closes, it cannot withstand any load.

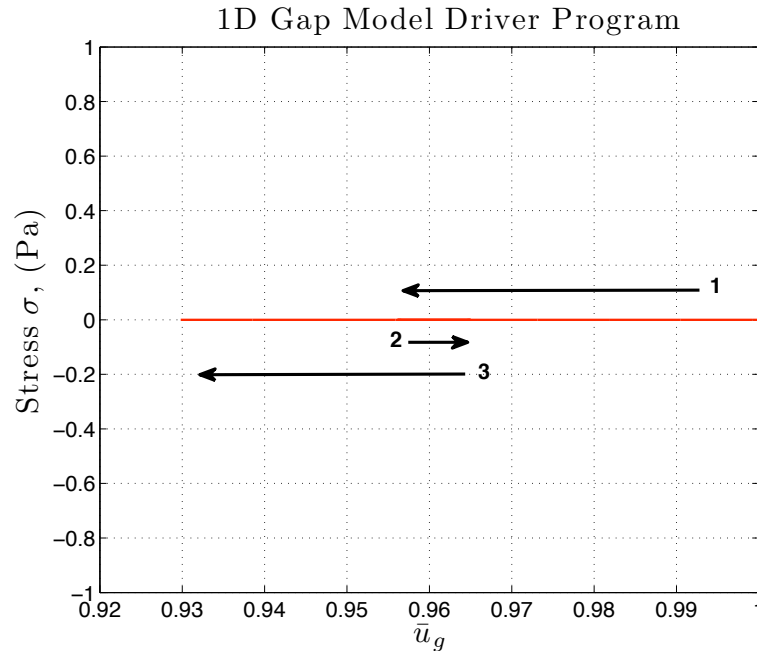


Figure 4.5: Driver program results, gap going through load-unload-load cycle, the first leg is labeled 1, second leg 2, third leg 3

## 4.4 1D Joint Model with Plasticity and Linear Elasticity

The 1D Joint Model of Section 4.1 is altered to allow for a portion of joint closure to be associated with linear elasticity. For a joint without linear elasticity, the dimensionless joint size  $\bar{u}_g$  closes along the “hardening” function  $g(\bar{u}_g)$  and unloads vertically. All of the initial strain increment  $\Delta\epsilon_{tot}^k$  at time  $t^k$  is first allocated to the elastic region of the element with which the joint is associated. With the decohesion function (4.1), the constraints on the decohesion function are not violated when the total increment in strain is allocated to the elastic region of the joint. This constitutive algorithm represents a plastic joint. Its formulation will be modified to create a constitutive algorithm for an elastic-plastic joint.

Based on the formulation of the 1D joint model, consider an initial joint discontinuity  $u_{g0}$  within an element of length  $h$ . The element also has a linearly elastic continuum of length  $h_c = h - u_{g0}$ . At time  $t^k$ , the continuum portion of the element has a strain  $\varepsilon_c$  and the joint has a current discontinuity of length  $u_g^k$ . The stress in the element is  $\sigma^k = E_c \varepsilon_c^k$  and continuity of the stress across the element  $\sigma^k$  is maintained.  $E_c$  is the modulus of elasticity for the the continuum portion of the element. In other words, the stress at the joint is also  $\sigma^k$ . The kinematic condition for strain across the element is

$$\varepsilon_{tot}^k h = \varepsilon_c^k h_c + \varepsilon_g^k u_{g0}. \quad (4.26)$$

The strains are defined as

$$\varepsilon_g^k = \frac{u_g^k}{u_{g0}} \quad (4.27)$$

$$\varepsilon_c^k = \frac{h_c - u_c^k}{h_c}, \quad (4.28)$$

where  $u_c^k$  is the amount of displacement that has occurred within the linearly elastic continuum portion of the element.

For the next time step, an increment in total strain  $\Delta \varepsilon_{tot}^{k+1}$  is prescribed. The increment in total strain in terms of an increment in displacement  $\Delta u_{tot}^{k+1}$  and the length of the element  $h$  is

$$\varepsilon_{tot}^{k+1} = \frac{\Delta u_{tot}^{k+1}}{h}. \quad (4.29)$$

The total strain increment is a sum of the increment in continuum strain as well as joint strain (4.30).

$$\Delta \varepsilon_{tot}^{k+1} = \frac{\Delta \varepsilon_c^{k+1} h_c + \Delta \varepsilon_g^{k+1} u_{g0}}{h} \quad (4.30)$$

Assume a linearly elastic constitutive relation for both the continuum and the joint. The modulus of elasticity of the joint  $E_g$  is not necessarily equal to the modulus of elasticity of the continuum  $E_c$ . To maintain continuity of stress, the following is enforced

$$\Delta \sigma = E_c \Delta \varepsilon_c^{k+1} = E_g \Delta \varepsilon_g^{k+1}. \quad (4.31)$$



Propose a dimensionless parameter  $\alpha_g$  derived from (4.30) and (4.31), where

$$\Delta \varepsilon_g^{k+1} = \frac{\Delta \varepsilon_{tot}^{k+1} h}{(1 + \alpha_g) u_{g0}}. \quad (4.32)$$

$\alpha_g$  expresses the strain in the continuum as,

$$\begin{aligned} \Delta \varepsilon_c^{k+1} &= \alpha_g \frac{\Delta \varepsilon_g^{k+1} u_{g0}}{h_c} \\ &= \frac{\alpha_g}{1 + \alpha_g} \frac{\Delta \varepsilon_{tot}^{k+1} h}{h_c}. \end{aligned} \quad (4.33)$$

From Equations (4.31), (4.32), and (4.33), the dimensionless parameter  $\alpha_g$  is,

$$\alpha_g = \frac{E_g h_c}{E_c u_{g0}}. \quad (4.34)$$

Propose an effective modulus  $E^*$  for the entirety of the element, such that  $\Delta \sigma = E^* \Delta \varepsilon_{tot}^{k+1}$ . To find  $E^*$ , solve the stress continuity equation of  $\Delta \sigma$  for the entire element and the continuum.

$$E^* \Delta \varepsilon_{tot}^{k+1} = E_c \Delta \varepsilon_c^{k+1} \quad (4.35)$$

Substitute (4.33) into (4.35) and solve for  $E^*$ . The expression for  $E^*$  is,

$$E^* = \frac{\alpha_g}{1 + \alpha_g} \frac{h}{h_c} E_c. \quad (4.36)$$

#### 4.4.1 Numerical Implementation of the Elastic-Plastic Joint Model

To implement the elastic-plastic joint model, the process is almost the same as that of the plastic-only joint model implementation in Section 4.2. The difference is that before calculating the value of the decohesion  $F$  function, the trial increments in strain for both the joint and the continuum regions are calculated. This differs from the fully plastic joint, where the total increment in strain is initially allocated to the elastic region. Assume an increment in total strain  $\Delta \varepsilon_{tot}^{k+1}$  is prescribed at time  $t^{k+1}$ . First, the equivalent modulus of elasticity is calculated following (4.36). The equivalent modulus  $E^*$  is then used from this point forward as the modulus of

elasticity  $Y$  used in Section 4.2. The term  $\alpha_g$  is calculated following (4.34). The trial increments in strain for the joint and the continuum region are

$$\Delta \boldsymbol{\varepsilon}_g^{k+1} = \frac{1}{1 + \alpha_g} \Delta \boldsymbol{\varepsilon}_{tot}^{k+1}, \quad (4.37)$$

$$\Delta \boldsymbol{\varepsilon}_c^{k+1} = \frac{\alpha_g}{1 + \alpha_g} \Delta \boldsymbol{\varepsilon}_{tot}^{k+1}. \quad (4.38)$$

With these as the trial increments in strain, the  $F$  function is calculated and the Newton-Raphson solver is followed if necessary just as outlined in Section 4.2. The modulus of elasticity used for the Newton-Raphson solver is  $E^*$ .

#### 4.4.2 Calculation of $E_g$

The modulus of elasticity for the joint can be allowed to vary with closure or be held constant. This is an option specifically implemented so as to better match the experimental data. Non-linear elasticity has been allowed but won't be presented.  $E_g$  can be a constant prescribed initially as a function of the joint function  $g(\bar{u}_{g,pres})$ , where  $\bar{u}_{g,pres}$  is a prescribed value of  $\bar{u}_g$ . Then,  $E_g$  is

$$E_g = \frac{\partial g(\bar{u}_{g,pres})}{\partial \bar{u}_{g,pres}}. \quad (4.39)$$

Another possibility, in holding  $E_g$  constant is setting it to the modulus of elasticity for the continuum.

$$E_g = E_c \quad (4.40)$$

The reasoning is that the elastic behavior of a joint composed of fractured parent rock particulate would have the same elastic behavior as the parent rock.

Also,  $E_g$  can be calculated to change through joint deformation based on the minimum joint size reached. As a joint closes, the minimum value of  $\bar{u}_g$  is captured as  $\bar{u}_{g,min}$ . The joint modulus is calculated as

$$E_g = b \frac{\partial g(\bar{u}_{g,min})}{\partial \bar{u}_{g,min}}. \quad (4.41)$$

$b$  is a non-dimensional factor that can be used to better fit experimental data and ensure that both elastic and plastic closure is occurring. If the joint was to unload, then  $E_g$  would be held constant during unloading. After the joint then has been closed again past  $\bar{u}_{g,min}$ ,  $E_g$  would change.

### 4.4.3 Results of Driver Program for 1D Elastic-Plastic Joint Model

A driver program was used to prescribe increments in strain for a joint and its associated elastic region. A load-unload-load routine was prescribed to demonstrate how the elastic-plastic model unloads. The results of the run are shown in Figure 4.6.

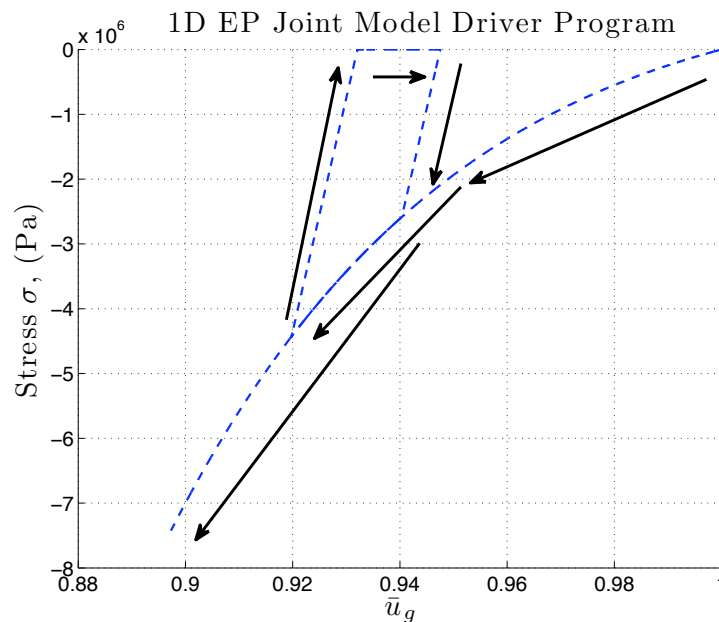


Figure 4.6: Driver program results for an elastic-plastic joint going through a load-unload-load cycle.

The results demonstrate that the elastic-plastic joint unloads linear elastically. The physical meaning is that as the joint closes both elastic and plastic deformation occurs. Elastic unloading will occur within the joint because of the equivalent mod-

ulus  $E^*$ . For the second load cycle, once the deformation causes  $F$  to increase to the value  $F = 0$ , then elastic-plastic deformation will resume. The elastic unloading is the reason for the difference between the elastic-plastic joint model and the joint model shown in Figure 4.4.

## 4.5 Experimental Validation of 1D Joint Model

The parameters used in the constitutive model have been chosen based on experimental data from a published experimental study of wave propagation across a filled rock joint (Li and Ma [13]). The authors used a Split-Hopkinson bar with a granular-filled joint between the incident and transmission bars confined by a PVC sleeve. The experimental set up is shown in Figure 4.7. The properties of the incident and transmission bars are a Young's modulus of 60 GPa, a density  $\rho$  of  $2650 \frac{\text{kg}}{\text{m}^3}$ , length  $L$  of 2 m, and a diameter of 50 mm. The material properties will be used in subsequent numerical simulations.

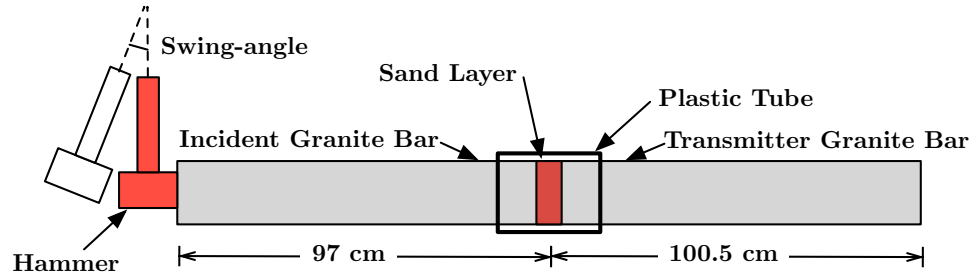


Figure 4.7: Experimental configuration

Using different hammer swing angles, Li and Ma found the stress-strain data lies on the same curve regardless of swing angle. The curve fit provided by the experimentalists is shown in Figure 4.8.

The developed constitutive model coincides with experimental data for a closure function  $g(\bar{u}_g)$  of the form:

$$g(\bar{u}_g) = \sigma_g \left( 1 - \frac{1}{\bar{u}_g^m} \right) (e^{-\bar{u}_g^m}). \quad (4.42)$$

The parameters  $\sigma_g$  and  $m$  best fit at values of 3.75 Gpa and 7.1, respectively. Using a driver program prescribing strain increments, the stress-strain curve was recreated with the constitutive model (Fig 4.8).

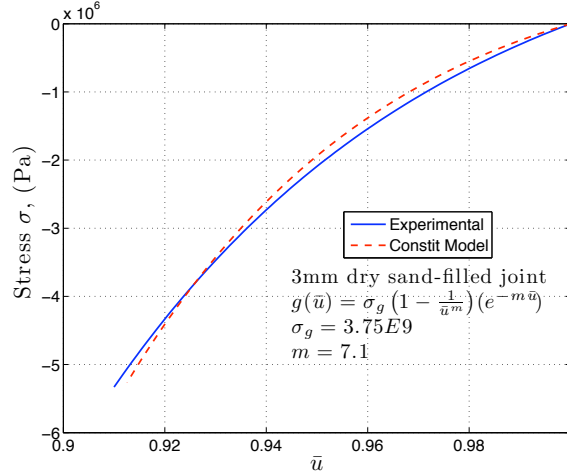


Figure 4.8: Driver output

These values of  $\sigma_g$  and  $m$  are used in the subsequent studies of joints with strength in closure. The experimental data do not give an indication of the joint behavior during unloading, so it is assumed that a joint could be modeled accurately with either an elastic-plastic model (linear joint unloading) or a fully plastic model (vertical joint unloading).

## 4.6 MPM Code, Gap Model, and Analytical Solution

Each of the three different constitutive models has been implemented into a one-dimensional Material Point Method (MPM) dynamic code. The studies conducted on these different models use the same code. To test the code and gap model, a one-dimensional solution was found for a bar with a gap in the middle. The bar is initially at rest with zero initial stress. The problem set up is that shown in Figure 4.9. A single gap exists at the middle of the bar, and the gap has an initial

discontinuity of  $u_0$ . A sinusoidal velocity  $v(t)$  is prescribed at the left boundary. The assumed function is

$$v(t) = \frac{v_{max}}{2} \left( 1 - \cos\left(\frac{2\pi t}{t_{wave}}\right) \right) \text{H}[t_{wave} - t] \text{H}[t]. \quad (4.43)$$

$\text{H}[t]$  denotes a Heaviside function.  $t_{wave}$  is the time span of the pulse, and  $v_{max}$  is the peak particle velocity of the pulse. The function has zero derivative at  $t = 0$  and  $t = t_{wave}$ . This “smoothness” tends to reduce numerical error.

For the run, a gap of initial discontinuity  $u_0 = 3\text{mm}$  was chosen. The peak particle velocity  $v_{max}$  is  $1\text{m/s}$ . The time span of the wave  $t_{wave} = 2.1\text{e}-4\text{s}$  (or  $1/2$  the length of time for a wave front to travel from one end of the bar to the other). The bar is discretized using 50 elements and one material point per element.

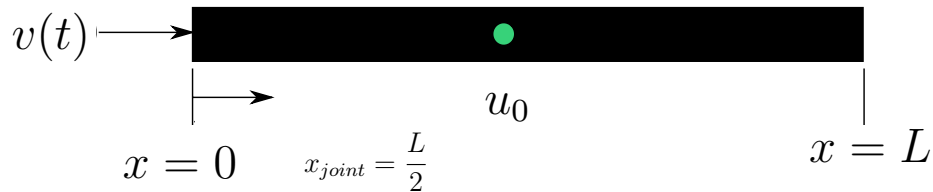
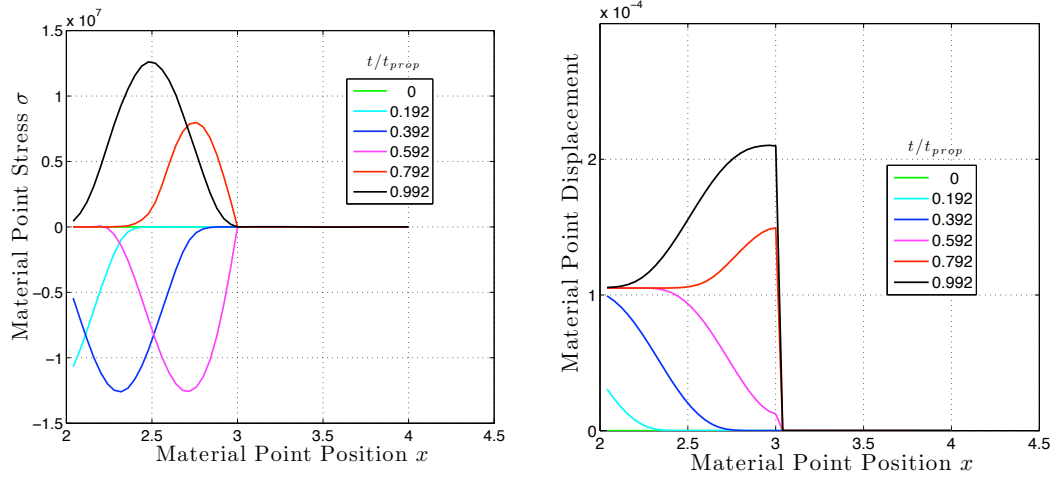


Figure 4.9: Verification run where the green dot represents a gap in the middle of the bar.

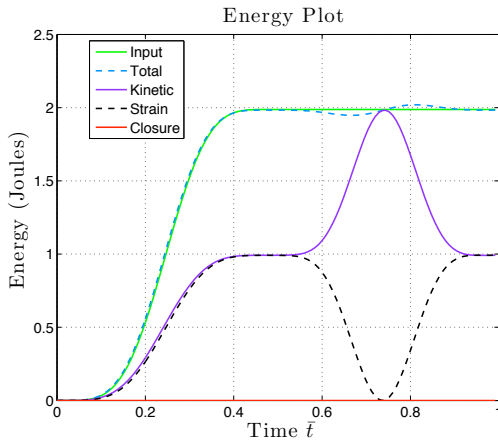
### 4.6.1 Gap Model Analysis

The behavior of a gap should be full wave reflection until total closure occurs. Until the gap width reduces to 0, none of the pulse should propagate past the gap. The gap behaves as a free surface because it has no resistance to closure (Fig 4.10(a)).



(a) Material Point Stress

(b) Material Point Displacement



(c) Energy in Bar

Figure 4.10: Response of the bar due to a velocity pulse as defined in Equation (4.43). Figure 4.10(a) is a plot of stress as a function of  $x$  for various times. Figure 4.10(b) is a plot of displacement as a function of  $x$  for various times. Figure 4.10(c) is a plot of various measures of energy as a function of time.

No displacement occurs at material points located beyond the joint because none of the wave propagates through (Fig 4.10(b)). The energy in the bar does not decrease because a gap has no resistance to closure so no energy is dissipated during closure (Fig 4.10(c)). Referring to the legend of Figure 4.10(c), the input energy is the energy introduced into the bar by the velocity boundary condition. The strain energy is the elastic energy in the material point summed along the bar, including the elastic energy in the parent rock for the region associated with the gap. The

kinetic energy is calculated using the velocity of each material point. The closure energy is the energy dissipated at the gap due to the a resistance to closure and is zero. The results in Figure 4.10 substantiate the intuitive behavior of the gap constitutive model, discussed below.

### 4.6.2 Analytical Solution to Determine Closure Potential

The analytical solution to a contiguous elastic bar is used to determine the maximum displacement that will occur for a sinusoidal wave reflecting off a free surface of a one-dimensional bar. This maximum displacement is then compared to the maximum closure of a gap having the same sinusoidal wave reflection. The gap closes the same amount as the motion of the free surface if the initial gap is large enough.

The governing partial differential equation to the one-dimensional elastic bar problem without body forces is

$$(Y u_{,x})_{,x} = \rho u_{,tt}. \quad (4.44)$$

The analytical solution to Equation (4.44) for the problem set up shown in Figure 4.9 (ignoring the gap) is

$$\begin{aligned} u(x, t) = & v_{max} \left\{ \left( t - \frac{x}{c} \right) - \frac{1}{\omega} \sin \left( \omega \left( t - \frac{x}{c} \right) \right) \right\} \left\{ H \left[ t - \frac{x}{c} \right] - H \left[ t - \frac{2\pi}{\omega} - \frac{x}{c} \right] \right\} \\ & + v_{max} \left\{ \left( t + \frac{x}{c} \right) + \frac{1}{\omega} \sin \left( \omega \left( t + \frac{x}{c} \right) \right) \right\} \left\{ H \left[ t - \frac{2L}{c} + \frac{x}{c} \right] - H \left[ t - \frac{2L}{c} - \frac{2\pi}{\omega} + \frac{x}{c} \right] \right\}, \end{aligned} \quad (4.45)$$

where

$$\omega = \frac{2\pi}{t_{wave}}, \quad (4.46)$$

$$c = \sqrt{\frac{Y}{\rho}}. \quad (4.47)$$

This solution is valid for time  $0 \leq t \leq 2t_{prop}$ , where  $t_{prop} = \frac{L}{c}$ .



The maximum displacement  $u_p$  at  $x = L$  occurs at time  $t_{prop} + t_{wave}$  and is called the closure potential where

$$u_p = \frac{v_{max}(2\pi)}{\omega} \quad (4.48)$$

or

$$u_p = v_{max}t_{wave}. \quad (4.49)$$

The expression in Equation (4.49) is also valid for an open gap. The displacement  $u_p$  is a function of the velocity boundary condition and can be used to characterize the initial velocity pulse. As long as the gap does not fully close, the maximum displacement at the gap after wave reflection is equal to  $u_p$ . For the boundary condition of Eq. (4.43),  $u_p$  is calculated to be  $2.1E-4$ m. If the initial gap width is larger than this value, no portion of the wave is transmitted through the gap.

Further, the analytical peak stress of the rightward propagating compressive wave is  $\sigma_{max} = -\rho cv_{max}$ . Using the imposed boundary condition, the peak stress is -12.6 MPa. This value agrees with the peak compressive stress of the sinusoidal wave before interacting with the gap in Figure 4.10(a).

### 4.6.3 Proposed Boundary Condition Characterization

The expression for  $u_p$  from Equation (4.49) is proposed to be the closure potential of the input wave. A gap of size  $u_{g0}$  with no resistance to closure will close an amount  $u_p$  for one sinusoidal wave reflecting off of it when  $u_{g0} > u_p$ . If  $\frac{u_p}{u_{g0}} > 1$ , the gap will fully close and some energy will be transmitted. If  $\frac{u_p}{u_{g0}} < 1$ , the gap will not close in a single wave reflection. Considering a joint of initial discontinuity  $u_{g0}$ , the same rule holds true. The resistance to closure of a joint implies that if  $u_p$  is equal to  $u_{g0}$ , the joint will still not fully close because a portion of the wave is reflected off of the joint, another portion is propagated past the joint, and the remaining portion is dissipated in closing the joint.

$\frac{u_p}{u_{g0}}$  is used as a non-dimensional variable to characterize the potential for closure for both gaps and joints. For subsequent studies, this expression is used to relate

the potential for closure possible from the velocity boundary condition to the initial joint size.

## Chapter 5

### Basic Features of Wave

### Propagation through a Joint

Three constitutive models are proposed in Chapter 4. The gap, plastic joint, and elastic plastic joint constitutive algorithms have each been implemented into a dynamic MPM code. The one-dimensional bar is discretized using elements with each element containing one material point. The location of the material points within cells is discussed further in Appendix D because it has an impact on the smoothness of the results. The purpose of the basic features study is to determine the qualitative characteristics of a gap or joint on wave propagation.

#### 5.1 One-Dimensional Bar Problem

With use of the one-dimensional dynamic code, numerical solutions are obtained for the bar problem shown in Figure 5.1. Whether single or multiple discontinuities are prescribed, the first discontinuity will be located in the middle of the bar at  $x_g = \frac{L}{2}$ . A discontinuity of length  $u_{g0}$  is prescribed as a single discontinuity or the sum of multiple discontinuities. The bar has a velocity boundary condition imposed at  $x = 0$  and a free surface boundary condition imposed at  $x = L$ . Initially, the bar is at rest with no prestress. The velocity boundary condition is imposed in the form

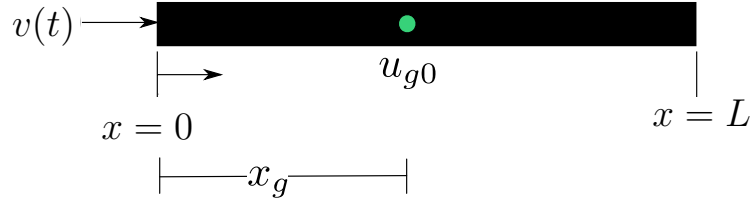


Figure 5.1: Notation for the problem of a bar with a single discontinuity

of a sinusoidal pulse as follows:

$$v(t) = \frac{v_{max}}{2} \left( 1 - \cos\left(\frac{2\pi t}{t_{wave}}\right) \right) \text{H}[t_{wave} - t] \text{H}[t]. \quad (5.1)$$

The prescribed velocity pulse contains two parameters consisting of:  $v_{max}$ , the peak particle velocity of the imposed wave, and  $t_{wave}$ , the duration of the sinusoidal pulse. As given in Eq. (4.49),  $u_p$  is the potential for closure as reflected through the dimensionless variable  $\frac{u_{g0}}{u_p}$ .

The parameters of the bar are:

- Length  $L = 2$  m,
- Density  $\rho = 2650$  kg/m<sup>3</sup>,
- Youngs modulus  $Y = 60$  GPa,
- Circular cross-sectional area  $A = 2$  mm<sup>2</sup>,
- Elastic wave speed  $c = \sqrt{\frac{Y}{\rho}} = 4758$  m/s,
- Location of the joint is  $x_g = \frac{L}{2}$ . For multiple joint studies, the first joint is located at  $x_g$  and subsequent joints are at specified points greater than  $x_g$ ,
- The spatial domain of the bar is discretized using 125 elements with one material point per element. 125 elements presents reasonable convergence with less noise, as shown in Appendix A.

The results of each study and bar parameters are nondimensionalized based on the scheme in Appendix C. Parameters with an over bar denote the dimensionless

value. For example,  $\bar{t}$  is the dimensionless time. The nondimensionalizing scheme results in a dimensionless elastic wave speed,  $\bar{c}$ , of unit value and the dimensionless length of the bar,  $\bar{L}$ , of unit value. This ensures the dimensionless propagation time,  $\bar{t}_{prop}$ , of an elastic wave traveling from one end of the bar to the other is also of unit value.

$$\bar{t}_{prop} = \frac{\bar{L}}{\bar{c}} = 1 \quad (5.2)$$

The parameters  $m$  and  $\sigma_g$  for  $g(\bar{u}_g)$  and the stated values of both are shown in Figure 4.8 and used for each numerical solution.

## 5.2 Gap, Plastic Joint, and Elastic-Plastic Joint Comparison

To illustrate the effects of the constitutive equations on the solution, consider a bar with a single discontinuity in the middle, as presented in Figure 5.1 and Section 5.1. The discontinuity can be characterized as a gap, a plastic joint, or an elastic plastic joint. The initial size of the discontinuity,  $u_{g0}$ , is 1 mm. An imposed sinusoidal velocity boundary condition has a peak particle velocity,  $v_{max}$ , of 8.31 m/s and a dimensionless wave time  $\bar{t}_{wave} = 0.43$ . The dimensionless wave time is large enough so that numerical dispersion is minimal for the numerical solution. The potential for closure of a discontinuity  $u_p$  is 1.5 mm for this boundary condition (Eqn (4.49)). This implies that a gap with no resistance to closure of initial discontinuity 1 mm will fully close from the propagated wave. A series of four computational runs, including a bar without a discontinuity, are presented to illustrate the impact of each constitutive algorithm on discontinuity behavior and wave propagation. The discontinuity is located halfway along the bar length at approximately  $\bar{x} = 1.5$ . The dimensionless bar length is of unit value and is centered in a computational domain of length 3.

### 5.2.1 No Discontinuity

Figures 5.2(a) and 5.2(b) show results for the elastic bar with no discontinuity. The compressive wave travels the length of the bar with no interruption, as one would expect. The sum of the kinetic and strain energies in the bar remain constant after the wave is fully into the bar. The red line of Figure 5.2(b) is the energy that would be dissipated in closing a discontinuity and is zero throughout the run because of the homogenous elastic bar.

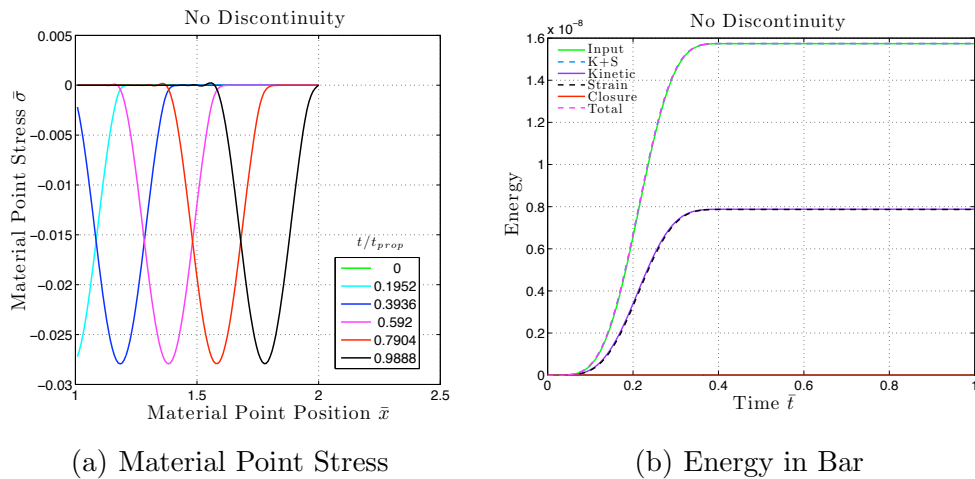


Figure 5.2: Results of wave propagation through a bar without a discontinuity

### 5.2.2 Gap Discontinuity

Figure 5.3 is the result of a bar with a gap. The gap has no resistance to closure and is identical to a free surface. The compressive wave will reflect off of it as a leftward traveling tensile wave until full closure occurs (Fig 5.3(a)). At time  $\bar{t} \approx 0.8$ , the discontinuity fully closes and no longer acts as a free surface. The remaining portion of the wave can then propagate through the discontinuity continuing as a compressive wave. The abruptness of this change and the nature of the dynamic code made for noisy results after gap closure (plotted times  $\bar{t} \approx 0.8$  and 1 (the black and red lines)). The tail end of the reflected tensile wave moving left of  $\bar{t} \approx 0.8$  oscillates

over a zero stress because of the abruptness. Therefore, once the joint fully closes, the tail of the reflected tensile wave will drop to zero and whatever remains of the initial compressive wave will propagate through the gap. The rightward portion of the initial compressive wave at  $\bar{t}$  of 0.8 is noisy but has the form of the pulse with an almost vertical front face and a tail that has the sinusoidal form of the initial compressive wave. When full closure of the gap occurs, the wave is split at the discontinuity. The front portion of the wave that was reflected as a tensile wave sharply drops to zero stress but its front moving face maintains the shape of the initial pulse. The front face of the continuing compressive wave is steep but the tail assumes the shape of the initial pulse.

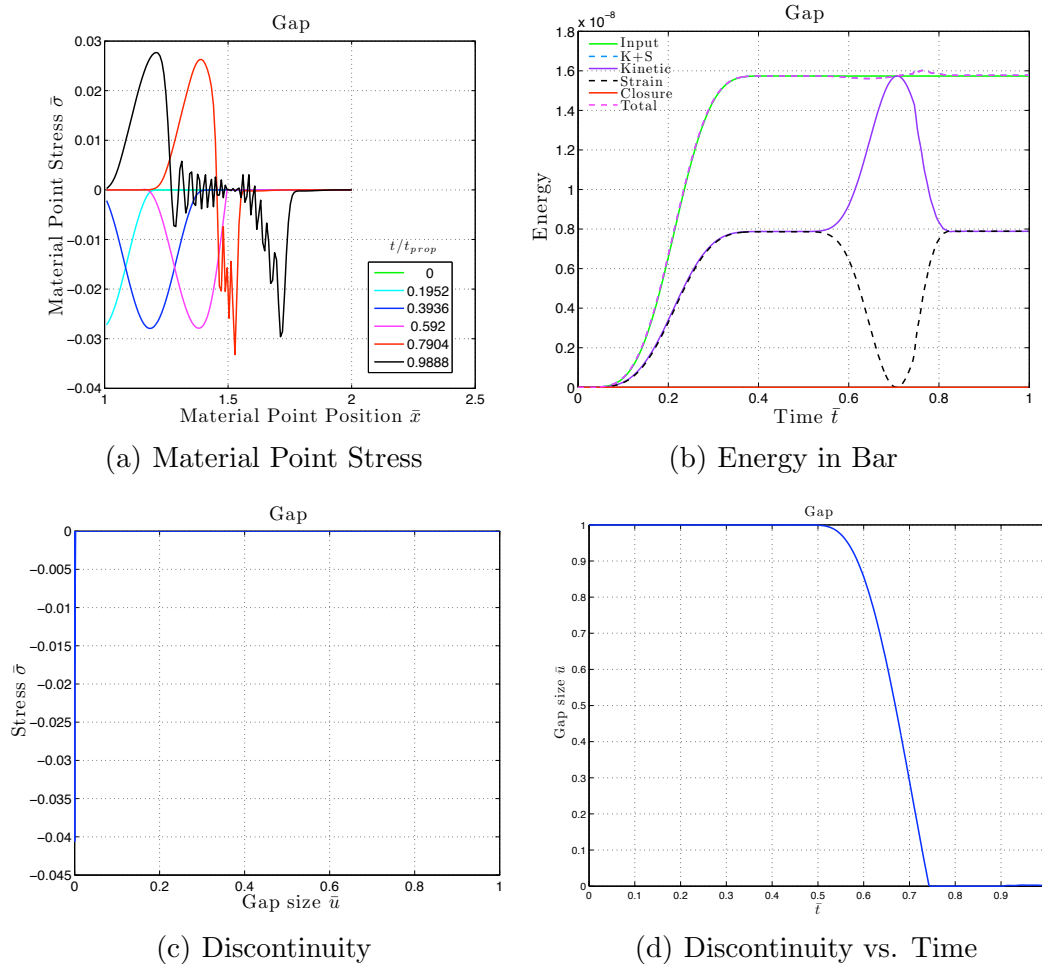


Figure 5.3: Results of wave propagation through a bar with a gap

The energy plot behaves as expected, as shown in Figure 5.3(b). The sum of the kinetic and strain energies remain constant after the wave is fully introduced and equal to that of the input energy. The reflection of the wave at the discontinuity starting initially at  $\bar{t} \approx 0.5$  causes equal increases in kinetic and decreases in strain energy so that the sum of the two values remains constant. This is identical to free surface reflection. The closure energy remains zero throughout because the gap dissipates no energy from the compressive wave.

Figure 5.3(c) is the plot of stress versus dimensionless discontinuity  $\bar{u}$ . The discontinuity is initially equal to 1. As the compressive wave interacts with it, the gap closes while not withstanding any compressive load. During this period, the wave is fully reflecting off of the discontinuity in the form of a leftward traveling tensile wave. At a discontinuity size  $\bar{u}$  equal to zero, the bar becomes continuous, which allows the remainder of the initial compressive wave to propagate past the gap. Figure 5.3(d) is a plot of  $\bar{u}$  versus time and is more insightful than Figure 5.3(c). At time  $\bar{t} \approx 0.5$ , the gap begins closing, and when  $\bar{t} \approx 0.75$ , the gap is completely closed.

### 5.2.3 Plastic Joint Discontinuity

Figure 5.4 is the result of wave propagation through a plastic joint. The discontinuity has resistance to closure and allows part of the initial compressive wave to propagate through before the joint is fully closed. The stress plot in Figure 5.4(a) shows the wave propagating through the joint with very little attenuation. The peak compressive stress after the joint appears to be approximately the same as the peak stress before the joint. A portion of the wave is reflected off of the joint as a tensile wave but the behavior is much smoother than the results for the gap shown in Figure 5.3(a). The majority of the tensile reflection occurs when the wave first interacts with the joint. The nonlinear resistance to closure is much less for a joint closing from  $\bar{u}_g = 1$  to  $\bar{u}_g = 0.9$  compared to a joint closing from  $\bar{u}_g = 0.7$  to  $\bar{u}_g = 0.6$ . Therefore, more of the front of the compressive wave will reflect off of the joint as a tensile wave because of the initially weaker resistance to closure of the joint.



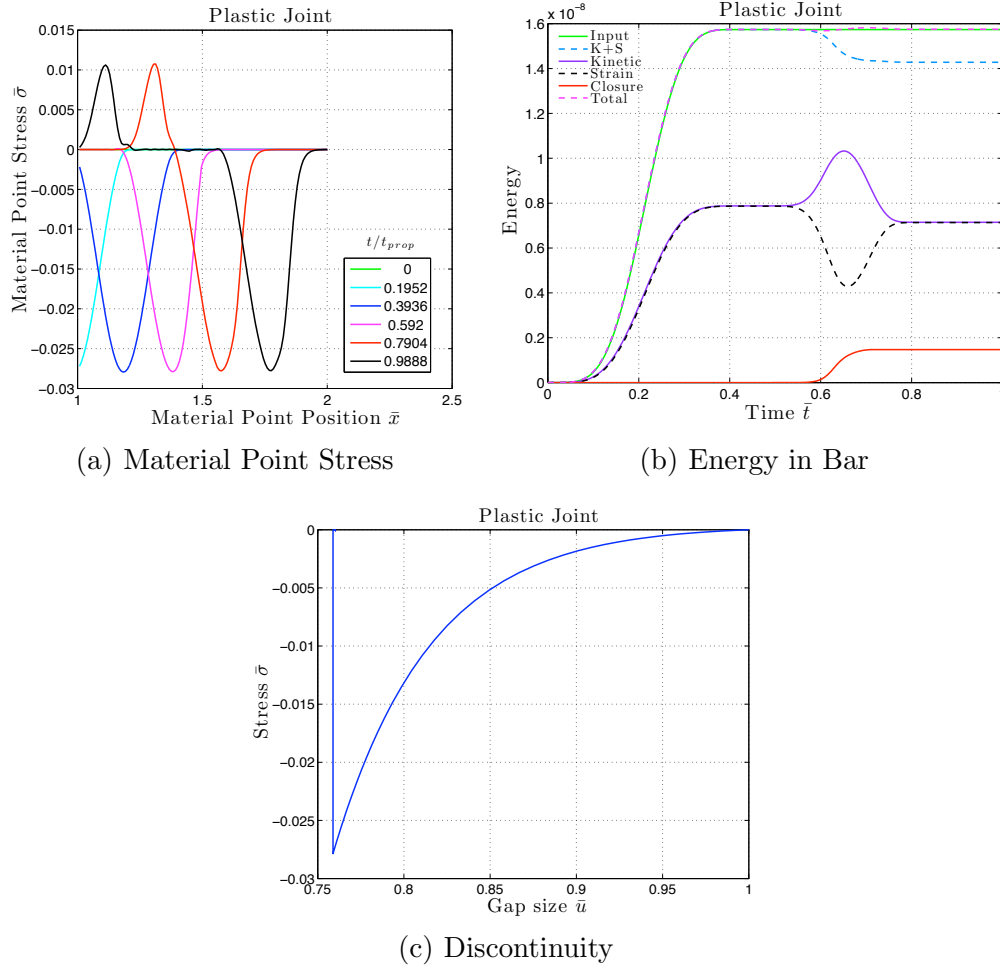


Figure 5.4: Results of wave propagation through a bar with a plastic joint

Once the joint has closed enough to resist any further closure, the majority of the compressive wave will propagate through the joint with little reflection. The length of the wave propagated through the joint is approximately the same length as the initial wave. The reflected tensile wave is much shorter because the joint closed quickly to a state of stress allowing the majority of the wave to continue through as a compressive wave with no further tensile reflection and no further increase in closure.

The plot of energy shown in Figure 5.4(b) demonstrates that the joint dissipates some energy during closure. The blue dotted line is the sum of the strain and kinetic energies in the bar. At dimensionless time  $\bar{t} \approx 0.5$ , the wave first interacts with the

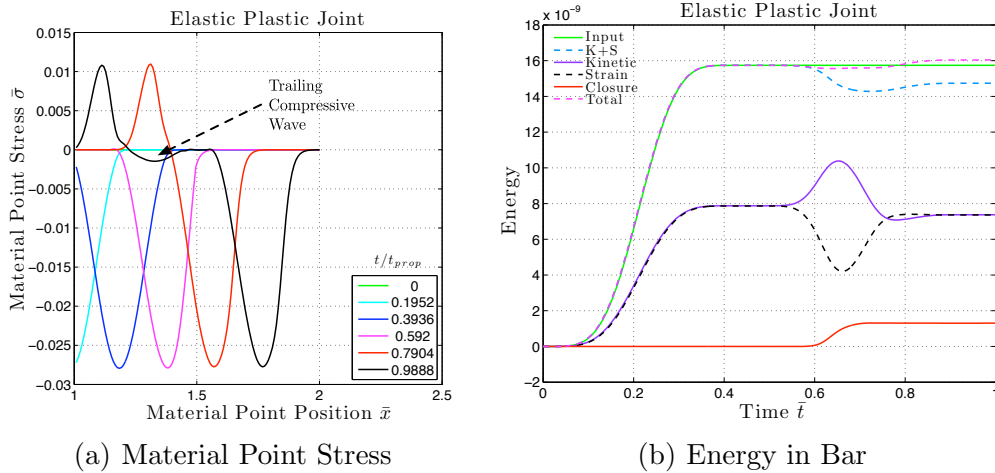
joint. The joint begins to close but not until  $\bar{t} \approx 0.6$  does the dissipated energy accumulate enough to be visualized on the plot. For  $\bar{t}$  between 0.5 and 0.6, the joint is closing but its resistance to closure is small enough that some of the wave reflects off of the joint as a tensile wave. The joint continues closing which requires an increase in energy dissipation until the stiffness of the joint is large enough that no more closure occurs. The closure energy increases while the sum of the strain and kinetic energies decreases. The total energy in the bar defined as the sum of the elastic, kinetic and closure energies remains constant during the joint interaction (the magenta dashed line in Fig 5.4(b)).

Figure 5.4(c) plots the stress at the joint as a function of  $\bar{u}$ . As the joint closes, the stress follows the gap function  $g(\bar{u}_g)$ . The joint closes to a minimum value of  $\bar{u} \approx 0.76$  and then unloads to a zero stress state. The unloading is plastic ( $\bar{u}$  remains constant), which produces a vertical unloading path. Correspondingly, the surrounding parent rock unloads elastically until zero stress is reached. The peak stress of the gap prior to unloading is  $\bar{\sigma} \approx -0.027$ . This is also the peak value of stress for the wave after propagating through the joint (Fig 5.4(a)).

### 5.2.4 Elastic-Plastic Joint Discontinuity

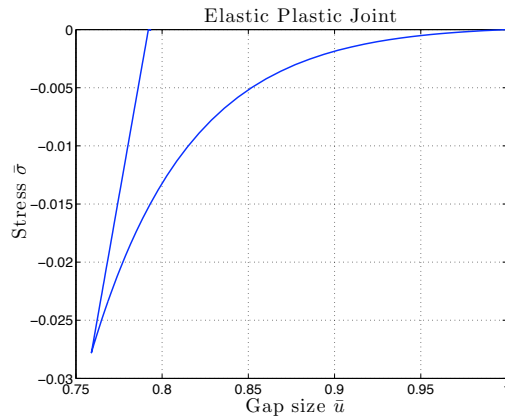
For the elastic-plastic joint, the modulus of elasticity for the joint was taken to be constant and is the slope of the function  $g(\bar{u}_g)$  when  $\bar{u}_g$  is 0.7. The reason for this choice is that for the assumed force on the boundary, the joint will not close below  $\bar{u}_g = 0.7$  and an unloading curve with a tangent to the loading cycle seems to agree with the experimental behavior of joints. The ratio of the elastic modulus of the parent rock to the joint modulus is,

$$\frac{E_j}{E_c} = 0.091. \quad (5.3)$$



(a) Material Point Stress

(b) Energy in Bar



(c) Discontinuity

Figure 5.5: Results of wave propagation through a bar with an elastic-plastic joint

Figure 5.5 provides plots of results obtained with an elastic-plastic joint in the bar. The elastic-plastic behavior is very similar to the plastic joint in Section 5.2.3. Comparing the stress plots of Figures 5.4(a) and 5.5(a), the compressive wave propagates towards the joint with a portion of the wave reflecting off of it and another portion propagating past and continuing on as a compressive wave. The peak values of the waves in each scenario are approximately the same. The key difference is the plastic joint does not have a compressive wave trailing the reflected tensile wave from the joint. However, the elastic-plastic joint at time  $\bar{t} \approx 1$  has a leftward moving compressive wave traveling behind the reflected tensile wave, indicated in Figure 5.5(a). The source of this phenomenon is likely the joint unloading elastically. The

modulus of elasticity of the joint is less than the modulus of the parent rock. The discontinuity in moduli might create a separate wave during unloading. Nonetheless, the impact of specifying an elastic-plastic joint as opposed to a plastic joint appears to be minimal.

The energy plot of Figure 5.5(b) does have some slight variance from the plastic joint energy plot. The total energy does move slightly above the input energy of the bar after the wave propagates through the joint. The scheme of using an effective modulus might be the source of the discrepancy. Nonetheless, the discrepancy is minimal.

The joint behavior in Figure 5.5(c) is almost identical to the plastic joint (Figure 5.4(c)). The peak stress at the joint and the shape of the loading curve is the same. Elasticity causes non-vertical unloading. The joint length  $\bar{u}$  does not remain constant due to elasticity as the joint stress unloads fully to zero strain.

## Chapter 6

# Effects of Parameters on Wave Propagation through Single Joint

### 6.1 Program of Single Joint Study

The focus of the one-dimensional study is to qualitatively determine the impact of each constitutive model on wave propagation for a single joint. Figure 6.1 illustrates the single joint study. A joint is placed in the middle of the bar with an initial discontinuity length  $u_{g0}$ . A wave is propagated down the bar as shown in Figure 5.1. The wave impulse, peak stress, and energy transmitted through the discontinuity are considered to determine the impact of the discontinuity on wave propagation. The form of the pulse is varied by the wave time  $\bar{t}_{wave}$  and peak particle velocity  $v_{max}$  to give the same potential for closure  $u_p$ . Also, the initial discontinuity size is varied. The values of the size of initial joint width and parameters of the propagated wave are shown in Table 6.1.



Figure 6.1: Single Discontinuity Study

(a) Boundary Conditions,  
 $u_p = 1.5\text{mm}$ 

Set	$v_{max}$	$\bar{t}_{wave}$
1	7.14 m/s	0.5
2	7.68 m/s	0.465
3	8.31 m/s	0.43
4	9.04 m/s	0.395
5	9.92 m/s	0.36
6	10.99 m/s	0.325
7	12.32 m/s	0.29
8	14.01 m/s	0.255
9	16.23 m/s	0.22
10	19.31 m/s	0.185
11	23.81 m/s	0.15

(b) Initial Discontinuity Size  $u_{g0}$ 

Set	$u_{g0}$
1	0 mm
2	0.15 mm
3	0.3 mm
4	0.45 mm
5	0.6 mm
6	0.75 mm
7	0.9 mm
8	1.05 mm
9	1.2 mm
10	1.35 mm
11	1.5 mm

Table 6.1: Inputs used for the single joint sets

## Study Outputs

Each study uses the same outputs to draw conclusions about wave-joint interaction. The outputs considered are the peak stress, the impulse of the wave, and the energy transmitted past the discontinuity. The peak stress past the discontinuity is related to the peak stress before the discontinuity by

$$\bar{\sigma}_{ratio} = \frac{\bar{\sigma}_{min,right}}{\bar{\sigma}_{min,left}}. \quad (6.1)$$

$\bar{\sigma}_{min,right}$  is the minimum peak stress after the wave has propagated beyond the discontinuity.  $\bar{\sigma}_{min,left}$  is the minimum peak stress before the wave has propagated through the discontinuity. Each of these is non-dimensionalized. The impulse value is calculated as

$$I_{ratio} = \frac{\bar{I}_{right}}{\bar{I}_{left}}. \quad (6.2)$$

Again, the subscript *left* and *right* denote the value before propagating past the discontinuity and after propagating past the discontinuity. Both the impulse and peak stress are values found at the material points and are more likely have unrealistic values because of numerical dispersion. The energy summed across the entire bar is  $\bar{E}_{total}$  and is the sum of the kinetic and strain energies for each material point in the

bar. The transmitted energy  $\bar{E}_{trans}$  is the sum of the kinetic and strain energies only for the material points to the right of the discontinuity. The energy is plotted with the expression

$$E_{ratio} = \frac{\bar{E}_{trans}}{\bar{E}_{total}}. \quad (6.3)$$

The energy values are less susceptible to dispersion because energy is a summed quantity of the the material point values.

## 6.2 Single Discontinuity Study

The first study is a single discontinuity. The gap, plastic joint, and elastic-plastic joint constitutive algorithms are each used for the discontinuity in the middle of the bar. The problem layout is shown in Figure 6.1. The input parameters in Table 6.1 are used for the closure potential  $u_p$  of 1.5 mm and the initial joint sizes.

### 6.2.1 Gap

The single discontinuity study begins with the gap. The corresponding results are shown in Figure 6.2. The gap enables intuitive expectations of the discontinuity behavior to be confirmed. When the initial discontinuity  $u_{g0}$  is zero, all of the wave energy should propagate past the gap. The peak stress and impulse should be the same on either side of the gap. Conversely, when  $u_{g0}$  is equal to  $u_p$ , the wave should not propagate past the gap. The impulse and peak stress should be zero past the gap. And, no energy should be transmitted through the gap.

In Figure 6.2(a), when  $\frac{u_{g0}}{u_p}$  is equal to one no energy is transmitted because total gap closure occurs at the end of the wave reflection. For  $\frac{u_{g0}}{u_p} = 0$ , all of the energy is transmitted past the gap. This behavior is the same for the impulse and peak stress in Figures 6.2(c) and 6.2(b), respectively.

The wave characteristics seem to have little impact on the amount of transmitted energy. Regardless of  $v_{max}$  and  $\bar{t}_{wave}$ , the results of transmitted energy plot on top

of one another (Fig 6.2(a)). This does not hold for the impulse or peak stress. The results for peak stress and impulse of each run are not fully shown in Figure 6.2. The wave impulse for each wave input lay close to one another (Fig 6.2(c)). But, the peak stress does not. For smaller  $\bar{t}_{wave}$  values, a larger peak stress occurs past the gap than before the gap. These results do not seem plausible and are due to numerical dispersion associated with a jump in stress once the gap closes. Individual material point quantities are particularly susceptible to numerical dispersion and make the results without much dispersion difficult to interpret on the same axis. The forcing function with small values of  $\bar{t}_{wave}$  result in significant dispersion. Peak stress and impulse are plotted for every run and shown in Figure E.1 in Appendix E.

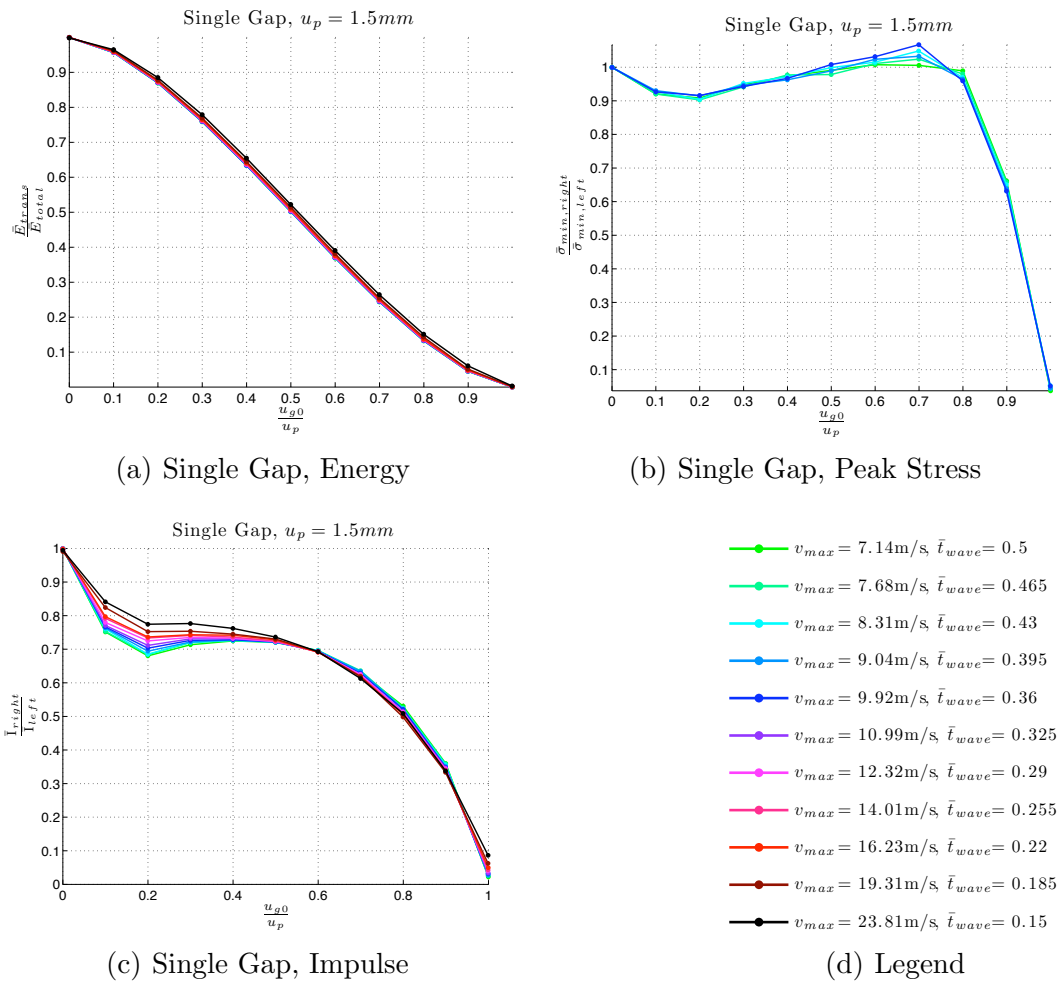


Figure 6.2: Plots of results for wave propagation through a single gap with  $u_p = 1.5mm$



### Conclusions of Single Gap Study

- The significant parameter for wave propagation through a single gap is  $\frac{u_{g0}}{u_p}$ .
- The energy transmitted past a gap is approximately constant regardless of the wave characteristics. As long as  $u_p$  is the same for a sinusoidal pulse,  $v_{max}$  and  $\bar{t}_{wave}$  do not impact the transmitted energy.
- The peak stress is very close to one when  $\frac{u_{g0}}{u_p}$  is less than one. This only applies to waves of  $\bar{t}_{wave} \geq 0.395$ .

### 6.2.2 Plastic Joint

The inputs of the single plastic joint study are the same as the single gap study. The results are presented in the same manner as well, shown in Figure 6.3. For an initial gap size of zero, the transmitted energy, peak stress, and wave impulse are the same for each wave input and are either one or close to one. These results are expected. The energy plot of Figure 6.3(a) shows that more energy is transmitted past the plastic joint for a longer wave time  $\bar{t}_{wave}$  for all values of  $\frac{u_{g0}}{u_p}$ . This conclusion is expected because a long wave interacts with a joint for a longer period of time allowing it to propagate more energy as opposed to reflecting off the joint quickly. The peak stress curves in Figure 6.3(b) lie on top of one another for the input parameters of  $\bar{t}_{wave}$  0.5, 0.465, 0.43, and 0.395. The peak stress drops slightly as  $\frac{u_{g0}}{u_p}$  is closer to one. The result is intuitive because the larger the joint, the more energy will be dissipated in closing it before a large portion of the energy can propagate through. However, for other input parameters, the peak stress result is greater than one. This should not occur with the constitutive algorithm. The behavior comes from numerical dispersion and the results are omitted. The full results are shown in Figure E.2. The peak stress grows for smaller wave times and appears to peak when  $\frac{u_{g0}}{u_p}$  is between 0.6 and 0.8 for the smaller wave times. The wave impulse decreases with larger  $u_{g0}$  (Fig 6.3(c)). The longer the wave the larger the impulse

Chapter 6. Effects of Parameters on Wave Propagation through Single Joint 52  
transmitted for wave times between 0.5 and 0.36. For wave times shorter than this,  
the characteristic breaks down due to numerical error.

The results for peak stress and impulse of each run are not fully shown in Figure E.2 of Appendix E. Individual material point quantities are particularly susceptible to numerical dispersion, which can skew the results. The input boundary conditions with small values of  $\bar{t}_{wave}$  result in significant errors. For  $\bar{t}_{wave}$  less than 0.36, the characteristic features break down due to numerical error.

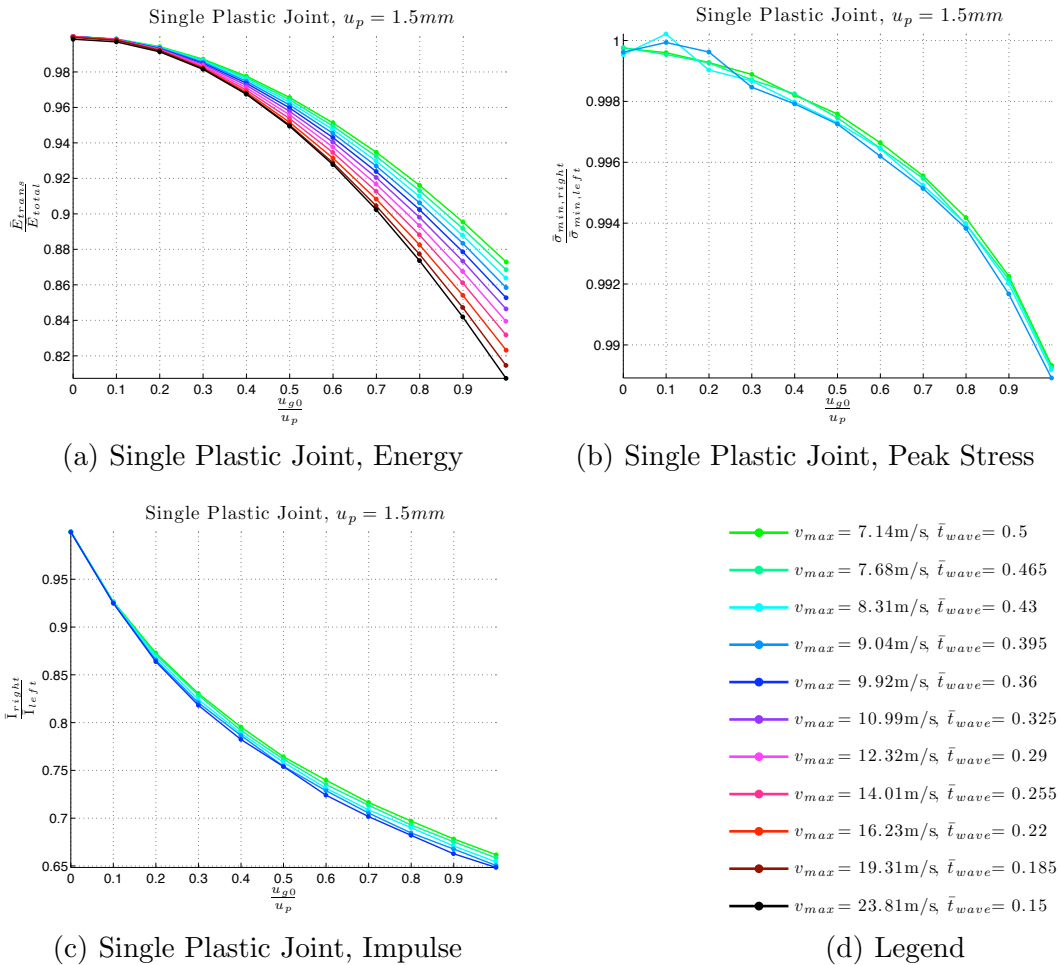


Figure 6.3: Plots of results for a wave transmitted through a single plastic joint with  $u_p = 1.5\text{mm}$ .

### **Conclusions of Single Plastic Joint Study**

- The longer the wave time, the more energy is transmitted past the plastic joint.
- The larger the initial discontinuity size, the less the peak stress transmitted past the joint. This only holds for wave times greater than 0.395 because numerical error makes determining the characteristics difficult.
- The wave impulse decreases with larger initial discontinuity size for wave times greater than 0.36.

### **6.2.3 Elastic-Plastic Joint**

The characteristic behavior of the single elastic-plastic joint is very similar to the plastic joint. The results of Figure 6.4 present similar qualitative characteristics as Figure 6.3.

#### **Conclusions of Single Elastic-Plastic Joint Study**

- The wave-joint interaction of an elastic-plastic joint has similar characteristics of a plastic joint.
- Slightly less energy is transmitted past an elastic-plastic joint than a plastic joint. The qualitative characteristics of both are the same.
- Slightly less peak stress is transmitted past an elastic-plastic joint than a plastic joint. The impact of wave characteristics on peak transmitted stress is the same.
- Slightly less impulse is transmitted past an elastic-plastic joint than a plastic joint. The impact of wave characteristics on wave impulse is the same.

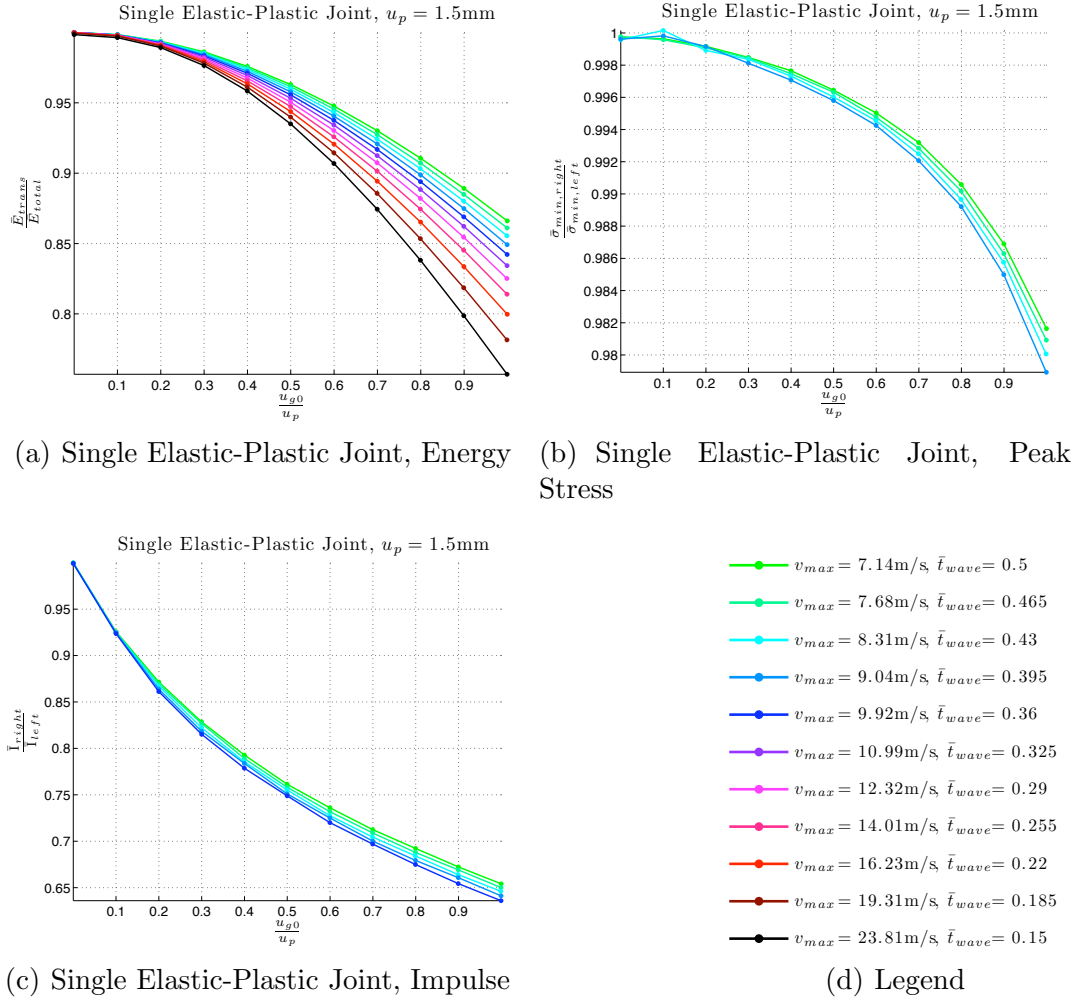


Figure 6.4: Plots of results for a wave transmitted through a single, elastic-plastic joint with  $u_p = 1.5\text{mm}$ .

### 6.3 Single Joint Conclusions

Overall, the study of single gaps and single joints yielded several conclusive results. The goal of the study was to determine the impact of wave parameters and initial joint size on energy transmission, impulse, and peak stress. Due to numerical errors introduced that are more pronounced by small values of  $\bar{t}_{wave}$ , the impulse and peak stress could not be concretely determined because each value is calculated at a material point. This was the case for a gap, a plastic joint, and an elastic-plastic joint. The results for energy transmission were less effected by numerical error because the

energy is summed over multiple material points. For a gap, energy transmission was the same for values of  $\frac{u_{g0}}{u_p}$ , and the wave parameters  $v_{max}$  and  $\bar{t}_{wave}$  had no impact. For a plastic joint, more energy was transmitted through the discontinuity for larger values of  $\bar{t}_{wave}$ . The reason for this is that a longer wave spends a longer period of time interacting with the joint. Because the joint has nonlinear resistance to closure, a longer wave-joint interaction time forces the joint to a stress state that can allow the remainder of the wave to propagate past. For an elastic-plastic joint, the results led to the same conclusion. The elastic-plastic joint does not behave significantly different from a plastic joint. The key difference between the two is that the amount of energy transmitted through an elastic-plastic joint is slightly less than that of a plastic joint for identical values of initial discontinuity size and wave parameters  $\bar{t}_{wave}$  and  $v_{max}$ .

## Chapter 7

# Effects of Parameters on Wave Propagation through Two Joints

Appendices F and G present two studies (and numerical results), which motivate this chapter. The intent of those studies was to find the impact of lumping joints into fewer joints and the spacing of two joints on wave propagation. After analyzing the results of the lumping gaps (Fig F.1), the issue arose that  $n$  gaps of equal initial size  $\frac{u_p}{n}$  allowed energy to be transmitted through the gaps. Whereas, a single gap of initial size  $u_p$  does not allow any energy to be transmitted past. Intuitively, whether a gap with no resistance to closure or two gaps with no resistance to closure, one would expect that no energy would be transmitted past them.

The results of the lumping gap study are plotted in Figure 7.1 (also included in Appendix F). One would expect no energy to propagate past the set of gaps when the sum of initial gap sizes  $u_{g0}$  is equal to the potential for closure of the input wave  $u_p$ . For a single gap, the results are as expected and satisfactory, as the entire compressive wave is reflected off of the gap. But, for multiple gaps, energy does propagate past the gaps. Further exploration is conducted to understand the impact of these unexpected results by increasing the distance between two gaps and analyzing the propagating wave.

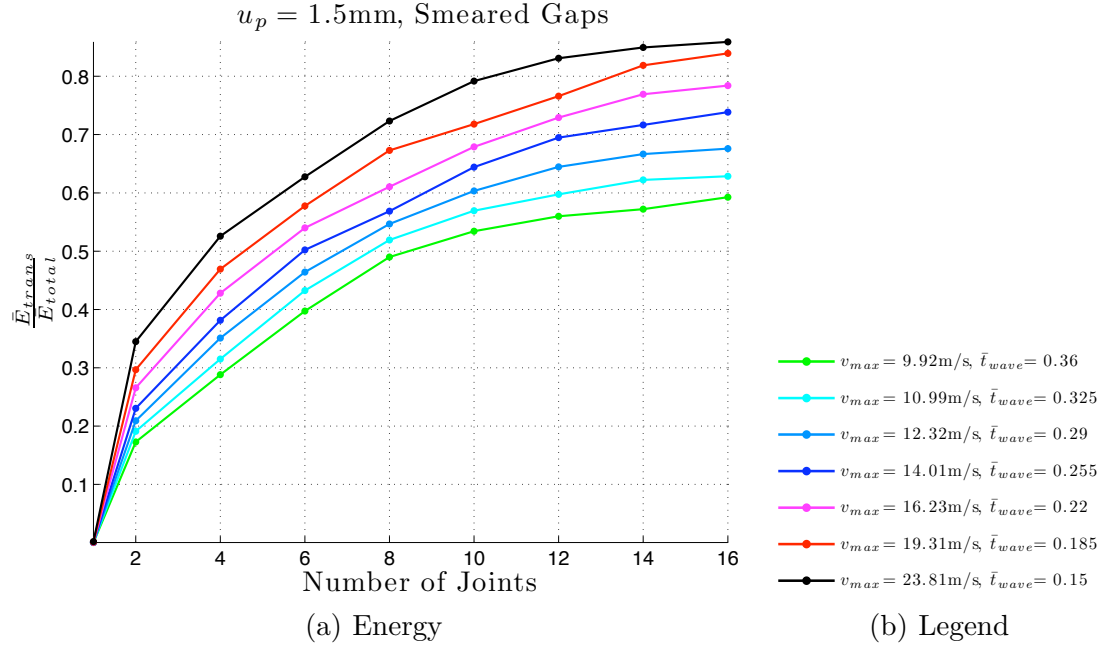


Figure 7.1: Transmitted energy results for multiple gap study

### Lumping Joints Study

As discussed above, the study of lumping multiple joints illustrated in Figure F.1 warranted further exploration. The results are provided in Appendix F. The key result is that more energy is transmitted through multiple joints than transmitted through one equivalent joint with the same total potential for closure. The study was conducted on gaps, plastic joints, and elastic-plastic joints with prescribed  $u_{g0} = 1.5\text{mm}$  and  $u_{g0} = 0.5\text{mm}$ .

### Joint Spacing Study

The numerical solutions to the study are provided in Appendix G. Two joints were prescribed in the middle of the bar, and the distance between the two was varied for each run. The tentative conclusion is that the more spacing between gaps, the less energy is transmitted. The results for plastic joints are not as susceptible to spacing issues as gaps. However, these results may not be conclusive because of

## 7.1 Two Gaps Study

To produce clearer numerical results, 250 material points and one material point per cell were prescribed to discretize the bar (rather than the previously proposed 125). The finer mesh was chosen because dispersion introduced by two discontinuities is less prominent with 250 versus 125 material points (Appendix B presents a convergence study for two gaps). The spacing between two gaps is varied by specifying the number of material points between the two gaps. The gaps have equal initial discontinuities of size  $\frac{u_{g0}}{2}$ , where  $u_{g0}$  is 1.5mm. The sinusoidal pulse is defined by parameter values of  $v_{max} = 9.92\text{m/s}$  and  $\bar{t}_{wave} = 0.36$ , which produces a value of  $u_p = 1.5\text{mm}$ . The initial total discontinuity size is  $u_{g0} = 1.5\text{mm}$ . The value of  $\bar{t}_{wave}$  was chosen to allow the full length of the wave to fit in the length of the bar to the right of the second discontinuity. The value of  $v_{max}$  produces a wave that has a potential for closure equal to the total initial discontinuity size. These values are reported in Table 7.0(a). The gaps are spaced by specifying the number of material points separating them. As shown in Table 7.0(b), the material point spacing is equivalent to  $\Delta\bar{x}_{gap}$ , which is the dimensionless length between the two material points with prescribed gaps. The dimensionless value  $\frac{\Delta\bar{x}_{gap}}{\bar{t}_{wave}}$  relates the gap spacing to the length of the wave. This value was chosen to better determine the relationship between gap spacing and wave length.

(a) Boundary Conditions,  $u_p = 1.5\text{mm}$

$v_{max}$	$\bar{t}_{wave}$
9.92 m/s	0.36

(b) Discontinuity Spacing

MP Spacing	$\Delta\bar{x}_{gap}$	$\frac{\Delta\bar{x}_{gap}}{\bar{t}_{wave}}$
10	0.04	0.111
20	0.08	0.222
30	0.12	0.333
40	0.16	0.444

Table 7.1: Inputs used for gap spacing



Stress at each material point is plotted at various times for each spacing in Figure 7.2. In each run, the results are similar regardless of gap spacing. The initial compressive pulse propagates to the first gap as expected. The first (left-most) gap will close upon wave-joint interaction. The closure introduces numerical dispersion because of the discontinuity in stress. The first portion of the wave reflects off the gap as a leftward traveling tensile pulse and the remainder propagates through the gap. The continuing compressive wave interacts with the second gap. Because the size of initial discontinuity of both gaps is  $\frac{u_p}{2}$ , the second gap also closes. During closure of the second gap, the compressive wave is reflected as a tensile wave traveling left. Gaps have no strength in tension, therefore, the now leftward traveling wave between the two gaps will reflect off of the first gap, which opens, and the pulse becomes a rightward traveling compressive wave. This event will be referred to as wave trapping. At this point, the right gap is already closed, and the trapped compressive wave propagates through it without disturbance. Wave trapping between gaps is the reason wave propagation was occurring through the sets of gaps for the lumping gap study. There is a noticeable slowing of the wave front due to the reflections. The greater the distance between gaps, the more time is required for the wave to propagate through the gaps to the right end of the bar. For  $\frac{\Delta \bar{x}_{gap}}{t_{wave}}$  values of 0.333 and 0.444,  $\bar{t} > 1.3$  when the wave front gets to the right end. Further, wave trapping increases the length of wave travel as it propagates from one end of the bar to other.

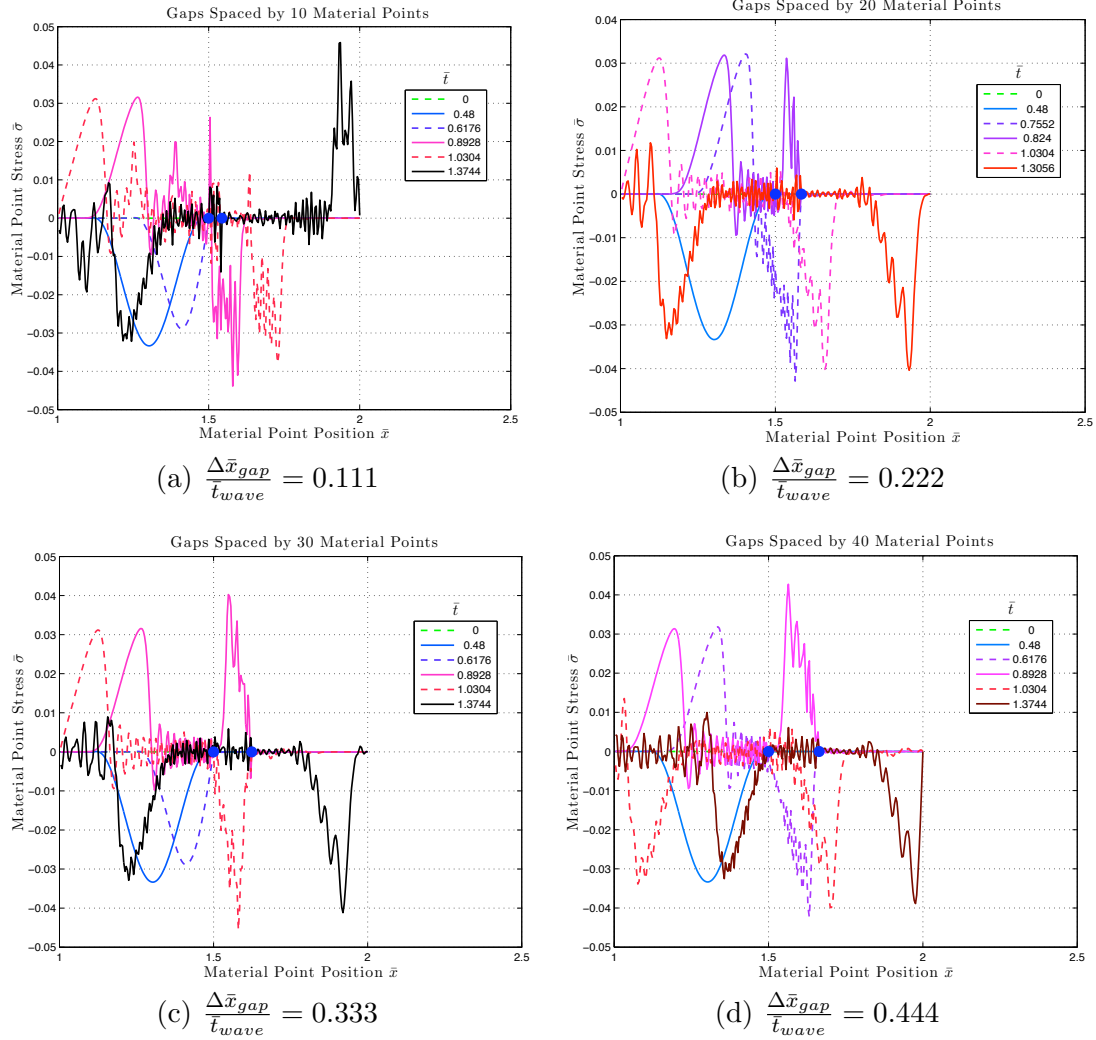


Figure 7.2: Plots of stress for different gap spacings (blue dots denote locations of gaps)

The energy transmitted through the gaps was also analyzed. Figure 7.3 shows the plots of energy transmitted through the gaps versus dimensionless time. Figures 7.3(b), 7.3(c), and 7.3(d) each show approximately 0.5 of total energy transmitted through the gaps at the end of each run. The run with a  $\frac{\Delta \bar{x}_{gap}}{t_{wave}}$  of value 0.111 is only 0.45 at the final time, which may be due to numerical error. When the gaps are close to one another, the discretization is not able to properly represent the wave. Nonetheless, if half of the total energy gets through the gaps, half of the wave energy is reflected off of the first gap. The second half of the wave is trapped in between

the gaps then eventually propagates through the second gap. Only half of the wave is reflected in closing the first gap of size  $\frac{u_p}{2}$ . And, half of the wave is reflected at the second gap. But after wave trapping, the wave can propagate through the closed second gap.

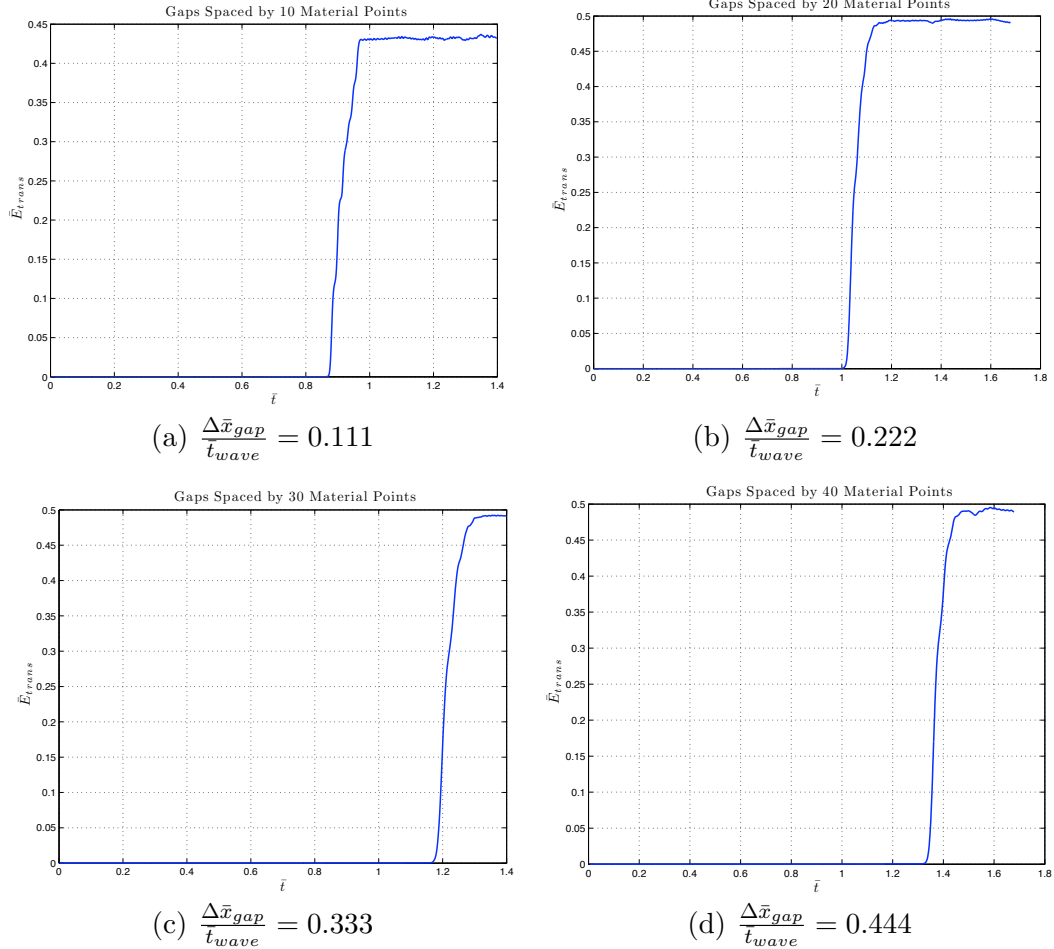


Figure 7.3: Results for transmitted energy due to gap spacing

### 7.1.1 Two Gaps In-Depth

The results of wave propagation through two gaps with a spacing value  $\Delta \bar{x}_{gap} = 0.16$  is shown in greater detail in Figure 7.4. Each plot is the material point stress at various times. (1) is the earliest plotted time, and (6) is the latest plotted time. Beginning with (1), the process of wave propagation is:

- (1) The compressive pulse **A** originates at the left end of the bar and propagates left towards the first gap.
- (2) Wave **A** closes the first gap, splitting the wave in half. Wave **B** reflects off of the first gap as a leftward traveling tensile wave. Wave **A** propagates through the closed first gap.
- (3) Wave **B** propagates towards the left end of the bar. Wave **A** closes the second gap and reflects off of it as a leftward traveling tensile pulse.
- (4) Wave **B** begins to reflect off of the left end of the bar. Wave **A** reflects off of the first gap and becomes a rightward traveling compressive pulse. The reflection of the tensile wave on the closed gap causes the first gap to open.
- (5) Wave **B** reflects off the left end of the bar. Wave **A** propagates through the closed gap.
- (6) Wave **B** and wave **A** are rightward traveling compressive pulses. The entirety of wave **A** has propagated through both gaps.

The close-open cycle of the first (left) gap is shown in Figure 7.5(a). The first gap opens because of the tensile reflection in Figure 7.4 at (3) after initially closing at (2). Figure 7.5(b) illustrates the closing of the second (right) gap versus time. The right gap closes at (2) in Figure 7.4 and remains closed.

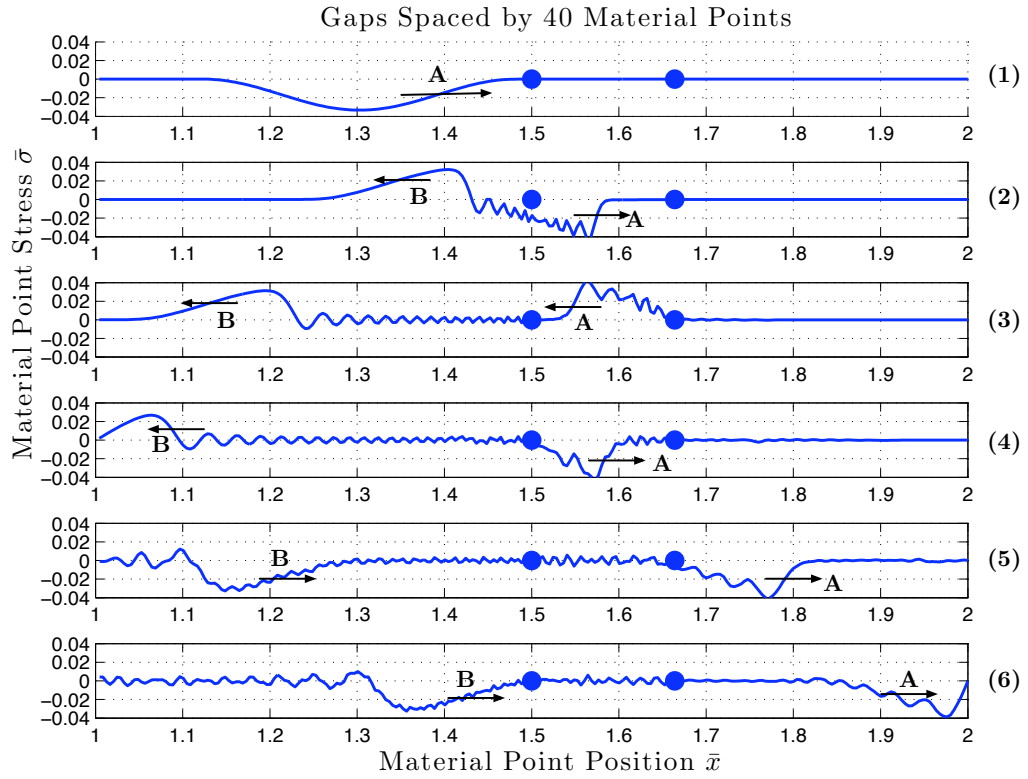


Figure 7.4: Stress plots at various time of wave propagation through two gaps spaced 40 material points apart (blue dots denote gap locations)

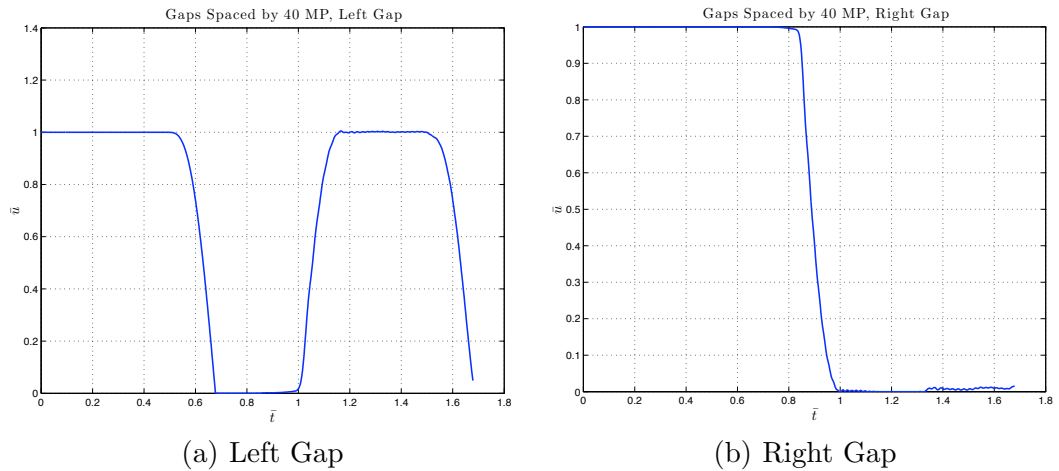


Figure 7.5:  $\bar{u}$  versus time for each gap

Runs with identical wave inputs to those shown in Section 7.1 were gathered for two plastic joints as well. Rather than analyzing a bar with two joints spaced by  $\Delta\bar{x}_{joint} = 0.04$  (the first run in the two gap study), a bar with a single joint was analyzed. Comparing the single joint results with joint spacing results can give clearer insight into the possibility of joint lumping.

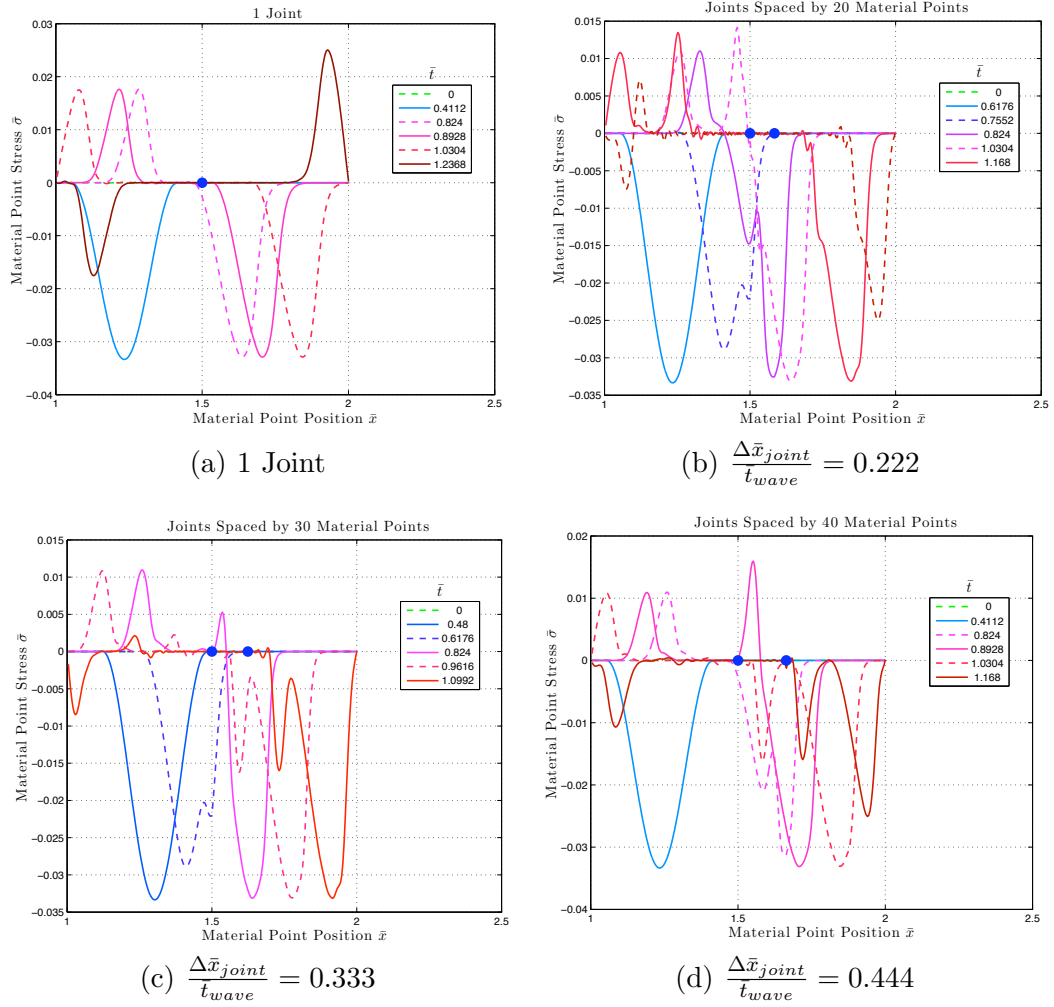


Figure 7.6: Plots of material point stress for multiple joint spacing (blue dots denote joint locations)

Figure 7.6 shows the plots of material point stress at various times. A single joint behaves as expected. The compressive wave is split into a tensile reflection off of the

joint and a continuing compressive pulse. For two joints, wave splitting occurs twice. Therefore, the original wave will split into three separate waves after propagating through both joints. For each run, there's an initial reflection off of the first joint and a continuing compressive wave. The continuing compressive wave propagates through the second joint but part of the wave is reflected as a tensile pulse. The tensile pulse is trapped between the two joints and reflects off of the first to continue through the second joint as a compressive pulse. At this point, there are two distinct waves that have propagated through the joints. The closer the joints are to one another, the more indistinguishable the two separate waves become. Also, the time required for the wave front to reach the right end of the bar is slightly greater than the elastic propagation time because of the increase in travel distance of the wave due to wave trapping

The energy plots were not considered for the two gap study because no energy dissipation occurs in closing gaps. For the two joint study, energy plots are important because energy is dissipated through joint closure. Figure 7.8 shows the plots of different energies versus time for each run. In each run, the kinetic and strain energy both began to alter at  $\bar{t} = 0.5$ . This is when the wave interacts with the first joint. For the spaced joints, a similar kinetic and strain energy attenuation occurs slightly thereafter because of the second joint. During these wave-joint interactions, the closure energy increases because the joints are being closed. Also, the sum of the kinetic and strain energies decrease, which is a result of the dissipated closure energy.

Table 7.2 displays the ratio of maximum closure energy for each run in relation to the maximum closure energy for a single equivalent joint. For a single joint, this value is one. For two joints of the prescribed spacings, the closure energy is 0.68% greater than the single joint. This implies that regardless of joint spacing, the same amount of energy will be dissipated in closing the joints. Also, if two joints only dissipate 0.68% more energy than a single joint, certain computations may warrant lumping multiple joints into fewer discontinuities to increase computing efficiency.

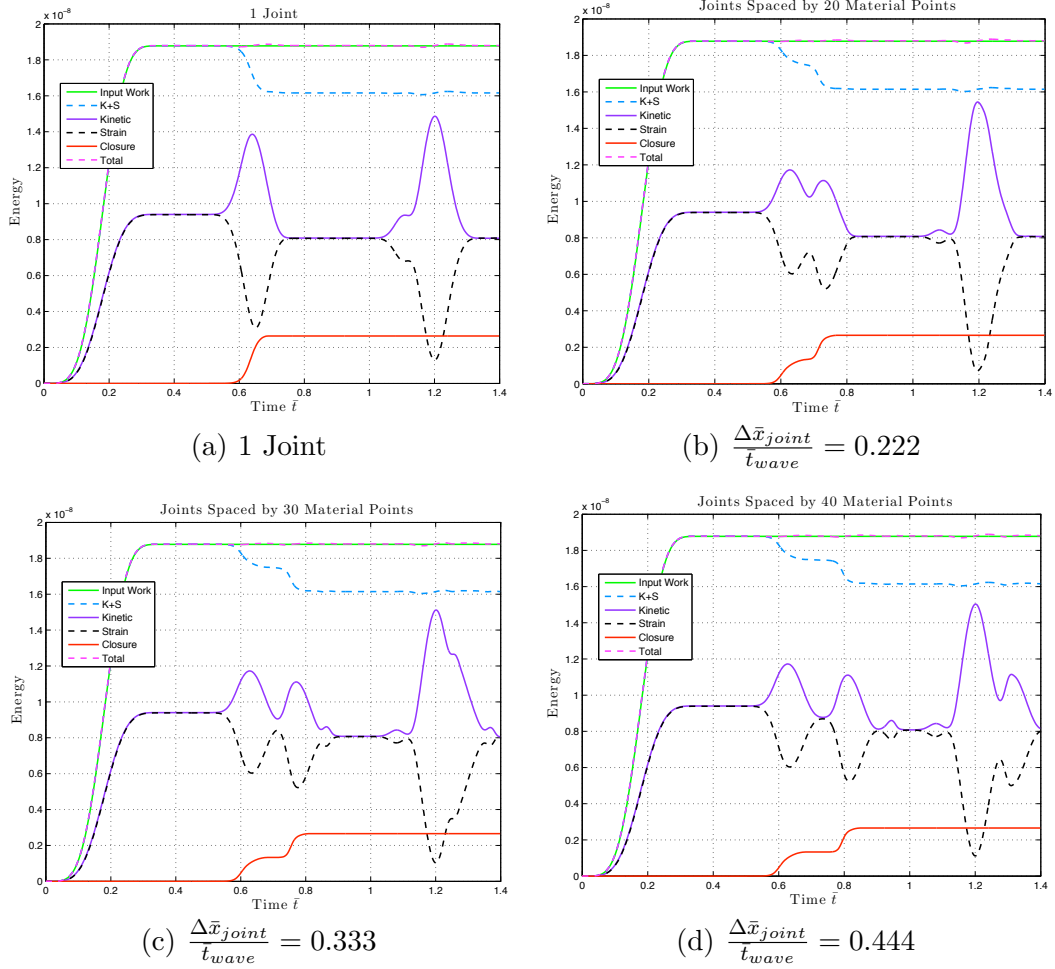


Figure 7.7: Energy versus time plots for multiple joint spacings

MP Spacing	$\frac{E_{close}}{E_{close,1joint}}$
1 Joint	1
20 MP	1.0068
30 MP	1.0068
40 MP	1.0068

Table 7.2: Energy dissipated in closing the joints

While the energy dissipated in propagating a wave through two joints is close to the energy dissipated through a single equivalent joint, the amount of energy transmitted through two joints is not the same as a single equivalent joint. Figure 7.8 illustrates the energy transmitted through the joints during wave propagation.



A single joint allows approximately 73% of the total energy to be transmitted. Two joints transmit 81% to 96% of the total energy, depending on spacing. The reason is that less of the wave is reflected off of the first joint (as compared to the single joint) and the portion of the wave reflected off of the second joint is trapped between the two joints and eventually propagates through the second joint after reflecting off the first. Multiple joints split up portions of the wave multiple smaller waves which become trapped between joints and eventually propagate through. Whereas, a single joint reflects a larger portion of the wave that will not reflect back through the initial joint because there isn't another joint for the tensile wave to reflect off of again. In other words, a single joint does not produce the wave trapping effects of multiple joints.

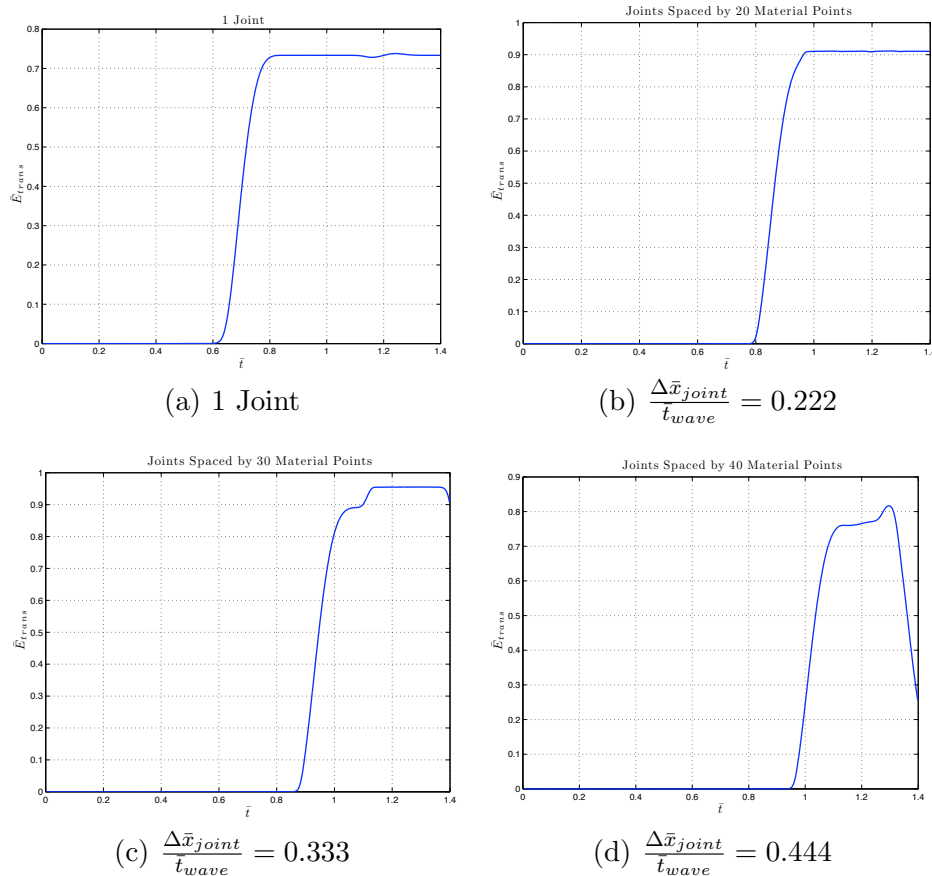


Figure 7.8: Energy transmission of multiple joint spacings

### 7.2.1 Two Joints In-Depth

The run with a spacing value  $\Delta\bar{x}_{joint} = 0.16$  study is further analyzed in a manner identical to the multiple gaps result of Section 7.1.1. Figure 7.9 shows the material point stress plotted at different times. (1) is the first time plotted. (6) is the last time plotted.

Beginning with (1), the process of wave propagation through two joints is:

- (1) The compressive pulse **A** propagates towards the first joint.
- (2) A portion of the compressive pulse **A** propagates through the joint. A smaller portion is reflected off of the joint and becomes the tensile leftward traveling wave **B**. The first joint closes to a stress state that allows wave transmission.
- (3) Wave **B** continues propagating. Wave **A** interacts with the second joint and again is broken into a continuing compressive wave **A** and a reflected wave **C**. At this current time, **C** has not reflected off of the joint fully and is still compressive. The second joint closes.
- (4) Wave **B** continues propagating. Wave **A** has propagated through the second joint and is continuing as a compressive wave. Wave **C** has reflected off of the second joint and is traveling left as a tensile pulse.
- (5) Wave **B** begins reflection off of the left end of the bar. Wave **A** continues propagating down the bar. Wave **C** reflects off of the first joint because joints have no strength in tension. Wave **C** is now a rightward traveling compressive pulse. The first joint opens because of this reflection.
- (6) Wave **B** reflects off of the end of the left bar and is traveling left as a compressive pulse. Wave **A** makes initial contact with the right end of the bar. Wave **C** propagates through the second joint with little attenuation because the joint has already closed to a stress state allowing the earlier transmission of wave **A**.

An interesting observation is that the peak stress of the tensile wave **B** is less than that of tensile wave **C**. This is most likely due to the altering of wave **A** after propagating through the first joint.

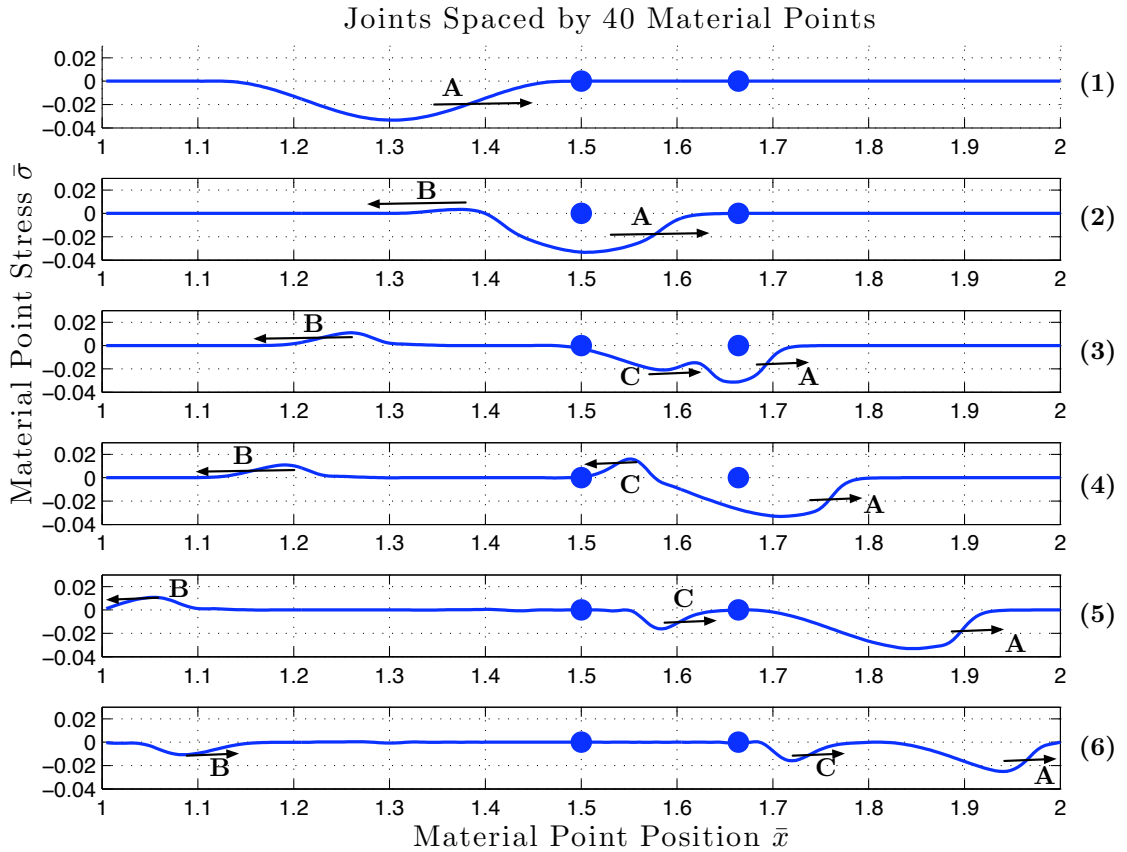
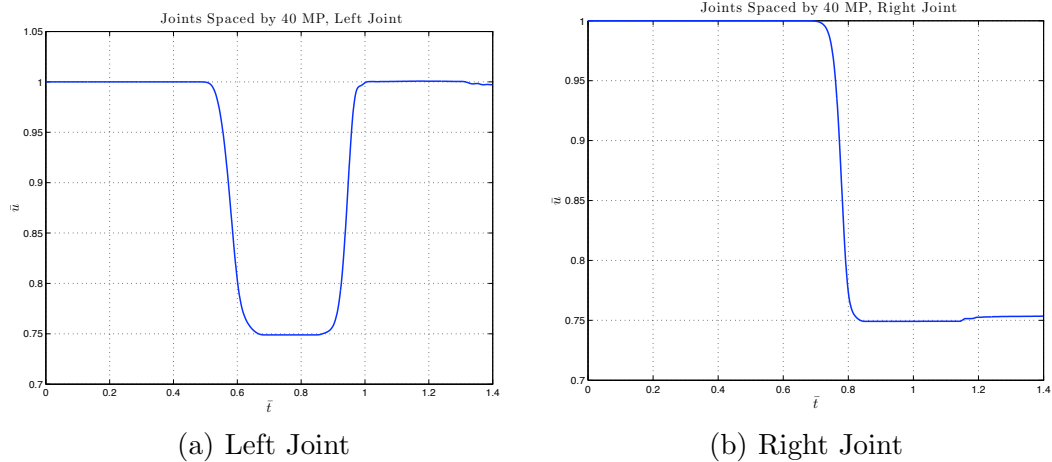


Figure 7.9: Material point stress plotted at different times (blue dots denote joint locations)

Figure 7.10 shows plots of the first and second joint sizes  $\bar{u}$  versus time. The left joint closes to approximately 0.75 from the initial propagation through the joint (Fig 7.10(a)). The wave then has a tensile reflection off of the second joint (wave **C** in Fig 7.9). When this tensile wave continues to the first joint, the joint opens up. This occurs at  $\bar{t} \approx 0.85$ . The second joint closes at  $\bar{t} \approx 0.8$ . Wave **C** propagates through the second joint without closing it further.

Figure 7.10:  $\bar{u}$  versus time for each joint

### 7.3 Summary of Multiple Joints

The analysis of two joints in this chapter clearly indicates that wave trapping occurs between two discontinuities, whether joints or gaps. The splitting of the initial wave at the second joint produces a tensile reflection that interacts with the first joint before propagating through the second. This phenomenon cannot be captured by a single joint. A single joint only has one tensile reflection which is not redirected back through the joint. For two joints, the second tensile reflection at the second joint does get reflected at the first joint and continues nearly uninterrupted propagation through the second joint. Therefore, more energy is transmitted through two joints than a single joint. The closure energy dissipated in two joints is very close to the energy dissipated in closing a single equivalent joint. Further, the closure energy of two joints is independent of joint spacing. Overall, the impact of two joints on wave propagation cannot be captured with a single joint.

# Chapter 8

## Conclusion

### 8.1 Summary

Rock joints are understood to be failures of the parent rock medium. Joints can either be filled with gouge and resist closure or be fresh and not resist closure (gaps). Typically, rock joints are characterized within a constitutive model that captures the effects of parent rock and joints as one. While reasonable for some simulations, this approach does not give a concrete indication of how individual joints interact and affect wave propagation. This research proposed several one-dimensional constitutive models suitable for normal loading of joints consisting of plasticity, elastic-plasticity, and gaps. With these models, the interactions of rock joints and wave propagation were explored.

The key results are the effects of wave parameters and the drawbacks of lumping multiple joints into an equivalent joint. A gap is shown to be indifferent to wave parameters and is only influenced by the closure potential  $u_p$  of the wave. A plastic joint transmits more energy for longer waves than shorter waves when both have equal values of the potential,  $u_p$ , for gap closure. The behavior of elastic-plastic and plastic joints is quite similar. Elastic unloading does not have a significant effect on wave propagation.

The work done with multiple joints shows that lumping joints does not capture the nuances of wave propagation. As a wave propagates through individual joints, it is attenuated and split. This can trap portions of the wave between joints until a certain amount of closure occurs, allowing the reflection to propagate through. Multiple joints have a net effect of allowing more of the original pulse to be transmitted in comparison with a single joint. Two joints have been shown to dissipate less than 1% more energy than a single joint. However, an equivalent single joint does not transmit as much energy as multiple joints because wave trapping does not occur.

## 8.2 Future Work

A continuation of the one-dimensional work to provide a deeper understanding of the impact of wave time on joint spacing would be helpful. Intuitively, a long wave has less reflected energy than a short wave. However, when multiple joints are prescribed, does wave length impact energy transmission as much it does for a single joint? Also, finding an effective manner to lump multiple joints while still capturing their overall effect may be beneficial for developing an efficient numerical algorithm. Implementation of a three-dimensional model to conduct studies similar to the one-dimensional study would be enlightening. Such studies could ascertain the impact of joint shearing on dynamic wave propagation in addition to the effects of normal joint closure reported herein.

## Appendix A

# Convergence Study with a Single Gap

The dynamic one-dimensional MPM code is specified to have a single gap in the middle of the bar. The bar is discretized with one material point per cell. Three runs are used to show convergence of the code by specifying 50, 125, and 250 material points to discretize the bar. The input wave is the sinusoidal pulse of  $v_{max} = 7.14\text{m/s}$  and  $\bar{t}_{wave} = 0.5$ . The wave has a closure potential  $u_p = 1.5\text{mm}$ . The discontinuity has an initial size  $u_{g0} = 0.5\text{mm}$ . The gap fully closes and a portion of the pulse propagates beyond the gap. The results of each run are illustrated in Figures A.1, A.2, A.3, and A.4.

The material point stress is plotted at different times along the bar for each mesh size in Figure A.1. As the number of material points is increased, the solution converges to the expected results of zero stress after the reflected tensile wave and the abrupt face of the continuing compressive wave through the gap after closure occurs.

The energy plot converges towards a constant total energy during the initial reflection of the wave off of the gap in Figure A.2. As the mesh is refined, less of a attenuation in total bar energy occurs. This is referring to the slight increase

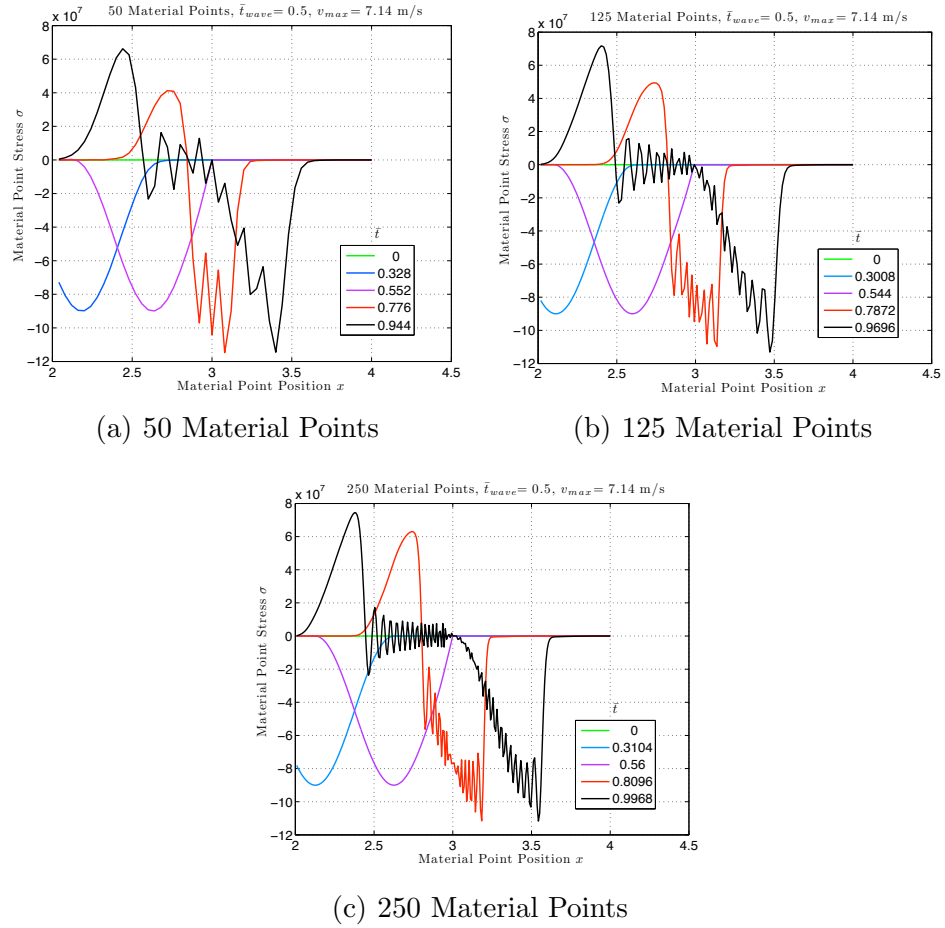


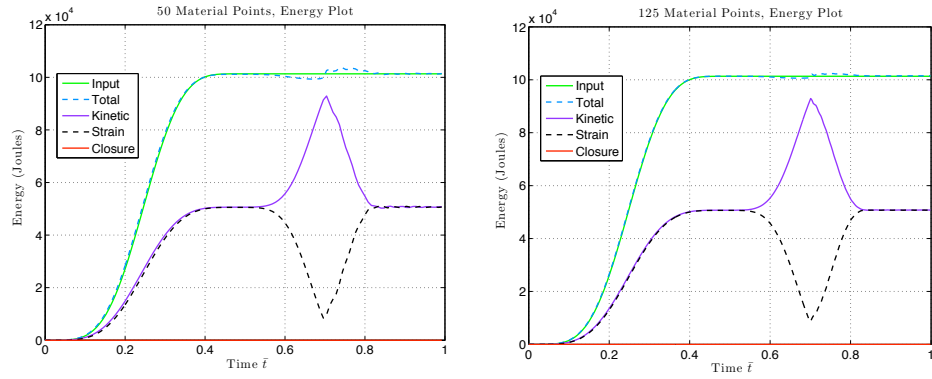
Figure A.1: Mesh refinement for wave propagation through a gap, 1 material point per cell

then decrease in total bar energy at time  $\bar{t}$  from 0.5 to 0.8. Also, the closure energy remains at zero because the gap has no resistance to closure.

The energy transmitted beyond the gap versus time in Figure A.3 is almost identical for each mesh refinement. Smoothing of the curve is noticeable between the 50 material point and 125 material point meshes during the period of energy being transmitted (Figs A.3(a) and A.3(b), respectively). For each mesh, the transmitted energy levels off to a constant value of approximately 0.72.

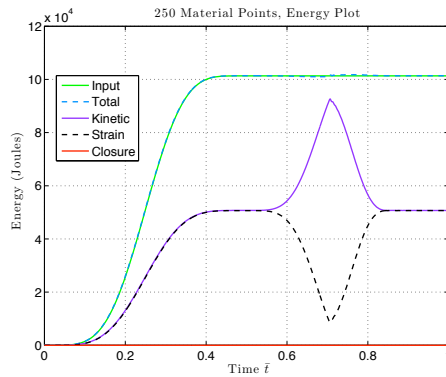
The gap size versus time in Figure A.4 is almost identical for each mesh refinement. The gap begins to close at  $\bar{t} \approx 0.5$  and closes fully at  $\bar{t} \approx 0.7$ .





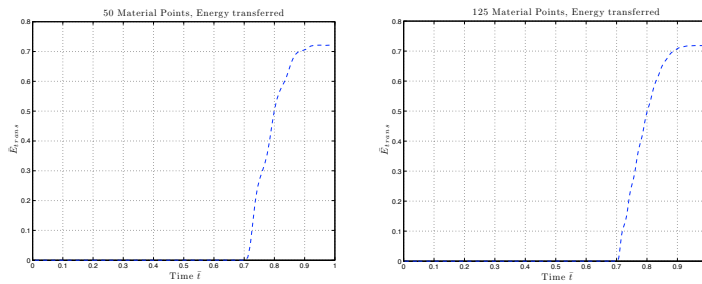
(a) 50 Material Points

(b) 125 Material Points



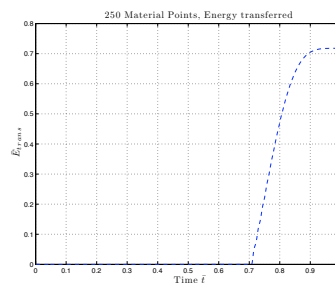
(c) 250 Material Points

Figure A.2: Mesh refinement for wave propagation through a gap, 1 material point per cell

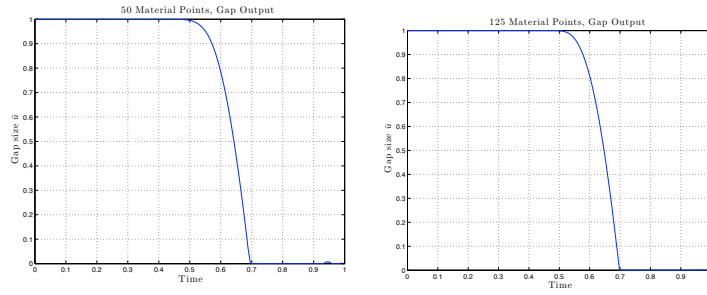


(a) 50 Material Points

(b) 125 Material Points

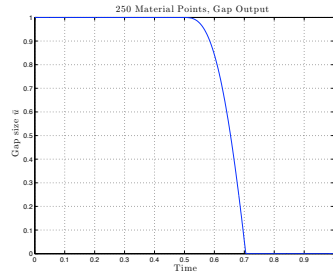


(c) 250 Material Points



(a) 50 Material Points

(b) 125 Material Points



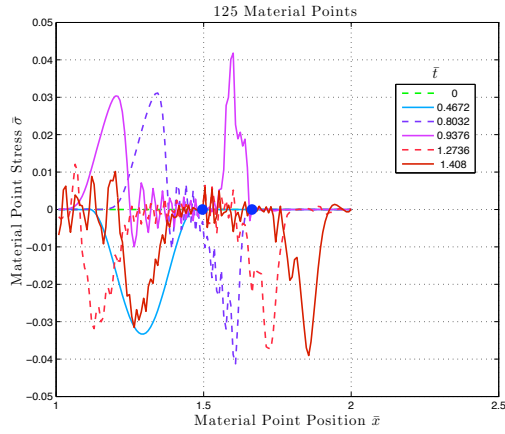
(c) 250 Material Points

Figure A.4: Mesh refinement for wave propagation through a gap, 1 material point per cell

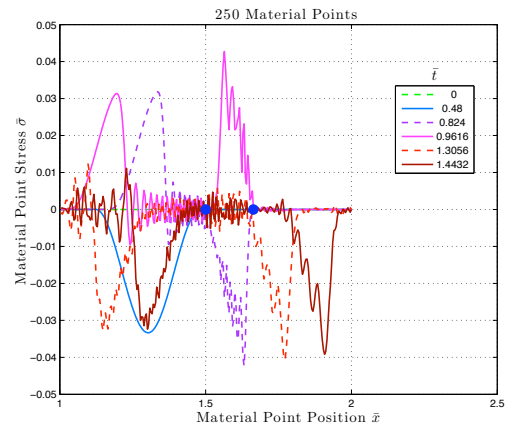
## Appendix B

# Convergence Study with Two Gaps

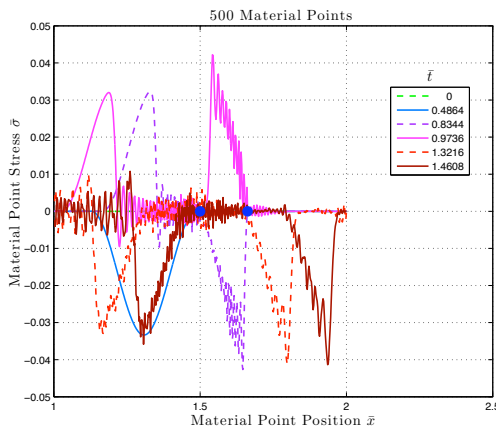
A second convergence study was conducted to show convergence with two prescribed gaps. The input wave has parameters  $v_{max} = 9.92\text{m/s}$  and  $\bar{t}_{wave} = 0.36$ . Figure B.1 shows convergence of stress plots when the bar discretization is refined from 125 to 250 to 500 material points. The energy plots also show smoother results due to refinement (Fig B.2). The plots of  $\bar{u}$  versus time for both the left and right gaps also converge when more material points are used (Fig B.3 and Fig B.4).



(a) 125 Material Points

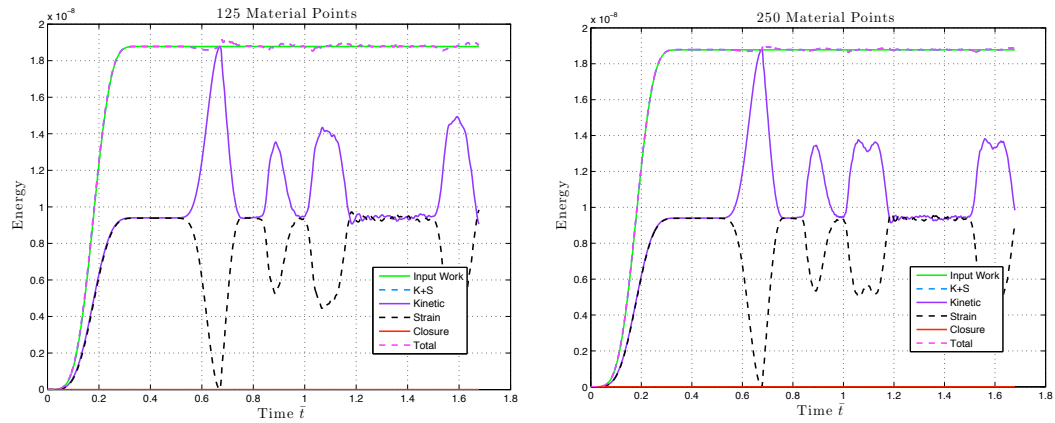


(b) 250 Material Points



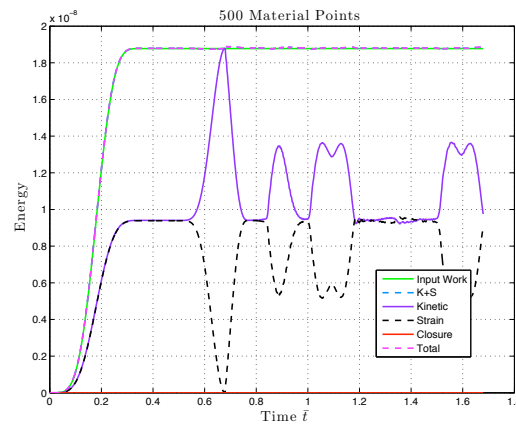
(c) 500 Material Points

Figure B.1: Mesh refinement for wave propagation through two gaps, 1 material point per cell



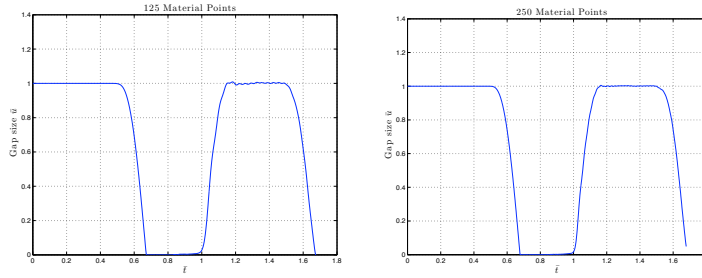
(a) 125 Material Points

(b) 250 Material Points

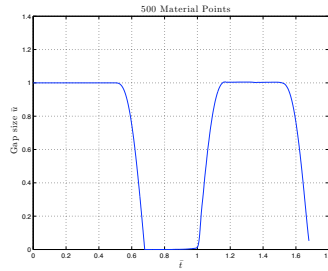


(c) 500 Material Points

Figure B.2: Mesh refinement for wave propagation through 2 gaps, 1 material point per cell

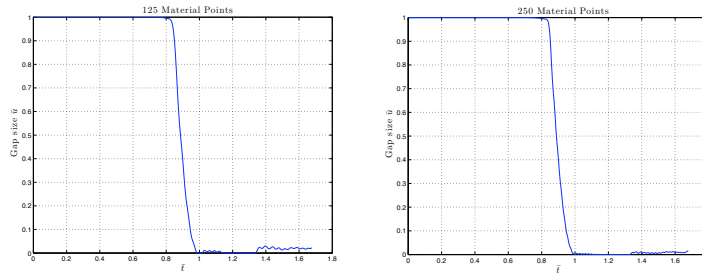


(a) 125 Material Points      (b) 250 Material Points

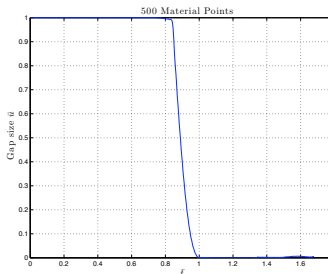


(c) 500 Material Points

Figure B.3:  $\bar{u}$  versus time for first gap



(a) 125 Material Points      (b) 250 Material Points



(c) 500 Material Points

Figure B.4:  $\bar{u}$  versus time for second gap

# Appendix C

## Nondimensionalization Scheme

The following Appendix outlines the scheme to nondimensionalize quantities for the numerical studies.

### C.1 Dimensioned Quantities

The dimensioned variables of the governing equation for the one-dimensional bar problem are as follows:

- (a)  $x$ , the cartesian coordinate along the length of the bar with dimension meters [m]
- (b)  $u$ , the displacement along the length of the bar with dimension meters [m]
- (c)  $t$ , time with dimension seconds [s]
- (d)  $\rho$ , density of the bar with dimensions  $\left[\frac{\text{kg}}{\text{m}^3}\right]$
- (e)  $Y$ , Young's modulus of the bar with dimensions  $\left[\frac{\text{kg}}{\text{m s}^2}\right]$
- (f)  $\sigma$ , the stress in the bar with dimensions  $\left[\frac{\text{kg}}{\text{m s}^2}\right]$

Also,  $\partial_x$  is the partial derivative operator. The partial derivative of  $u$  with respect to  $x$  is symbolically  $u_{,x}$ . The second partial derivative of  $u$  with respect to  $x$  is symbolically  $u_{,xx}$ .

## C.2 Equations

Ignoring body forces, the governing equation for the motion of a bar in 1D is

$$\sigma_{,x} = \rho u_{,tt}. \quad (\text{C.1})$$

The linear elastic constitutive equation in one-dimension is

$$\sigma = Y \varepsilon, \quad (\text{C.2})$$

where  $\varepsilon$  is the strain in the bar. The kinematic relationship for strain in terms of displacement is

$$\varepsilon = u_{,x}. \quad (\text{C.3})$$

When Equations (C.1), (C.2), and (C.3) are combined, the 1D wave equation is

$$(Yu)_{,x} = \rho u_{,tt}. \quad (\text{C.4})$$

## C.3 Proposed Dimensionless Quantities

The reference dimension quantities are

- (a)  $x_{ref} = L$ , the length of the bar
- (b)  $\sigma_{ref} = \frac{\sigma_g}{1000}$ , the value  $\sigma_g$  comes from the gap closure “hardening” function  $g(\bar{u}_g)$
- (c)  $Y_{ref} = \sigma_g$ , the proposed reference Young’s modulus
- (d)  $t_{ref} = \frac{L}{c}$ , the reference time, where  $c$  is the elastic wave speed  $\sqrt{\frac{Y}{\rho}}$



(e)  $\varepsilon_{ref} = 1000$ , the reference strain

When the reference values are combined with the variables of the wave equation, the dimensionless quantities follow

$$(a) \quad \bar{x} = \frac{x}{L}$$

$$(b) \quad \bar{u} = \frac{u}{u_{ref}}$$

$$(c) \quad \bar{t} = \frac{t}{t_{ref}}$$

$$(d) \quad \bar{Y} = \frac{Y}{\sigma_g}$$

$$(e) \quad \bar{\sigma} = \frac{\sigma}{\sigma_g}$$

$$(f) \quad \bar{\rho} = \frac{\rho}{\rho_{ref}}$$

The undefined reference values  $u_{ref}$  and  $\rho_{ref}$  are determined for convenience later on.

Substitute the expressions involving reference values and dimensionless variables into Equation(C.1) to get a dimensionless equation

$$\bar{\sigma}_{,\bar{x}} = \bar{\rho}\bar{u}_{,\bar{t}\bar{t}}. \quad (C.5)$$

Upon substitution of dimensionless values, Equation (C.1) reduces to

$$\frac{1}{1000L}\sigma_g(\bar{\sigma})_{,\bar{x}} = \frac{\rho_{ref}u_{ref}}{t_{ref}^2}\bar{\rho}(\bar{u})_{,\bar{t}\bar{t}}. \quad (C.6)$$

So that Equation (C.6) reduces to Equation (C.5), the the reference density  $\rho_{ref}$  comes out as,

$$\rho_{ref} = \frac{\sigma_g t_{ref}^2}{1000L u_{ref}}. \quad (C.7)$$

Then with Equation (C.2) following a similar substitution procedure, the constitutive equation reduces to

$$\frac{\sigma_g}{1000}\bar{\sigma} = \left(\frac{\sigma_g u_{ref}}{L}\right)\bar{Y}\bar{u}_{,\bar{x}}. \quad (C.8)$$

$u_{ref}$  is conveniently chosen to be

$$u_{ref} = \frac{L}{1000}, \quad (\text{C.9})$$

which gives an equation of the form

$$\bar{\sigma} = \bar{Y} \bar{u}_{,\bar{x}}. \quad (\text{C.10})$$

Substitute  $u_{ref}$  into (C.7) and simplify to get the reference density  $\rho_{ref}$  (C.11).

$$\rho_{ref} = \frac{t_{ref}^2 \sigma_g}{L^2} \quad (\text{C.11})$$

By non-dimensionalizing the governing equation in this manner, the dimensionless elastic wave speed  $\bar{c}$ , which is  $\sqrt{\frac{\bar{Y}}{\bar{\rho}}}$ , reduces to,

$$\bar{c} = 1. \quad (\text{C.12})$$

A elastic wave speed of unit value gives a dimensionless wave propagation time  $\bar{t}_{prop}$  of,

$$\bar{t}_{prop} = \frac{\bar{L}}{\bar{c}} \quad (\text{C.13})$$

$$= \frac{L/L}{\bar{c}} \quad (\text{C.14})$$

$$= 1. \quad (\text{C.15})$$

A unit dimensionless wave speed and wave propagation time is easy to interpret in the plots of results.

## Appendix D

# Material Point Placement

The material point method allows for any number of material points to be located within a cell (or element). For the one-dimensional computations exploring the effects of joints, only one material point is used per cell. Typically, the single material point is placed initially in the middle of the cell. In developing the one-dimensional material point method code, the material points were inadvertently placed a distance  $\epsilon$  from the left node of the cell.  $\epsilon$  is a value slightly larger than machine precision. This placement results in unusually smooth numerical results. The effects of such a placement were further investigated compared to the typical placement of material points centered within the cells.

Considering discontinuities, the cell boundary material point locations is helpful. For small deformations, the material points map the majority of their values to a single node because the unit hat basis functions are  $\approx 1$  for a node and  $\approx 0$  for another node when evaluated at the material points. Therefore, material point information does not get mapped in front of the elastic wave as it propagates and helps to clearly identify existing discontinuities with minimal noise.

Four runs demonstrate the impact of material point location. The last two runs shown in Figures D.3 and D.4 have a zero strength gap in the middle of the bar showing the features when the material points are placed in the middle of the cells. For a zero strength gap, the wave should just reflect off of the gap. These are all one

material point per cell and the values are plotted at material points (not mapped to the cells).

Also, the dimensionless times listed in the legend are  $\bar{t} = \frac{t}{t_{propagation}}$

- Bar length  $L = 2 \text{ m}$
- Density  $\rho = 2000 \text{ kg/m}^3$
- Young's modulus  $Y = 50 \text{ Gpa}$
- Cross sectional area  $A = 1 \text{ m}^2$
- Number of elements, either 50 or 128 depending on where the material points are placed in the cell, 50 when the material point is close to cell boundary, 128 when the material point is in middle of cell boundary
- 1 material point per cell
- Total run time is 1.5 wave propagations or  $t_f = 0.0006 \text{ s}$
- Velocity boundary condition, left boundary  $v_{left} = \frac{v_{max}}{2} (1 - \cos(\frac{2\pi t}{t_{input}}))$ , where  $v_{max} = 1 \text{ m/s}$  and  $t_{input} = 0.0002 \text{ s}$
- $\Delta t = 0.9 \frac{h_{cell}}{c}$  where  $c = \sqrt{\frac{Y}{\rho}}$

Figures D.1 and D.2 are the results for a bar without a gap in the middle. When the material point is on the cell boundary, numerical results are much smoother (Fig D.1). When the material point is centered in the cell, the results are not nearly as smooth as the cell boundary-placed material points (Fig D.2). The conclusion of this investigation is that computational results are significantly smoother when the material point is placed on the cell boundary.

Figures D.3 and D.4 are the results of placing a gap in the middle of the bar. Figure D.3 shows that material points close to the cell boundaries allow for gap behavior without noticeable numerical values passing through the open gap. But,

Figure D.4 does have unrealistic numerical values to the right of the gap. When material points are centered in the cells, material point quantities will map to two nodes equally. Similarly, nodal quantities map to two material points. This allows for quantities to propagate past the gap and allow for non-zero stresses to the right of the gap. When material points are placed on cell boundaries, the majority of material point quantities only map to one node and vice-versa. Therefore, numerical errors from the mapping are not as apparent. For this reason, the joint and gap studies place the material points close to cell boundaries during numerical discretization of the bar.

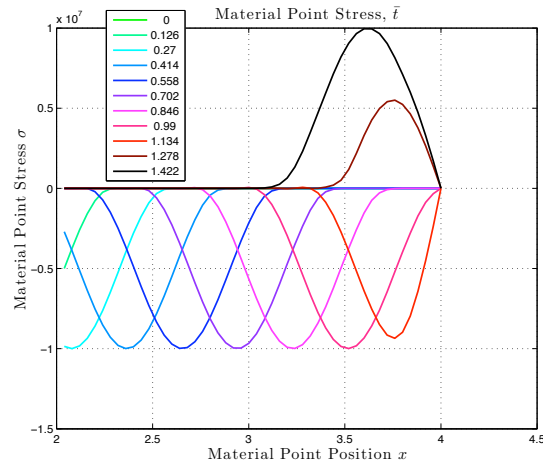


Figure D.1: Stress as a function of  $x$  for different times using 50 material points located close to the cell boundary to discretize the bar

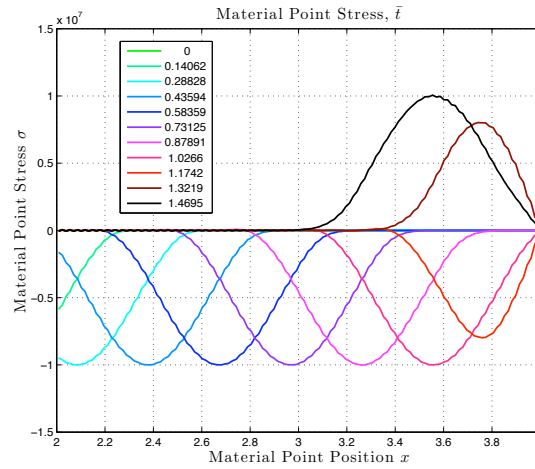


Figure D.2: Stress as a function of  $x$  for different times using 128 material points centered in the cells to discretize the bar

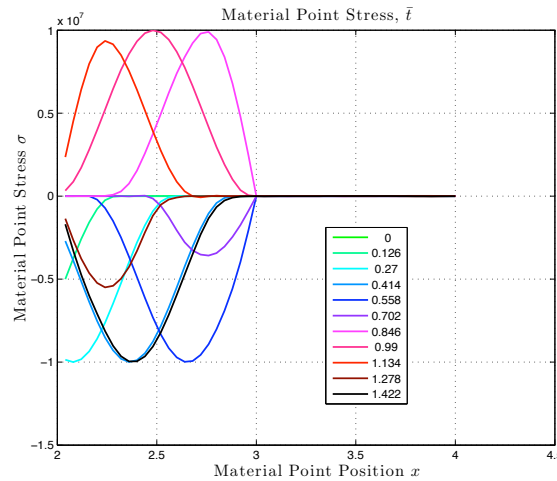


Figure D.3: Stress as a function of  $x$  for different times using 50 material points located close to the cell boundary to discretize the bar with a gap in the center of the bar

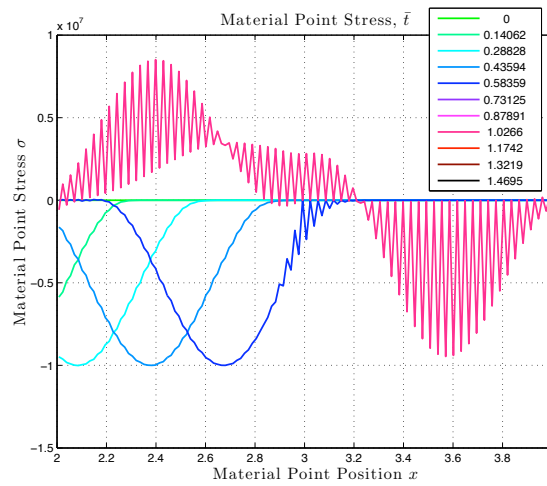


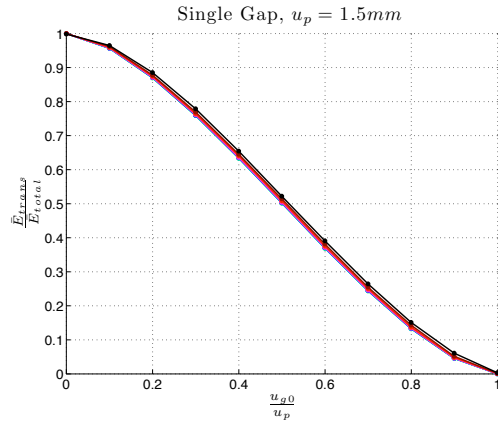
Figure D.4: Stress as a function of  $x$  for different times using 128 material points centered in the cells to discretize the bar with a gap in the center of the bar

# Appendix E

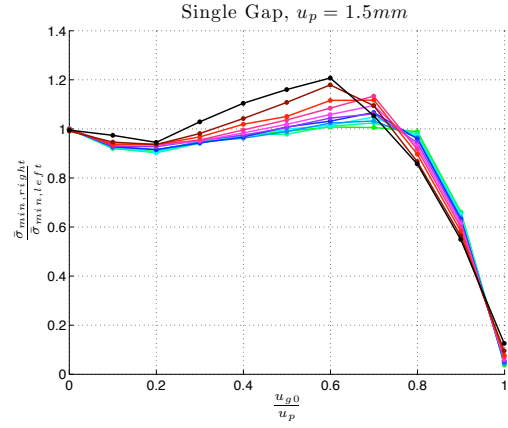
## Complete Figures

The following figures include all of runs from the single discontinuity study. In the main text, certain runs with large amounts of numerical dispersion were removed.

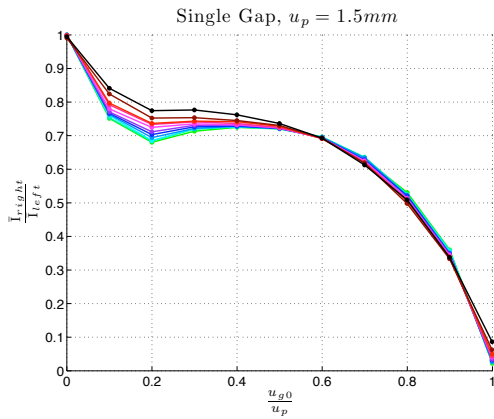




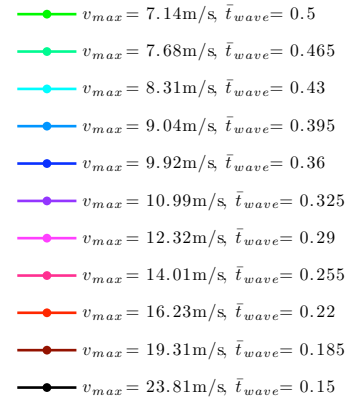
(a) Single Gap, Energy



(b) Single Gap, Peak Stress



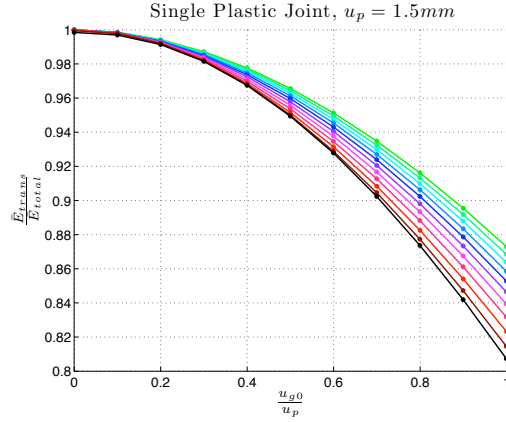
(c) Single Gap, Impulse



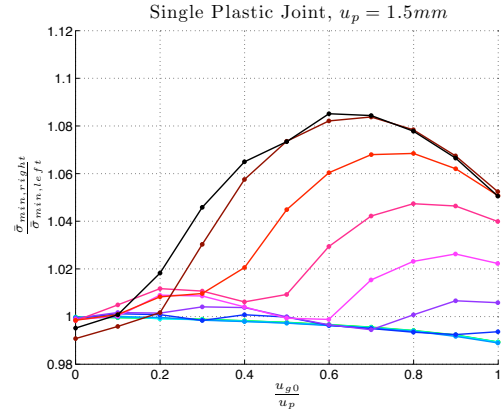
(d) Legend

Figure E.1: Results of single gap study,  $u_p = 1.5mm$

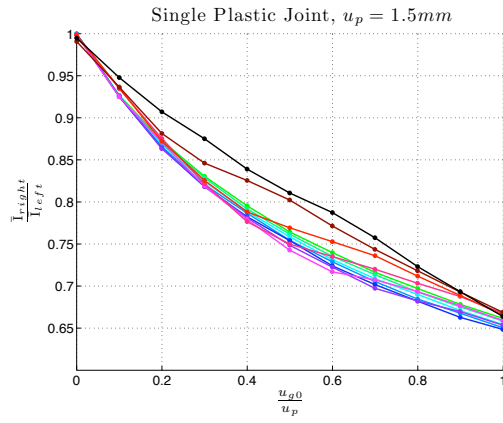
## E.2 Single Plastic Joint



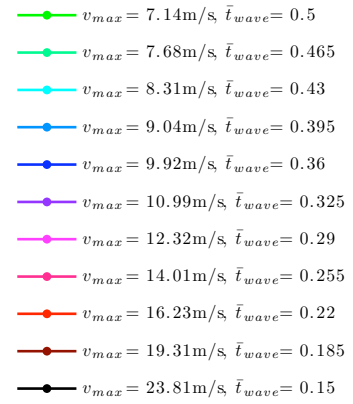
(a) Single Plastic Joint, Energy



(b) Single Plastic Joint, Peak Stress



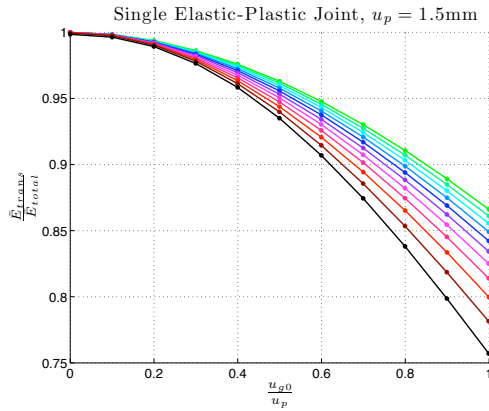
(c) Single Plastic Joint, Impulse



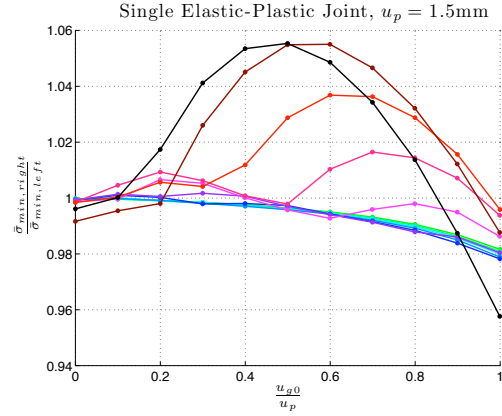
(d) Legend

Figure E.2: Results of single plastic joint study,  $u_p = 1.5mm$

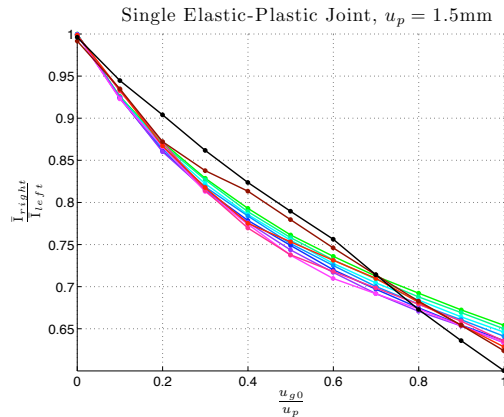
### E.3 Single Elastic-Plastic Joint



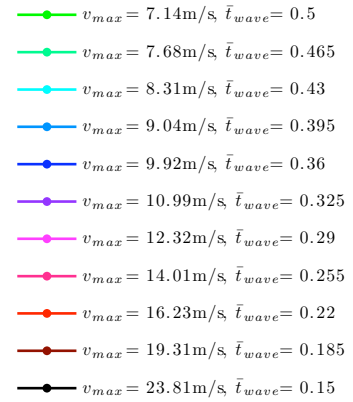
(a) Single Elastic-Plastic Joint, Energy



(b) Single Elastic-Plastic Joint, Peak Stress



(c) Single Elastic-Plastic Joint, Impulse



(d) Legend

Figure E.3: Results of single elastic-plastic joint study,  $u_p = 1.5\text{mm}$

# Appendix F

## Lumping Joints Study

Figure F.1 illustrates the investigation of the effects of multiple joints with the restriction that the sum of the initial joint lengths is a constant. This process is called lumping the joints. In this context, lumping joints places multiple discontinuities into fewer or a single discontinuity. Conversely, smearing discontinuities places a single discontinuity into multiple discontinuities. One issue of interest in connection with computing efficiency on a large scale is whether or not several joints can be modeled as one “equivalent” joint. The study will consider 16 individual discontinuities (whose initial discontinuities sum to  $u_{g0}$ ) and their impact on wave propagation. Then, for the same sum of initial discontinuity, use only 14 discontinuities. The pattern continues until only one discontinuity is used with an initial size of  $u_{g0}$ . Table F.1 provides a summary of values for parameters defining the sizes of the initial joint and forcing function.

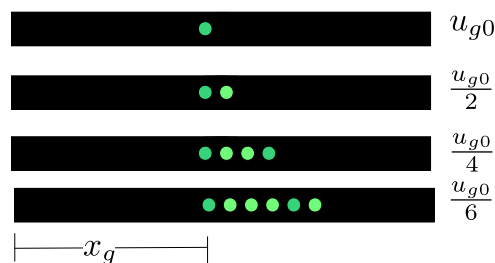


Figure F.1: Layout of Discontinuity Lumping Study

(a) Boundary Conditions,  
 $u_p = 1.5\text{mm}$

Set	$v_{max}$	$\bar{t}_{wave}$
1	9.92 m/s	0.36
2	10.99 m/s	0.325
3	12.32 m/s	0.29
4	14.01 m/s	0.255
5	16.23 m/s	0.22
6	19.31 m/s	0.185
7	23.81 m/s	0.15

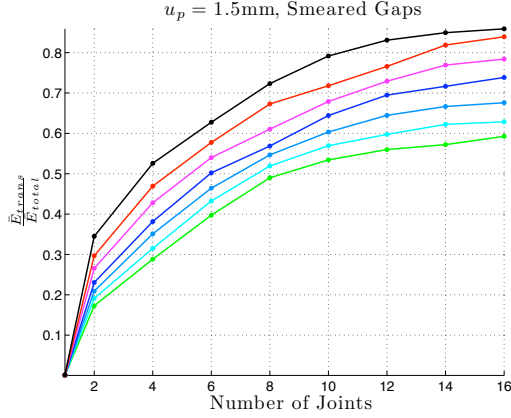
(b) Initial Discontinuity Size  $u_{g0}$

Set	$u_{g0}$
1	1.5 mm
2	0.5 mm

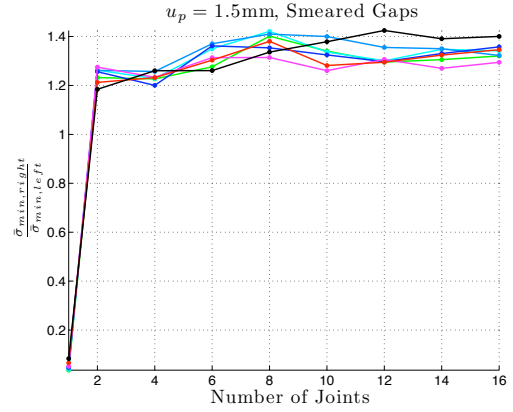
Table F.1: Inputs used for multiple joints

The following figures are the full results of the joint lumping study. The results indicate that the fewer discontinuities used, the less energy is transmitted through. This trend applies to gaps, plastic joints, and elastic-plastic joints.

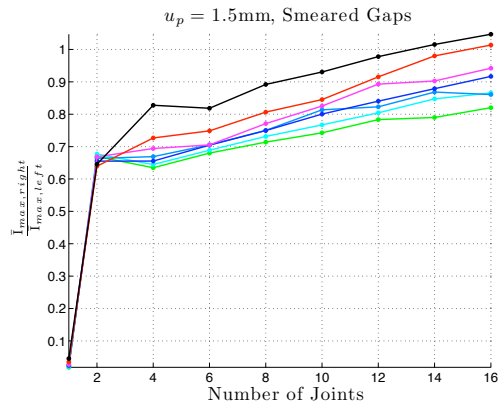
**F.1 Gaps,  $u_{g0} = 1.5\text{mm}$**



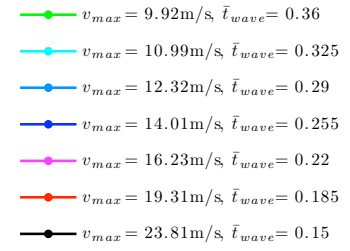
(a) Energy



(b) Peak Stress



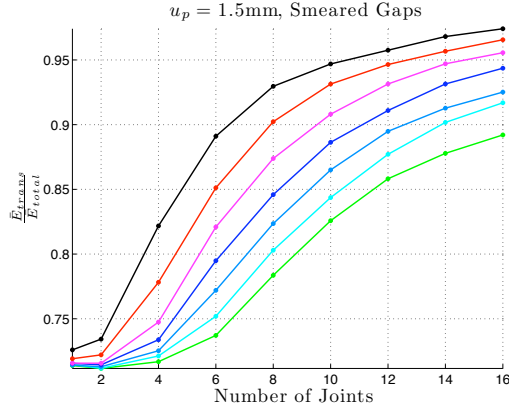
(c) Impulse



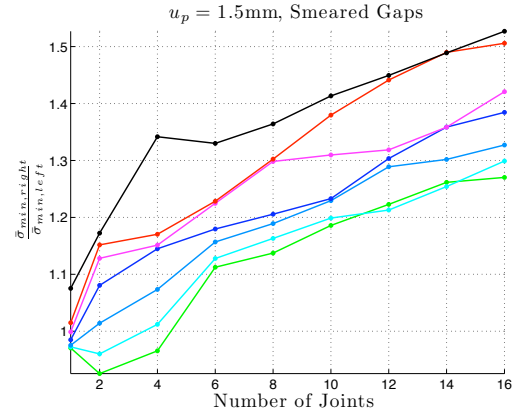
(d) Legend

Figure F.2: Results of lumping multiple gaps,  $u_{g0} = 1.5\text{mm}$

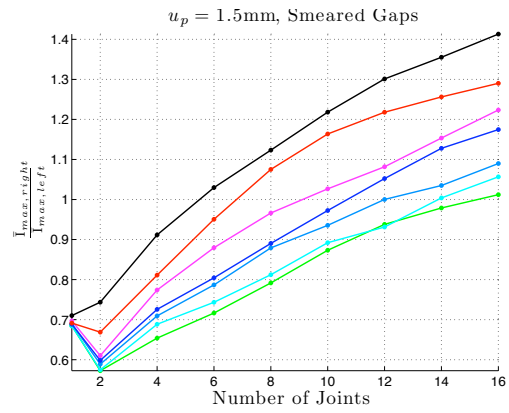
**F.2 Gaps,  $u_{g0} = 0.5\text{mm}$**



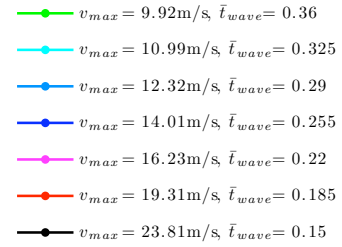
(a) Energy



(b) Peak Stress



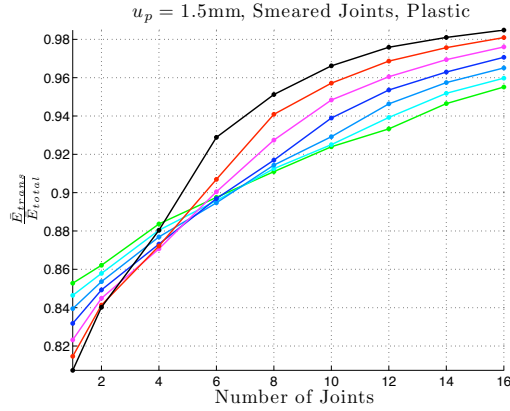
(c) Impulse



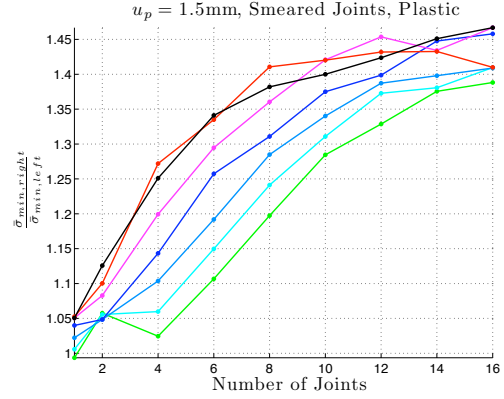
(d) Legend

Figure F.3: Results of lumping multiple gaps,  $u_{g0} = 0.5\text{mm}$

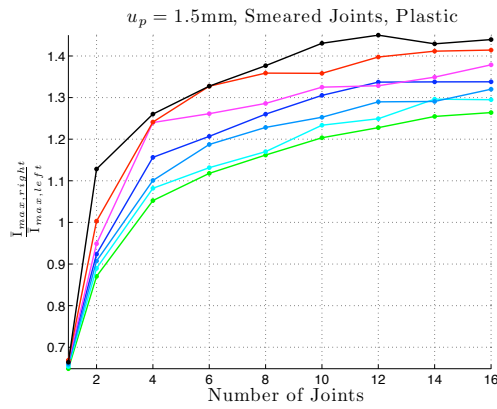
### F.3 Plastic Joints, $u_{g0} = 1.5\text{mm}$



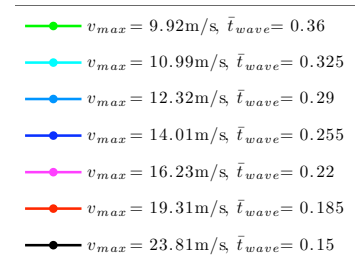
(a) Energy



(b) Peak Stress



(c) Impulse



(d) Legend

Figure F.4: Results of lumping multiple plastic joints,  $u_{g0} = 1.5\text{mm}$



### F.4 Plastic Joints, $u_{g0} = 0.5\text{mm}$

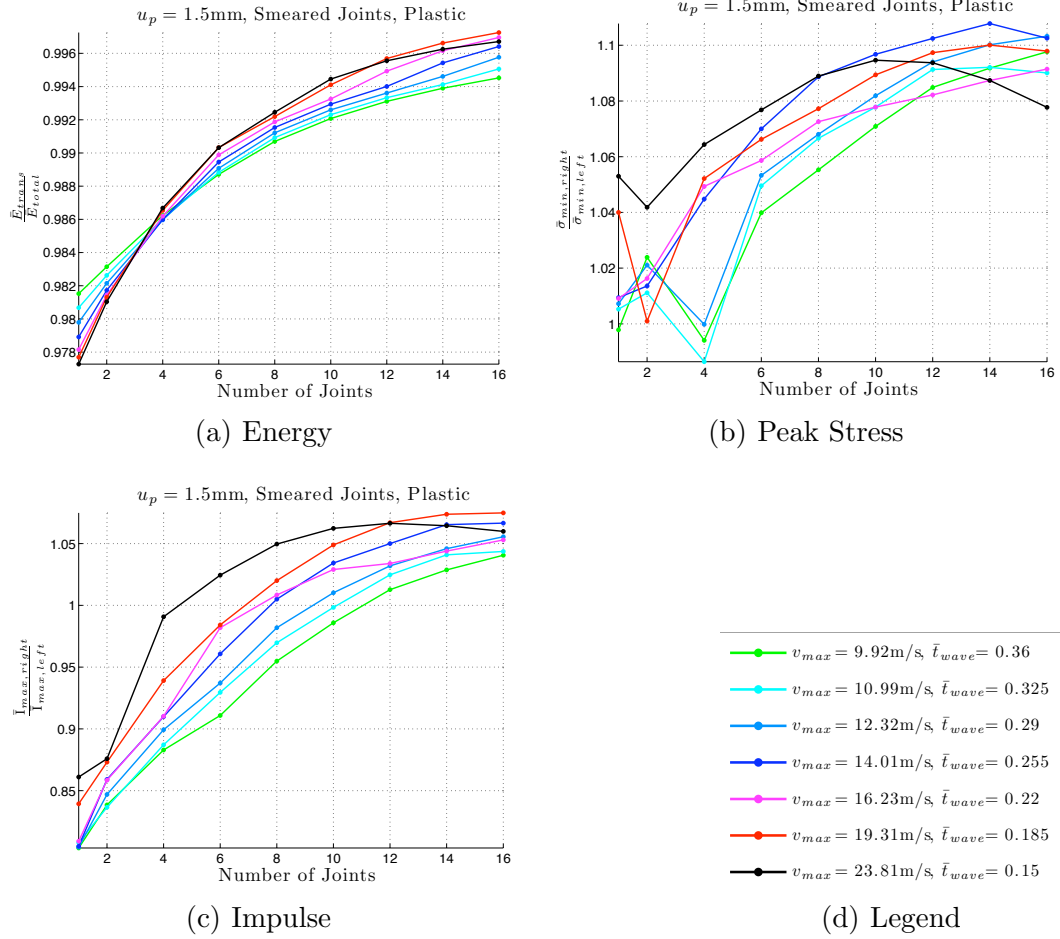


Figure F.5: Results of lumping multiple plastic joints,  $u_{g0} = 0.5\text{mm}$

### F.5 Elastic-Plastic Joints, $u_{g0} = 1.5\text{mm}$

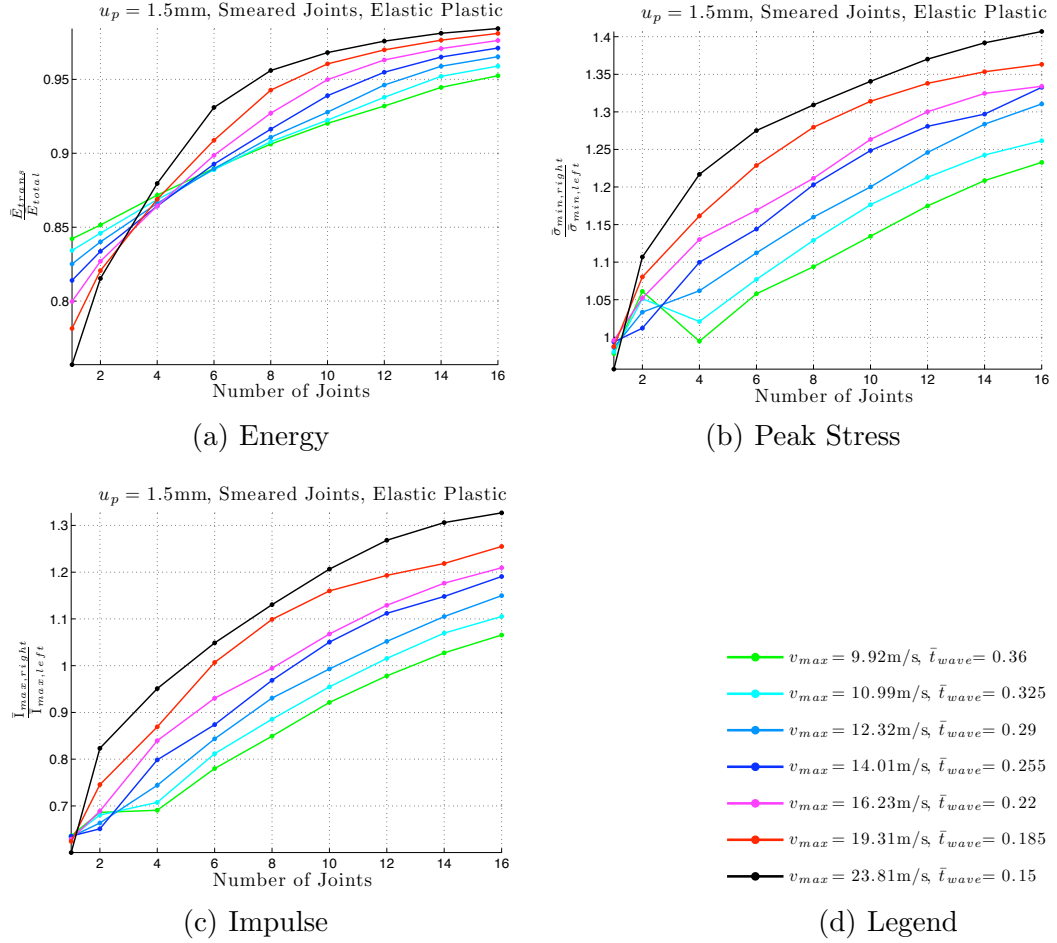


Figure F.6: Results of lumping multiple elastic-plastic joints,  $u_{g0} = 1.5\text{mm}$

### F.6 Elastic-Plastic Joints, $u_{g0} = 0.5\text{mm}$

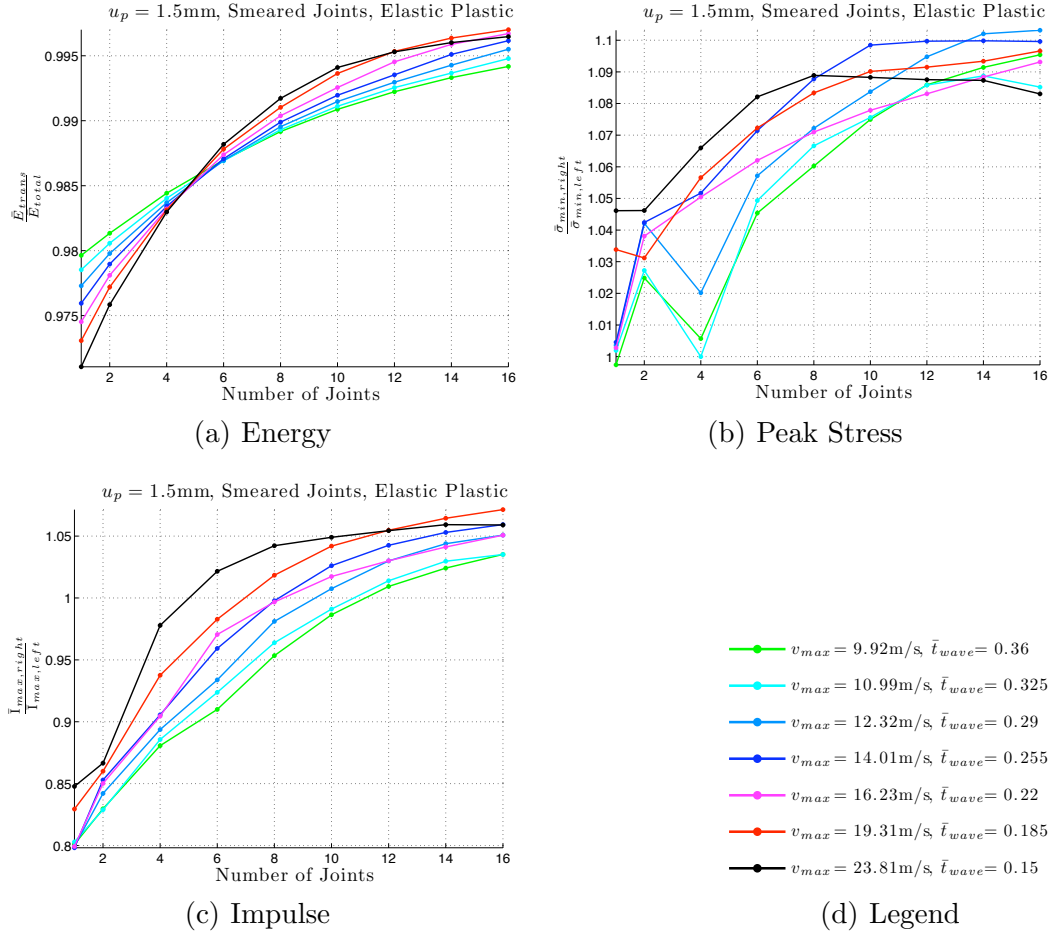


Figure F.7: Results of lumping multiple elastic-plastic joints,  $u_{g0} = 0.5\text{mm}$

# Appendix G

## Joint Spacing Study

The joint spacing study seeks to indicate the relationship between joint spacing and wave time  $\bar{t}_{wave}$ . The dimensionless parameter to relate joint spacing and wave time is as follows:

$$\Delta\bar{x}/\frac{\bar{t}_{wave}\bar{c}}{\bar{L}}. \quad (\text{G.1})$$

Because the non-dimensionalizing scheme sets  $\bar{c}$  and  $\bar{L}$  to unit values, the parameter  $\Delta\bar{x}/\frac{\bar{t}_{wave}\bar{c}}{\bar{L}}$  is equal to  $\frac{\Delta\bar{x}}{\bar{t}_{wave}}$

Figure G.1 illustrates the study. Two discontinuities with the same initial size are spaced equidistant from one another starting in the middle of the bar. The distance is increased to determine the impact of spacing on wave propagation. Table F.1 provides the initial total discontinuity sizes and sinusoidal wave parameters for the runs in the study.

$\bar{x}_{joint}$  is the distance between joints. And,  $\frac{\bar{t}_{wave}\bar{c}}{\bar{L}}$  is the spatial length of the input velocity pulse.

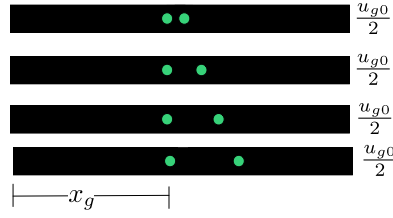


Figure G.1: Layout of Discontinuity Spacing Study

(a) Boundary Conditions,  
 $u_p = 1.5\text{mm}$

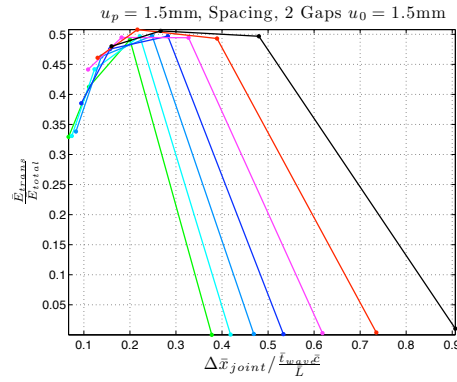
Set	$v_{max}$	$\bar{t}_{wave}$
1	9.92 m/s	0.36
2	10.99 m/s	0.325
3	12.32 m/s	0.29
4	14.01 m/s	0.255
5	16.23 m/s	0.22
6	19.31 m/s	0.185
7	23.81 m/s	0.15

(b) Initial Discontinuity Size  $u_{g0}$

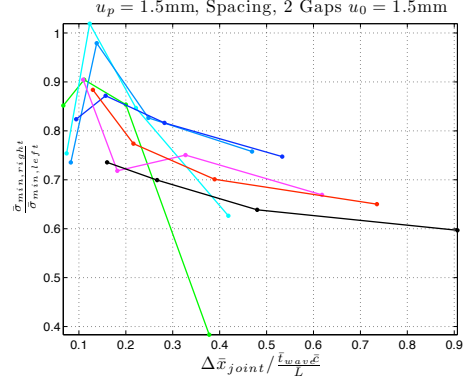
Set	$u_{g0}$
1	1.5 mm

Table G.1: Inputs used for joint spacing

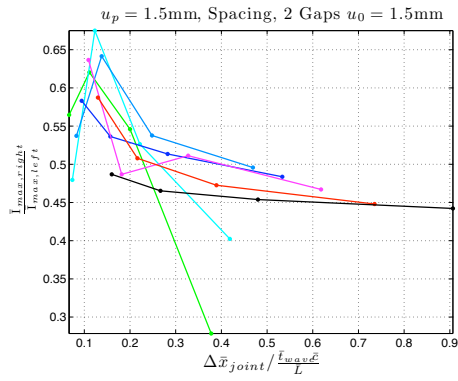
A tentative conclusion of these results is that the more space between gaps, the less energy is transmitted through the gaps. However, these results were collected before thoroughly understanding the implications of multiple joint wave propagation discussed in Chapter 7. The energy transmitted may increase if each simulation ran for a long enough time to allow the wave front to propagate to the end of the bar.



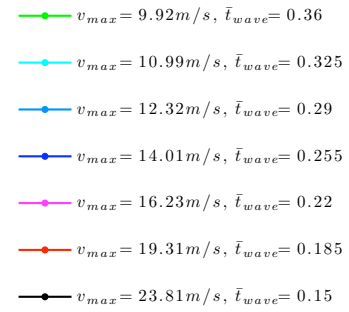
(a) Energy



(b) Peak Stress



(c) Impulse



(d) Legend

Figure G.2: Results of spacing two gaps,  $u_{g0} = 1.5\text{mm}$

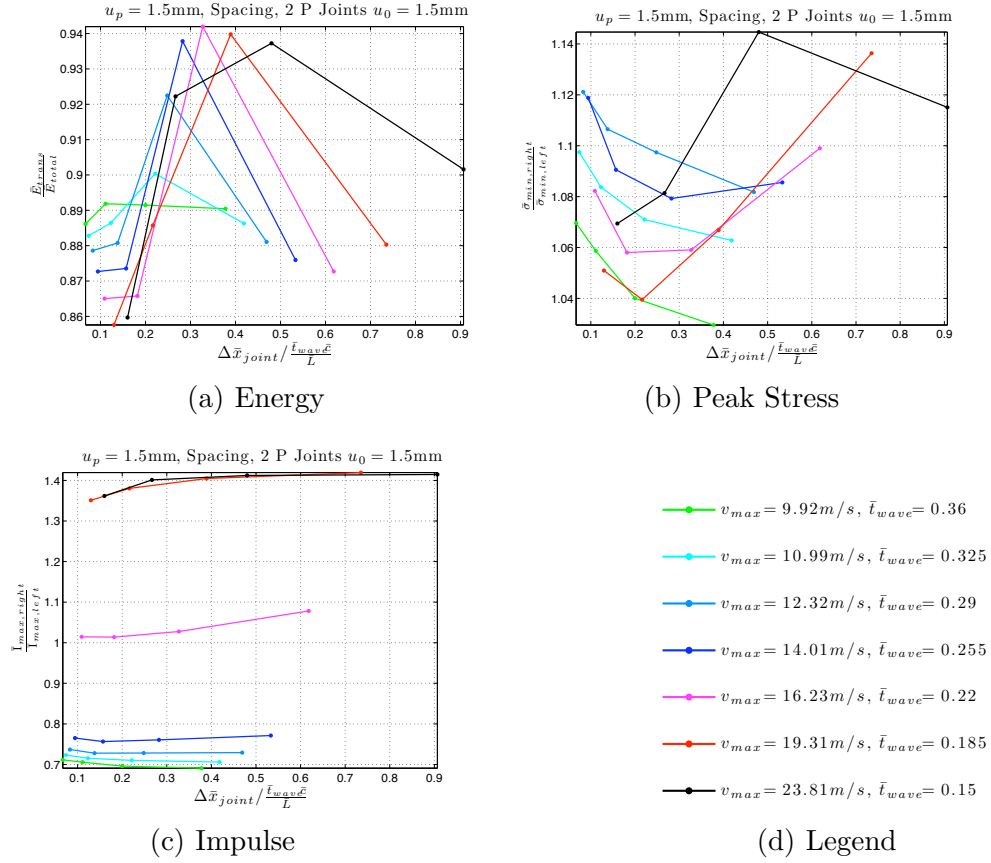


Figure G.3: Results of spacing two plastic joints,  $u_{g0} = 1.5\text{mm}$

## References

- [1] N.R. Barton. A model study of rock-joint deformation. *International Journal of Rock Mechanics and Mining Sciences*, 9:579–602, 1972.
- [2] Zdenek P. Bazant. Problems of softening damage, localization, scaling and energy release in simulation of ground shock in jointed rock. In *Ground Shock in Faulted Media Workshop*, Washington, D.C., January 2010.
- [3] Zdenek P. Bazant and Goangseup Zi. Microplane constitutive model for porous isotropic rock. *International Journal for Numerical and Analytical Methods in Geomechanics*, 27:25–47, 2003.
- [4] Rebecca Brannon. A homogenized rock-joint (fault) formulation for computational material models. In *Ground Shock in Faulted Media Workshop*. University of Utah, January 2010.
- [5] Ming Cai and Hideyuki Horii. A constitutive model of highly jointed rock masses. *Mechanics of Materials*, 13:217–246, 1992.
- [6] Michel Chalhoub and Ahmad Pouya. Numerical homogenization of a fractured rock mass: A geometrical approach to determine the mechanical representative elementary volume. *Electronic Journal of Geotechnical Engineering*, 13, 2008.
- [7] A. F. Fossum and Rebecca Brannon. On a viscoplastic model for rocks with mechanism-dependent characteristic times. *Acta Geotechnica*, (1):89–106, 2006.
- [8] Richard E. Goodman. *Introduction to rock mechanics*. Number 0-471-81200-5. John Wiley, 2nd edition, 1989.



- [9] D.W. Hu, Q.Z. Zhu, H. Zhou, and J.F. Shao. A discrete approach for anisotropic plasticity and damage in semi-brittle rocks. *Computers and Geotechnics*, 37: 658–666, 2010.
- [10] T.H. Huang, C.S. Chang, and C.Y. Chao. Experimental and mathematical modeling for fracture of rock joint with regular asperities. *Engineering Fracture Mechanics*, 69:1977–1996, 2002.
- [11] L. Jing. A review of techniques, advances and outstanding issues in numerical modeling for rock mechanics and rock engineering. *International Journal of Rock Mechanics and Mining Sciences*, 40:283–353, 2003.
- [12] Usik Lee. A theory of smeared continuum damage mechanics. *Journal of Mechanical Science and Technology*, 12(2):233–243, 1998.
- [13] J.C. Li and G.W. Ma. Experimental study of stress wave propagation across a filled rock joint. *International Journal of Rock Mechanics and Mining Sciences*, 46:471–478, 2009.
- [14] Michael E. Plesha. Constitutive models for rock discontinuities with dilatancy and surface degradation. *International Journal for Numerical and Analytical Methods in Geomechanics*, 11:345–362, 1987.
- [15] J.F. Shao and J.W. Rudnicki. A microcrack-based continuous damage model for brittle geomaterials. *Mechanics of Materials*, 32:607–619, 2000.
- [16] Ashutosh Trivedi. Strength and dilatancy of jointed rock with granular fill. *Acta Geotechnica*, 5:15–31, 2010.
- [17] J.G. Wang, Y. Ichikawa, and C.F. Leung. A constitutive model for rock interfaces and joints. *International Journal of Rock Mechanics and Mining Sciences*, 40:41–53, 2003.